Functional characterization of filamin proteins in *Dictyostelium discoideum* and neutrophils

Dissertation
der Fakultät für Biologie der
Ludwig-Maximilians-Universität München
zur Erlangung des akademischen Grades
„Doktor der Naturwissenschaften“
(Dr. rer. nat.)

vorgelegt von
Heike Roth

München, 2015

Eidesstattliche Erklärung

Ich versichere hiermit an Eides statt, dass die vorgelegte Dissertation von mir selbständig und ohne unerlaubte Hilfe angefertigt ist.

München, den 20. Juli 2015

Heike Roth

Ort der Durchführung

Der experimentelle Teil dieser Dissertation wurde von September 2011 bis Juli 2015 im Labor von Frau PD Dr. Annette Müller-Taubenberger und Herrn Prof. Dr. Michael Schleicher am Institut für Anatomie (Lehrstuhl III / Zellbiologie) der Ludwig-Maximilians-Universität München ausgeführt.

1. Gutachter: PD Dr. Annette Müller-Taubenberger

2. Gutachter: Prof. Dr. Elisabeth Weiß

Eingereicht am: 22. Juli 2015

Tag der mündlichen Prüfung: 10. November 2015

Publications

Journals

2015 **Roth H**, Samereier M, Trommler G, Noegel AA, Schleicher M, Müller-Taubenberger A (2015) Balanced cortical stiffness is important for efficient migration of *Dictyostelium* cells in confined environments *Biochemical and Biophysical Research Communications* 467: 730 – 735

In preparation. **Roth H**, Samereier M, Brechtefeld D, Walzog B, Schleicher M, Müller-Taubenberger A (2015) Filamin A exhibits regulatory functions in neutrophil motility but is not essential for efficient adhesion and migration

In preparation. Batsios P, Ishikawa-Ankerhold H, Samereier M, **Roth H**, Schleicher M, Müller-Taubenberger A (2015) Ate1-mediated posttranslational arginylation affects substrate adhesion and cell migration in *Dictyostelium discoideum*

In preparation. Samereier M, **Roth H**, Schleicher M, Müller-Taubenberger A (2015) EB1 contributes to proper front-to-back polarity in neutrophils

Poster presentations

03/2012 **Roth H**, Samereier M, Schleicher M, Müller-Taubenberger A, Filamin in *Dictyostelium* amoebae and leukocytes, Annual Meeting of the German Society for Cell Biology, 2012, Dresden, Germany, Eur. J. Cell Bio. 91, PS5-12

Table of content

Abstract

Dictyostelium discoideum and neutrophils are very similar in their modes of directed cell movement. *D. discoideum* migration is necessary for uptake of the bacterial food source, for the development and for fruiting body formation in the unique life cycle. Neutrophils are very important for cell-mediated immune responses and antagonize invading pathogens. To this end, they execute a variety of different cellular functions including adhesion, spreading, directed migration and phagocytosis. All these processes require an accurately regulated actin network as well as the activation and adjustment of different signaling pathways. Filamin (FLN) proteins are highly conserved large F-actin binding proteins that crosslink actin into orthogonal networks and are sensible candidates to be involved in these processes.

D. discoideum contains one FLN isoform (ddFLN). Deficiency of ddFLN resulted in a surprisingly subtle phenotype and had no effect on cell motility. A similar phenomenon was observed for other actin-binding proteins as well, which triggered the hypothesis of redundancy, i.e. actin-binding proteins can compensate for each other in order to guarantee different cellular processes. In the first part of the study, the function of ddFLN during cell migration was analyzed in more detail. A ddFLN overexpressing strain was generated by transforming wild-type cells with a full-length ddFLN-GFP construct. Additionally, a strain expressing a truncated ddFLN protein lacking the actin-binding domain (GFP-ddFLN(rod1-6)) was created in the wild-type background. Migration of these ddFLN mutant strains was analyzed in comparison to the primary ddFLN null mutant strain HG1264 and wild-type cells. Cell migration was investigated in the well-established micropipette assay where cells crawl on a flat surface in buffer along a gradient of chemoattractant. In addition, an under-agarose assay was executed to assess cell migration under restrictive conditions, and a new 3D migration assay was developed to study cell motility during 3D movement within a collagen matrix. The use of the evaluation software Imaris allowed the in-depth examination of the ddFLN mutant strains in different modes of migration. The subtle phenotype of the ddFLN null strain HG1264 that displayed only minor effects on 3D migration was confirmed. However, the analysis indicated an important role of ddFLN in cell motility. Overexpression of ddFLN revealed a function of ddFLN in maintaining the stability of the cell cortex and the leading edge. The results of the GFP-ddFLN(rod1-6) expressing strain hinted toward different kinds of migration modes used by *D. discoideum* cells under restrictive conditions (under-agarose assay) and in 3D (collagen assay) as compared to movement on a 2D

surface in buffer (micropipette assay). The data clearly suggested that ddFLN plays different roles for various migration types.

In the main part of the project, the function of human FLN proteins in neutrophils was assessed. The human promyelocytic leukemia cell line HL60 was used as a neutrophil model. Treatment with DMSO induced the differentiation of the cells into the neutrophil-like state. The mammalian FLN family consists of three different isoforms: FLNa, FLNb and FLNc. In a first part of the study, FLNa was identified as the major isoform in the neutrophil-like HL60 cells. Additionally, a peculiar localization of FLNa was found at the uropod of migrating cells. FLNa deficient HL60 cell lines were generated by shRNA mediated knockdown to investigate the functional relevance of FLNa in detail. Knockdown of FLNa resulted in a decreased speed of migration on a flat surface (2D), that could be the consequence of a diminished activation of myosin II. FLNa deficient cells also displayed a reduced motility in 3D migration, presumably caused by the same defect in myosin II activation. There were no or only minor effects of FLNa on adhesion and cell spreading but a so far undescribed role of FLNa in neutrophil phagocytosis, probably in the pattern recognition receptor (PRR) mediated recognition of pathogens, was detected. Subsequently, a hitherto unknown FLNa interaction with coronin 1A, mediated by FLNa repeats 9 to 18 was identified. In summary, FLNa deficiency resulted in a surprisingly subtle phenotype. There were no indications of an involvement of FLNa in the modulation of F-actin network dynamics. Instead, in neutrophils FLNa seems to play a more regulatory role with respect to functions relevant for motility.

Zusammenfassung

Dictyostelium discoideum und Neutrophile sind sich im Hinblick auf die Art und Weise ihrer gerichteten Zellmigration sehr ähnlich. Migration von *D. discoideum* ist notwendig für die Aufnahme der bakteriellen Nahrungsquellen, für die Entwicklung und die Bildung des Fruchtkörpers innerhalb des einzigartigen Lebenszyklus. Neutrophile sind sehr wichtig für die Zell-basierte Immunantwort und bekämpfen eingedrungene Pathogene. Zu diesem Zweck üben sie eine Anzahl verschiedener zellulärer Funktionen aus, wie z.B. Adhäsion, Spreiten, gerichtete Migration und Phagozytose. Für die Ausführung all dieser verschiedenen Prozesse ist ein präzise reguliertes Aktin-Netzwerk und gleichzeitig die Aktivierung sowie Regulierung verschiedener Signalwege nötig. Filamin (FLN) Proteine sind stark konservierte, große Aktin-Bindeproteine, die F-Aktin in rechtwinklige Netzwerke quervernetzen, und stellen geeignete Kandidaten dar, um an der Regulation dieser Prozesse beteiligt zu sein.

In *D. discoideum* gibt es nur eine FLN Isoform (ddFLN). Verringerung der ddFLN Expression verursachte einen überraschend schwachen Phänotyp und hatte keinen Effekt auf die Beweglichkeit der Zellen. Ein ähnliches Phänomen wurde für andere Aktin-Bindeproteine beobachtet, woraus die Hypothese der Redundanz abgeleitet wurde: Aktin-Bindeproteine können einander ersetzen, um die Ausübung bestimmter zellulärer Prozesse zu garantieren. Im ersten Teil der Arbeit wurde die Funktion von ddFLN während der Zellmigration im Detail untersucht. Ein ddFLN überexprimierender Stamm wurde erzeugt, indem ein Vollelänge-ddFLN Konstrukt in Wildtyp-Zellen transformiert wurde. Zudem wurde ein Stamm hergestellt, der im Wildtyp-Hintergrund ein verkürztes ddFLN Protein exprimierte, welchem die Aktin-Bindedomäne fehlte (GFP-ddFLN(rod1-6)). Migration dieser verschiedenen ddFLN Mutanten-Stämme wurde im Vergleich zur ersten ddFLN-Null-Mutante (HG1264) und zu Wildtyp-Zellen analysiert. Zellmigration wurde mithilfe des etablierten Mikropipetten-Versuches untersucht, bei dem sich die Zellen auf einer flachen Oberfläche in Puffer entlang eines Lockstoff-Gradienten bewegen. Zusätzlich wurde ein Unter-Agarose-Versuch verwendet, mit dem Zellmigration unter einschränkenden Bedingungen charakterisiert wird. Ein neuer 3D-Migration-Versuch wurde entwickelt, der die Analyse der Zellen während ihrer 3D-Bewegung durch eine Kollagen-Matrix erlaubt. Die Verwendung der Analyse-Software Imaris ermöglichte die detaillierte Untersuchung der unterschiedlichen ddFLN-Mutanten Stämme in verschiedenen Arten der Migration. Der schwache Phänotyp der ddFLN-Null-Mutante, die ausschließlich geringe Effekte in der 3D Migration zeigte, wurde bestätigt. Dennoch gab es starke Hinweise auf eine wichtige Rolle von

ddFLN in der Beweglichkeit der Zellen. Die Überexpression des ddFLN Proteins offenbarte eine Funktion von ddFLN in der Aufrechterhaltung der Stabilität des Zellkortex und der Vorderfront der migrierenden Zelle. Die Ergebnisse des GFP-ddFLN(rod1-6) exprimierenden Stammes deuteten darauf hin, dass *D. discoideum* Zellen unter einschränkenden Bedingungen (im Unter-Agarose-Versuch) und während der Migration in 3D (im Kollagen-Versuch) andere Arten der Migration aufwiesen als während der Bewegung auf einer flachen 2D Oberfläche in Puffer (im Mikropipetten-Versuch). Die Daten legten eindeutig nahe, dass ddFLN in den unterschiedlichen Arten der Migration verschiedene Funktionen ausübte.

Im Hauptteil des Projektes wurde die Funktion von humanen FLN in Neutrophilen untersucht. Die humane promyelozytische Leukämie-Zelllinie HL60 wurde als Neutrophilen-Model verwendet. Behandlung mit DMSO induzierte die Differenzierung der Zellen in den Neutrophilen-ähnlichen Zustand. Die Familie der Säuger FLN Proteine besteht aus drei verschiedenen Isoformen: FLNa, FLNb und FLNc. Im ersten Teil der Arbeit wurde FLNa als Haupt-Isoform in den Neutrophilen-ähnlichen HL60 Zellen identifiziert. Zusätzlich wurde eine auffällige Lokalisation des FLNa Proteins am Hinterende der migrierenden Zellen gefunden. Um die funktionelle Relevanz des FLNa Proteins im Detail zu analysieren wurden HL60 Zelllinien mit vermindertem FLNa Proteingehalt mithilfe von shRNS vermittelter Herunterregulation der Expression hergestellt. Die Verminderung des FLNa Expressionlevels führte zu einer verringerten Migrationsgeschwindigkeit der Zellen auf einer flachen Oberfläche (2D), was die Konsequenz einer reduzierten Aktivierung von Myosin II sein könnte. Die Zellen mit mangelhafter FLNa Expression zeigten ebenso eine verminderte Geschwindigkeit in der 3D Migration, was vermutlich durch den gleichen Defekt in der Myosin II Aktivierung hervorgerufen wurde. FLNa hatte keine oder nur sehr geringe Effekte von FLNa auf Adhäsion und Zell-Spreiten. Allerdings zeigte sich eine bisher noch nicht beschriebene Rolle von FLNa in der Neutrophilen-Phagozytose, wahrscheinlich in der Mustererkennungsrezeptoren (*pattern recognition receptor*, PRR) vermittelten Erkennung der eingedrungenen Pathogene. Zudem wurde eine bis dato unbekannte Interaktion von FLNa mit Coronin 1A, welche von den FLNa Wiederholungs-Sequenzen 9 bis 18 vermittelt wird, identifiziert. Zusammenfassend verursachte der Mangel an FLNa einen überraschend schwachen Phänotyp. Es gab keine Hinweise darauf, dass FLNa an der Modulation der Dynamik von F-Aktin Netzwerken beteiligt ist. Stattdessen scheint FLNa eine eher regulatorische Rolle im Hinblick auf Funktionen zu haben, die die Beweglichkeit der Zellen betreffen.

1 Introduction

1.1 The model organism *Dictyostelium discoideum*

The amoeboid soil organism *Dictyostelium discoideum* (*D. discoideum*) is a haploid eukaryote that was first isolated and characterized by Kenneth B. Raper (Raper, 1935). Phylogenetically, *D. discoideum* belongs to the phylum Mycetozoa and developed form the animal-fungal lineage after the divergence of plants (Eichinger et al., 2005). As a social amoeba, *D. discoideum* exhibits a unique life cycle comprising unicellular and multicellular stages (Figure 1). In the vegetative state, the cells live as individual amoebae in the soil, feed on bacteria via phagocytosis and multiply by mitotic division. Under adverse conditions like for example starvation, the cells become responsive to cAMP released by other amoebae and begin to form streams, aggregates and often a multicellular, well-organized 'slug' with distinguishable cell types. The slug is motile and migrates in a phototactic and thermotactic manner to an optimal location, where the formation of a fruiting body and finally the release of spores are initiated (Kessin, 2001).

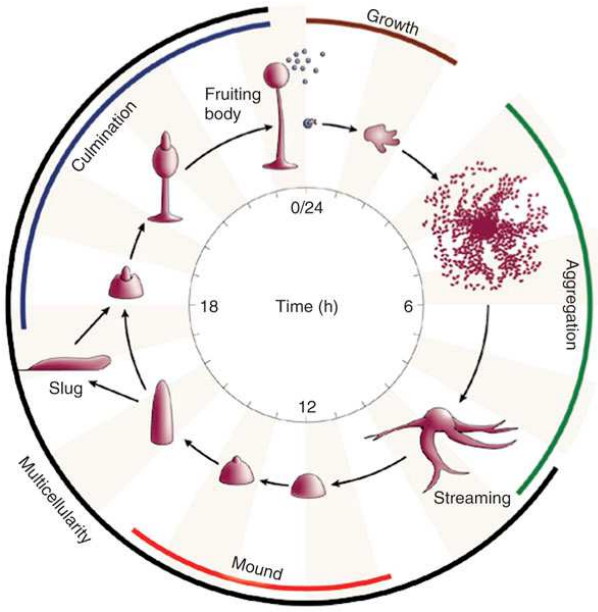

Figure 1: The life cycle of *D. discoideum*
In the growth phase, the *D. discoideum* cells live as amoebae. Upon starvation, the cells enter the aggregation phase and begin to stream together mediated by chemotaxis toward cAMP. As a result, a multicellular mound is formed which then can form a slug or start culmination without entering the slug stage. Finally, the fruiting body consists of a disc, the stalk and the spore mass at the top. New vegetative amoebae can hatch from the released spores and the life cycle begins anew. Under laboratory conditions a full cycle requires about 24 hours. Picture taken from Chisholm and Firtel (2004).

D. discoideum is a widely used model organism to study cell motility, chemotaxis, phagocytosis, cell division, mitosis, morphogenesis or cell type differentiation. The cells can be easily cultured either on bacterial lawns, cell culture plates or in shaking cultures. They exhibit a relatively short generation time of about 8 hours so that large quantities of cells can be quickly obtained. Furthermore, the genome of *D. discoideum* is completely sequenced and the haploid nature of the cells enables the fast and relatively easy generation of mutants (Eichinger et al., 2005).

Minus mutants and mutant strains expressing selected fusion proteins can be precisely analyzed with cell biological techniques and can be used for fixed cell microscopy, live-cell imaging and protein interaction studies (Faix et al., 2004; Kuspa et al., 1995; Parent, 2001). *D. discoideum* is a prime model organism to study cell motility and cytoskeletal dynamics, especially as its actin cytoskeleton and many of its actin-binding proteins share high similarities with cytoskeletal components of motile cells of higher organisms (Eichinger et al., 1999; Noegel and Luna, 1995; Zigmond et al., 1997).

1.2 Neutrophils

1.2.1 Neutrophils in the innate immune system

Neutrophils are white blood cells or leukocytes that mature in and are released from the bone marrow. Together with the eosinophils and basophils they form the class of polymorphonuclear cells (PMNs) or granulocytes. With 50 – 70% they are the most abundant circulating leukocytes in human blood (Mestas and Hughes, 2004). Neutrophils are characterized by a segmented nucleus, specific granules, including primary, secondary and tertiary granules, and secretory vesicles within the cytoplasm that are sequentially generated during maturation (Borregaard and Cowland, 1997).

In general, neutrophils are considered as very short-lived cells with a lifespan of approximately 10 hours in the peripheral blood. However, a previous study reported a substantially longer lifespan of 5.4 days, but this remains to be confirmed (Li et al., 2011; Pillay et al., 2010; Tofts et al., 2011). Nevertheless, neutrophils are the first immune cells recruited in an inflammatory process to oppose invading pathogens. Therefore, the cells have to leave the circulation and transverse into the tissue to arrive at the site of infection or inflammation in a multistep process called transendothelial migration (TEM) (Figure 2). This recruitment process is initiated by tissue resident leukocytes that secret cytokines e.g. tumor necrosis factor (TNF) or interleukin-1β (IL-1β) in response to invading pathogens (Nauseef and Borregaard, 2014). Activated endothelial cells express high levels of E- and P-selectins, membrane glycoproteins that interact with surface receptors as P-selectin glycoprotein ligand (PSGL)-1 and other glycosylated ligands on neutrophils. Selectin-ligand interactions are necessary to capture neutrophils from the blood stream (Zarbock and Ley, 2009). Chemokines either secreted directly by inflamed endothelial cells or by activated mast cells and platelets are immobilized on the luminal site of the endothelium and activate another group of important surface receptors on neutrophils, the

integrins (Massena et al., 2010). Integrins are heterodimeric glycoproteins consisting of an α-chain non-covalently bound to a β-chain. Activation of integrins is accompanied by conformational changes from a low affinity state over an intermediate affinity to a high affinity conformation (Zhang and Chen, 2012). At least 24 different integrin molecules are known in human. They are composed of the 18 different α- and 8 different β-subunits. Mainly β_2 integrins are expressed on neutrophils with $\alpha_M\beta_2$ (macrophage-antigen, Mac-1) and $\alpha_L\beta_2$ (lymphocyte function-associated antigen, LFA-1) as the most important integrins (Zarbock and Ley, 2009). The activation of integrins (inside-out signaling) in neutrophils occurs either via signaling pathways activated after binding of chemoattractant receptors to chemokines or directly through selectin mediated signaling. Subsequent integrin-ligand interaction (outside-in signaling), in particular the binding of LFA-1 to the intracellular adhesion molecule-1 (ICAM-1) on endothelial cells, activates signaling pathways in neutrophils involving protein lipase C (PLC), small GTPases and actin-binding proteins as talin. Effectively these signaling pathways result in slowing of neutrophil rolling, arrest and spreading on the vessel wall (Ley et al., 2007; Nauseef and Borregaard, 2014). Subsequently, the cells crawl Mac-1-ICAM-1 dependent on the vessel wall to a site where they can leave the vasculature either by using the paracellular route through endothelial junctions or the transcellular route, directly through an endothelial cell (Muller, 2011; Phillipson et al., 2006). After traversing the basement membrane, neutrophils perform chemotaxis toward the complement factor C5a or bacteria derived chemoattractants as N-formylmethionyl-leucyl-phenylalanine (fMLP) and migrate through the tissue to the sites of inflammation or infection (Kolaczkowska and Kubes, 2013).

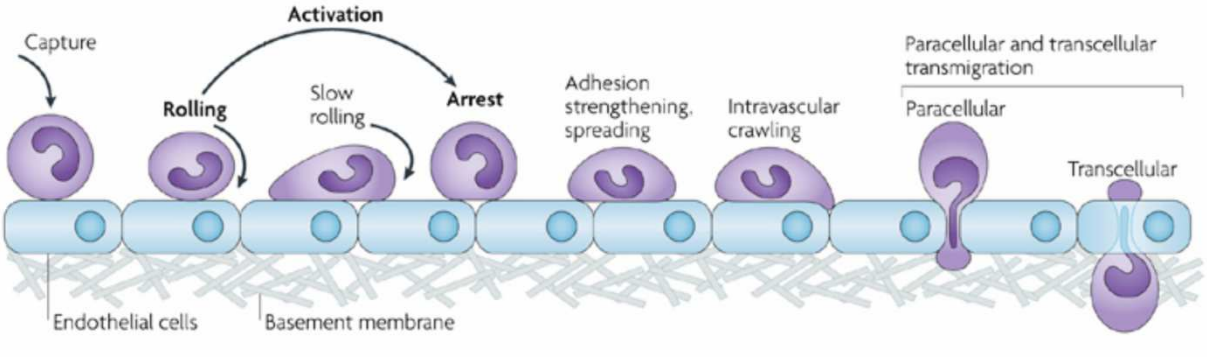

Figure 2: Leukocyte adhesion cascade
Leukocytes are captured from the blood by activated endothelial cells by selectin-ligand interactions. They roll along the endothelium and become activated. Further selectin-ligand interactions, LFA-1 and Mac-1 binding to ICAM-1 on the endothelium mediate slow rolling, arrest and subsequent firm adhesion and spreading of the leukocytes. After Mac-1-ICAM-1 dependent intravascular crawling, the leukocyte traverse the endothelium either by paracellular or transcellular transmigration and arrive in the tissue. Picture taken and modified form Ley et al. (2007).

Once the neutrophil encounters the invading pathogen, it can execute different killing mechanisms, among them phagocytosis. Invading pathogens become usually opsonized, that means their surface is coated with complement factors and IgGs. This 'coat' facilitates their recognition and elimination through phagocytes. Therefore, phagocytes are equipped with different Fcγ receptors that can interact with IgGs or complement receptors, like Mac-1, a receptor for the complement factor iC3b (Langereis, 2013; Vidarsson and van de Winkel, 1998). Additionally, pattern recognition receptors (PRRs) are also present that can interact with invariant structural motifs on pathogens, the pathogens-associated molecular patterns (PAMPs) (Thomas and Schroder, 2013). After the pathogen is recognized and engulfed by the neutrophil, it is trapped within the cell in a phagosome. Primary and secondary vesicles fuse with the phagosome and the pathogen is killed by their antimicrobial contents and the production of reactive oxygen species (ROS) (Kruger et al., 2015). Neutrophils also execute extracellular killing mechanisms by generating a powerful oxidative burst, by releasing antimicrobial and proteolytic proteins stored in the granules or by the formation of NETs, extracellular DNA traps (Brinkmann et al., 2004; Kruger et al., 2015; Nauseef and Borregaard, 2014). While neutrophils play an essential role during the first immune response to acute inflammations, they also display anti-inflammatory characteristics, are involved in wound healing by for example removal of dead cells and debris and are able to modulate the adaptive immune response through interactions with dendritic cells, B- and T-cells (Kolaczkowska and Kubes, 2013).

1.2.2 The HL60 cell line – a neutrophil model

Studying neutrophil functions is always a problematic endeavor due to the limited life span of these cells. While the development of knockout and mutant mice models made the analysis of the functions of mouse neutrophils possible, the examination of human neutrophil mechanisms remains difficult. Although it is possible to isolate granulocytes from the peripheral blood, the small amounts of isolated cells, the variability between different donors, the short life span and the difficulties in genetic manipulation of these cells prevent extensive analysis of human neutrophil functions. Different leukemia cell lines offer an alternative option. The human promyelocytic leukemia cell line HL60 was established in 1977 from the peripheral blood of a female patient suffering from acute promyelocytic leukemia (Collins et al., 1977). The immortal cell line can proliferate growth-factor-independently in suspension with a doubling time of 20 to 48 hours (Birnie, 1988). The HL60 cells exhibit mutations in some typical oncogenes, including a point mutation in *N-ras*, an amplified *c-myc* gene, and they are deficient for *p53* (Collins, 1987).

Leukemia cells are typically characterized by a disrupted hematopoiesis (Tsiftsoglou et al., 2003). Under physiological conditions, neutrophils are generated in the bone marrow where hematopoietic stem cells give rise, over a continuum of different progenitors, to terminal differentiated blood cells. The first step in the hematopoietic process is the division into a lymphoid branch that results in natural killer cells, B- and T-lymphocytes and a myeloid branch (Larsson and Karlsson, 2005). The myeloid branch is further subdivided into to the megakaryocyte/erythrocyte lineage and the granulocyte/macrophage lineage (Akashi et al., 2000). The first progenitor cell type within the latter branch is the myeloblast that develops via further progenitors as for example promyelocytes and myelocytes into mature granulocytes (neutrophils, basophils and eosinophils) or alternatively, via monoblasts and monocytes, into mature macrophages (Rozenberg, 1996). The vast majority of the HL60 cells display a myeloblast/promyelocytic morphology with large round nuclei, basophilic cytoplasm, azurophilic granules and surface antigens characteristic for immature myeloid cells. The untreated cell culture usually contains 5 – 10% cells which underwent spontaneous differentiation into more mature cells as myelocytes, monocytes or granulocytes (Birnie, 1988). However, the pluripotent cells can be also directly induced to differentiate either into monocyte-, macrophage-, eosinophil-like or granulocyte-like stages by the addition of certain substrates. A few examples for the different inducing agents are summarized in table 1.

Table 1: Inducers of HL60 differentiation (Collins, 1987; Collins et al., 1978; McCachren et al., 1986)

Induced cell type			
Monocytes	Macrophages	Granulocytes	Eosinophils
Vitamin D_3 Sodium butyrate Differentiating-inducing factor (DIF) Interferon-γ (IFN-γ) Tumor necrosis factor	Phorbol esters (TPA) Teleocidin	Dimethyl sulfoxide (DMSO) Retinoic acid Actinomycin D Dimethylformamide (DMF) Dibutyryl-cAMP	Alkaline media Butyric acid GM-CSF

Differentiation along the granulocyte- or neutrophil-like pathway is accompanied by a decrease in cell size, in the nuclear-to-cytoplasm ratio, in myeloperoxidase (MPO) activity, in the cytoplasmic basophilic properties and by an increase in nuclear segmentation in 90 – 95% of the cells. Alterations in gene and protein expression lead to a changed surface marker expression characteristic for mature granulocytes. This renders the HL60 cell line a useful model to study neutrophil functions (Birnie, 1988; Fleck et al., 2005). While the mechanism by which retinoic acid induces differentiation is well understood, the mode of action of DMSO is not precisely

known, but seems to involve changes in *c-myc* and *p53* expression, impairment of PKC signaling and increased calcium uptake (Tsiftsoglou et al., 2003). It is an important finding that different inducers mediate differentiation via variable signaling pathways and result into differentiated cells with slightly diverse properties (Carrigan et al., 2005; Sjögren et al., 2000). Additionally, numerous HL60 wild-type strains of different origin exhibit also variable characteristics and display in part varying susceptibilities toward the inducers (Fleck et al., 2005). All this makes a highly standardized protocol for the induction of differentiation of HL60 cells necessary. In the present study, 1.3% DMSO were used for induction of differentiation as previously described (Millius and Weiner, 2010). DMSO differentiated HL60 cells are well suited to study neutrophil chemotaxis and motility. After differentiation by DMSO the cells display high surface expression levels of different chemoattractant receptors for fMLP, LTB_4 and C5a, other complement receptors and different Fc receptors (Fleck et al., 2005; Jacob et al., 2002; Klinker et al., 1996). The cells also express the typical neutrophil cell surface receptors Mac-1, LFA-1 and L-selectin. In contrast, retinoic acid and dibutyryl-cAMP differentiated HL60 cells exhibit an only low Mac-1 surface expression and L-selectin expression is also diminished after differentiation with retinoic acid (Carrigan et al., 2005; Sjögren et al., 2000). Additionally, treatment with DMSO increases the percentage of cells, capable of phagocytosis from 5–10% to 85–90% (Collins et al., 1978). A previous study comparing DMSO differentiated HL60 cells with primary human neutrophils revealed high similarities between both cell types with regard to migration speed in chemotaxis and chemokinesis, G-protein coupled receptor, phosphatidylinositol (4,5)-bisphosphate 3-kinase (PI3K), Rho kinase and phosphatase 1/2A signaling pathways (Hauert et al., 2002). However, it is important to note that neutrophil-like HL60 cells are not identical with primary neutrophils. DMSO differentiated HL60 cells display differences in protein kinase C signaling pathways that are associated with a decreased phosphorylation of the mitogen-activated protein kinase (MAPK) and express only low levels of interleukin-8 (IL-8) receptors in comparison with primary neutrophils (Hauert et al., 2002). Furthermore, while differentiated HL60 cells contain primary azurophilic granules, secondary granules and secretory vesicles are completely absent and many proteins, localized normally inside those granules are not expressed (Johnston et al., 1992; Nordenfelt et al., 2009).

1.3 Cell migration

The ability of cells to perform migration is essential for a vast number of cellular processes including embryogenesis, wound healing, angiogenesis, nerve growth, hunting and killing of

bacteria for example by immune cells or *D. discoideum*. In contrast, improper cell migration can cause pathological conditions for example in cancer metastasis or inflammatory diseases as asthma or arthritis. In general, cell migration can be divided in either collective or single-cell movement in either 2D or 3D environments. Single cells can migrate using a mesenchymal migration mode that is defined by a strong adhesiveness mediated by focal adhesion and is characterized by proteolytic degradation of the surrounding matrix in 3D. This type of migration is typically detectable in fibroblasts, myoblasts, neural crest cells and different cancer cells from solid tumors. These cells exhibit a rather low migration speed (0.1 – 1 µm/min). In contrast, cells like *D. discoideum* and leukocytes, including neutrophils and dendritic cells display the amoeboid migration mode that is characterized by the lack of focal adhesions and stress fibers. These cells are rather poorly adhesive, migrate with considerably higher speed of approximately 10 µm/min and do not perform proteolytic remodeling of the surrounding matrix when migrating in 3D. However, it is important to note that this classification is rather arbitrary and still incomplete, and that single cells can definitely switch between the different modes of migration depending on different environmental conditions or cell properties (Friedl et al., 2001; Friedl and Wolf, 2010).

Both neutrophils and *D. discoideum* cells can migrate via pseudopodial amoeboid crawling. This cyclic process is characterized by the periodic protrusion of the cell front (pseudopodium) mediated by actin polymerization, contraction of the cell body and retraction of the cell's rear via an actomyosin driven motor (Bastounis et al., 2014; Cai and Devreotes, 2011). The cells can migrate either randomly or they can sense chemical cues in the environment and perform directed movement in a process called chemotaxis. During chemotactic migration, the gradient of an extracellular chemoattractant is detected by the cells and converted into an inhomogeneous intracellular signaling cascade that allows the establishment of cell polarity. Thereby, different cytoskeletal components and signaling molecules are recruited to either the anterior or the posterior of the cells, which allows migration in direction of the highest concentration of the chemoattractant (Cai and Devreotes, 2011). Either folic acid or cAMP can act as chemoattractant for *D. discoideum* cells depending on the life cycle phase, whereas a variety of different factors like fMLP secreted by bacteria, complement factor C5a, chemokines or growth factors can function as stimuli for neutrophil chemotaxis (Bagorda et al., 2006; Lämmermann and Germain, 2014). However, the underlying signaling pathways are surprisingly similar in *D. discoideum* and neutrophils (Devreotes and Zigmond, 1988; Jin et al., 2009). In both cases, chemotaxis is initiated by the binding of the respective chemoattractant to G-protein coupled receptors (GPCRs). GPCRs are a large seven-transmembrane receptors coupled to

G-proteins that consist of α-, β- and γ-subunits. Upon stimulation, the βγ-dimer dissociates from the α-subunit and both subunits can subsequently recruit and activate various downstream effectors (Bagorda et al., 2006). The GPCRs are thereby uniformly distributed in the plasma membrane indicating that the spatial distribution of the signaling pathways occurs downstream of the receptors (Servant et al., 1999; Xiao et al., 1997). These signaling pathways lead to the recruitment and activation of a variety of different downstream effectors, among them phosphatidylinositol (4,5)-bisphosphate 3-kinases (PI3Ks) and small GTPases. PI3Ks, that can be directly activated by the Gβγ complex, are translocated to the cell front and are responsible for the accumulation of phosphatidylinositol (3,4,5)-triphosphate (PIP_3). Simultaneous recruitment of the PIP_3 5-phosphatase PTEN, a PI3K antagonist, to the rear of the cell results in a locally restricted production of PIP_3 that reflects the external chemical gradient in neutrophils and *D. discoideum* (Bagorda et al., 2006; Parent, 2004). PIP_3, accumulated at the leading edge, can bind various downstream effector proteins for example via a pleckstrin homology (PH) domain. In *D. discoideum*, the PH-domain containing proteins CRAC (cytosolic regulator of adenylyl cyclase), PhdA (PH domain-containing protein A), Akt/PKB (protein kinase B) or Scar1, an adaptor protein related to the Wiskott-Aldrich syndrome protein (WASP) family in mammals are recruited to the leading edge (Cai and Devreotes, 2011; Friedl et al., 2001). These effector proteins are responsible for the induction of polarity and trigger actin polymerization (Cai and Devreotes, 2011). For example Scar1 can directly control the activity of the Arp2/3 complex that contributes to the nucleation of actin polymerization (Higgs and Pollard, 1999; Ura et al., 2012). Among the PIP_3 binding proteins identified, Akt/PKB was also found in neutrophils (Servant et al., 2000). Additionally, regulators of the small GTPases, for example the Rac-GEFs P-Rex (PIP_3-dependent Rac exchanger) or Vav-1, are recruited via PIP_3 (Kim et al., 2003; Welch et al., 2002). GEFs (guanine nucleotide-exchange factors) activate GTPases by mediating the release of GDP and thereby enabling the binding of GTP. The small GTPases Rac and Cdc42 are crucial for actin polymerization, formation and stabilization of a leading edge in neutrophils (Srinivasan et al., 2003). For example, Cdc42 interacts with WASP that in turn activates the Arp2/3 complex (Rohatgi et al., 1999). While no homologues for Cdc42 and Rho could be found in *D. discoideum*, 15 Rac homologues have been identified. The exact functions for all these Rac proteins are not entirely understood so far. However, RacB, RacC and Rac1 were already identified to play a role during directed cell movement (Chung et al., 2000; Han et al., 2006; Park et al., 2004). In both neutrophils and *D. discoideum*, alternative PI3K independent pathways, involving for example Ras proteins, target of rapamycin complex 2 (TORC2) or phospholipase A_2 (PLA_2) are present that are

also capable of signal transduction from the chemoattractant receptor to cytoskeletal components, again underlining the similarities between *D. discoideum* and neutrophil chemotaxis (Artemenko et al., 2014). In both cell types, the signaling pathways ultimately result in the regulation of actin polymerization and expansion at the leading edge. Besides the Arp2/3 complex, other homologous actin-binding proteins (ABPs) are predicted to be involved in the modulation of the actin network, as for example spectrin or filamin (Friedl et al., 2001).

Following the protrusion of the leading edge, the pseudopod then establishes a low adhesive interaction with the substrate. While adhesion in neutrophils is mostly mediated by ECM-binding integrins via outside-in signaling, no integrin homologs have been identified so far in *D. discoideum*. The exact mechanism of adhesion and the involved receptors in *D. discoideum* remain to be determined (Friedl et al., 2001).

The last step in chemotaxis, the contraction and retraction of the cell's rear, the so-called uropod, is mediated by myosin II filaments. While myosin II is located at the rear in *D. discoideum* and neutrophils, the signaling pathways that lead to myosin II assembly and contraction are distinct (Parent, 2004). In *D. discoideum* cells, either Akt/PKB or cGMP mediated signaling is responsible for myosin II contraction (Chung et al., 2001; Veltman et al., 2005). In contrast, uropod retraction in neutrophils is controlled by RhoA and its downstream effector ROCK (Rho-associated protein kinase) that leads to the phosphorylation and thereby activation of myosin II (Niggli, 1999; Xu et al., 2003).

Neutrophils and *D. discoideum* can also migrate in 3D environments. In their natural habitat, *D. discoideum* crawls in the soil and single cells also migrate within the multicellular organisms formed in the developmental phase. Neutrophils and of course other leukocytes have to transverse the interstitial tissue in order to arrive at the sites of injury or inflammation. Different leukocytes, like dendritic cells or T cells were shown to migrate in an integrin-independent manner in 3D. While the movement within a matrix is primarily driven by actin protrusion, myosin II contractility is here again important and functions in mediating squeezing of the cell through narrow gaps in the meshwork (Lämmermann et al., 2008; Woolf et al., 2007). In contrast, not many details are known about the mode of migration of *D. discoideum* cells in 3D. However, the cells can adopt a second type of amoeboid movement that involves membrane blebbing and seems to be prominent in 3D environments (Fackler and Grosse, 2008; Yoshida and Soldati, 2006). In general, blebs are rounded bulky protrusions of the plasma membrane that are used to extend the leading edge. The initial step in blebbing involves the local disruption of plasma membrane-cytoskeleton interactions and the subsequent protrusion of the membrane is either mediated by

the cells internal hydrostatic pressure or by actomyosin driven contractility. Notably, actin polymerization does not occur in this initial step, but it is necessary in the following steps to retain bleb expansion. Actomyosin contractility is responsible for bleb retraction (Charras and Paluch, 2008; Fackler and Grosse, 2008). Rac GTPases as RacB and RacE have been identified in *D. discoideum* to be involved in bleb formation (Lee et al., 2003; Zatulovskiy et al., 2014). The bleb driven migration mode in *D. discoideum* is also preferentially initiated under conditions of increased mechanical resistance and can occur in cooperation with pseudopods leading to the formation of hybrid structures called blebbopods (Tyson et al., 2014; Zatulovskiy et al., 2014). In some mammalian cells, blebbing can also occur and it is regulated by RhoA-ROCK-myosin and Rac GTPase signaling pathways (Fackler and Grosse, 2008). In mammalian systems, blebbing is of particular interest in the context of cancer cells as this mode of migration seems to support the invasive properties of a tumor cell (Sahai and Marshall, 2003; Wyckoff et al., 2006). While bleb driven migration was indeed also observed in neutrophils during migration in confined spaces, not much is known about the regulation and occurrence of blebs in leukocytes (Wilson et al., 2013).

1.4 Filamin proteins

Filamin (FLN) protein was first purified accidentally from rabbit macrophages in 1975 and displayed characteristic actin-binding properties (Hartwig and Stossel, 1975). Subsequently, FLN homologues were found in different cells of other vertebrates, as in chicken or guinea pig, in fibroblasts and platelets but also in muscle cells (Bechtel, 1979; Shizuta et al., 1976; Wallach et al., 1978; Wang et al., 1975). Additionally, various non-vertebrates as *Drosophila melanogaster*, *Entamoeba histolytica*, *Caenorhabditis elegans* or *D. discoideum* were also shown to contain FLN-like-proteins (John Condeelis, 1982; Kovacevic and Cram, 2010; Li et al., 1999; Sokol and Cooley, 1999; Vargas et al., 1996). In general, all FLNs display a similar structure (Figure 3). With exception of a *Drosophila* FLN isoform, they all contain an N-terminal actin-binding domain (ABD) that is highly similar to those of other actin-binding proteins (ABPs) including spectrin, α-actinin or dystrophin (Noegel et al., 1989). The ABD consists of two tandem calponin homology domains and encompasses ~250 amino acids (Stossel et al., 2001; van der Flier and Sonnenberg, 2001). The ABD is always followed by a flexible rod segment consisting of a varying number of repetitive repeats. Each repeat comprises approximately 96 amino acids that are arranged in seven β-strands that adopts an immunoglobulin-like (Ig-like) fold (Fucini et al., 1997b). The last of these so called Ig-like repeats always mediates dimerization, making FLN proteins to large

homodimers (Fucini et al., 1999; Fucini et al., 1997a). Human FLNs exhibit two additional hinge domains, located between repeats 15 and 16 (hinge 1, H1) and repeats 23 and 24 (hinge 2, H2) that are highly flexible and contain cleavage sites for the protease calpain (Nakamura et al., 2011; Popowicz et al., 2006).

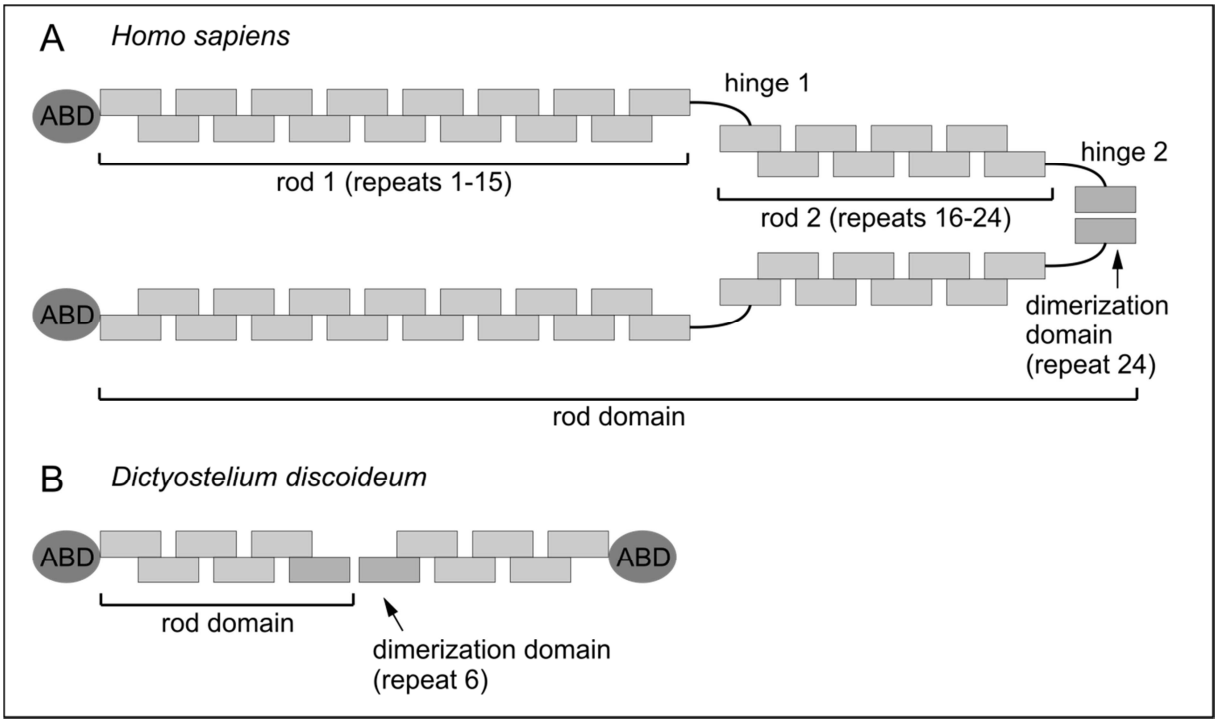

Figure 3: Schematic representation of the human and *Dictyostelium* FLN
Both FLN proteins have an N-terminal actin-binding domain (ABD) that is followed by a rod segment consisting of Ig-like repeats. The last Ig-like repeat mediates the homodimerization. A) Human FLN exhibit 24 Ig-like repeats. Two additional hinge domains subdivide the rod segment into rod 1 (repeats 1 to 15), rod 2 (repeats 16 to 23) and the dimerization domain repeat 24. B) *Dictyostelium* FLN contains six Ig-like repeats.

In human FLNs (huFLNs), the dimerization domain is similar to the other Ig-like repeats, whereas the *Dictyostelium* FLN (ddFLN) dimerization domain displays some differences in contrast to the other repeats. This results in differences in the dimerization interface which is strong and rigid in ddFLN, but considerable weaker and more flexible in huFLN (McCoy et al., 1999; Popowicz et al., 2006; Pudas et al., 2005). However, both huFLN and ddFLN are described as potent actin crosslinking proteins that promote high-angle branching of the actin filaments. The resulting orthogonal actin networks are characterized by a high elasticity and viscosity (Janssen et al., 1996; Niederman et al., 1983; Wolosewick and Condeelis, 1986). Furthermore, huFLNs either crosslink actin filaments in 3D networks or mediate the formation of actin bundles depending on their concentration (Tseng et al., 2004). Single Ig-like repeats from ddFLN and huFLN can reversibly unfold under force. It was proposed that the unfolding of the FLN protein may play a role in

mechanoprotection and may lead to dissociation or association of diverse binding partners from the protein (Furuike et al., 2001; Kolahi and Mofrad, 2008; Schwaiger et al., 2004; Schwaiger et al., 2005; Yamazaki et al., 2002).

1.4.1 Filamin in *D. discoideum*

DdFLN, the single FLN isoform in *D. discoideum*, was shown to localize to newly formed pseudopods during migration (Condeelis et al., 1988; Lemieux et al., 2014). A first ddFLN null mutant (HG1264) was generated by nitrosoguanidine-mutagenesis in 1990. Surprisingly, this mutant showed normal motile behavior, normal growth, normal actin filament assembly and in general a very subtle phenotype (Brink et al., 1990). The only prominent effect of the ddFLN deficiency was detected during the development, where ddFLN is required at the tip of the migrating slug to mediate properly oriented phototaxis (Fisher et al., 1997; Khaire et al., 2007). Although the exact mechanism by which ddFLN regulates phototaxis remains to be completely solved, the Ig-like repeats 2 to 6 were already identified as the crucial FLN domains involved in this process (Annesley et al., 2007). Furthermore, it was suggested that ddFLN acts as scaffold for a multi-protein signaling complex during phototaxis involving the proteins RasD, protein kinase B, the gelsolin-related protein 125 (GRP125) and the extracellular signal-regulated kinase 2 (ErkB) (Bandala-Sanchez et al., 2006). However, mutants deficient in other actin-binding proteins like α-actinin, severin, 34 kDa actin-bundling protein and cortexilin I and II displayed also no or only moderate phenotypes (Andre et al., 1989; Faix et al., 1996; Rivero et al., 1996a; Schleicher et al., 1988; Wallraff et al., 1986). In order to explain this apparent lack of functions of the different actin-binding proteins, a model of functional redundancy and thus the existence of a stabilizing network of different actin-binding proteins that guarantees major cellular functions were suggested. In line with this hypothesis, double mutants lacking α-actinin and ddFLN and triple mutants deficient in α-actinin, ddFLN and either 34 kDa actin-bundling protein or severin exhibited clearly more severe phenotypes that could be rescued by re-expression of only one of the proteins (Eichinger et al., 1996; Rivero et al., 1999; Rivero et al., 1996b; Schindl et al., 1995; Witke et al., 1992). A double knockout of ddFLN and α-actinin resulted in a decreased phagocytosis and disrupted motility. Re-expression of ddFLN was sufficient to rescue these defects (Rivero et al., 1996b). A previous study suggested a role for ddFLN in cytokinesis and an involvement of ddFLN in complex with Rac and the IQGAP-related protein GAPA in the regulation of actin remodeling (Mondal et al., 2010). Despite these findings, the exact role and function of ddFLN in particular during the vegetative state is not completely understood yet.

It is important to mention that simultaneously to the HG1264 cell line, another ddFLN null mutant (ABP-120$^-$) was generated by homologous recombination. This ddFLN null mutant displayed a more prominent phenotype with a severe locomotion defect (Cox et al., 1992; Cox et al., 1996). It was first suggested that these differences might be due to multiple, potential compensatory, genetic alterations in the HG1264 strain caused by the nitrosoguanidine treatment. However, it is more likely that the different *D. discoideum* parent strains, used for both ddFLN null mutants (AX2 for HG1264, AX4 for ABP-120$^-$) are the reason for the varying results. A ddFLN null strain in an AX2 background was subsequently generated by homologous recombination and verified the subtle phenotype of the primary HG1264 strain (Eichinger et al., 1996; Rivero et al., 1999; Rivero et al., 1996b).

1.4.2 Human filamins

The human FLN family consists of three isoforms: FLNa, FLNb and FLNc. FLNa and FLNb are both ubiquitously expressed with FLNa as the most abundant and also, so far, best studied isoform (Stossel et al., 2001). Expression of FLNc is restricted largely to skeletal and cardiac muscle. However, evidences of low FLNc expressions in some non-muscle cells arose (Baldassarre et al., 2009; Feng and Walsh, 2004). The three FLN isoforms share a high sequence similarity (amino acid identity of 70%) with only slightly higher divergence at the hinge domains (amino acid identity of 45%). Additionally, FLNc exhibits an unique 82-amino-acid insertion within the Ig-like repeat 20. As the FLN isoforms show overlapping expression patterns, it might be possible that they execute similar functions or are able to compensate for each other (Kesner et al., 2010; Zhou et al., 2010).

1.4.2.1 Filamin interaction partners

The first identified and most important interaction partner for FLNs was actin and FLNs are in general described as F-actin crosslinker. The crosslinking properties of FLNs are the result of their homodimeric structure. In addition to the N-terminal ABD, a second actin-binding domain lies within the repeats 9 to 15 of the FLN protein and is necessary for high avidity binding. The flexibility of the repeats 1 to 8 provides the repeats 9 to 15 with the required mobility to find the proper alignment on the actin filament (Figure 4). The repeats 16 to 24 are not involved in F-actin binding (Nakamura et al., 2007). Calmodulin binds Ca^{2+}-dependent to the N-terminal ABD and thereby dissociates FLN from the actin filament (Nakamura et al., 2005).

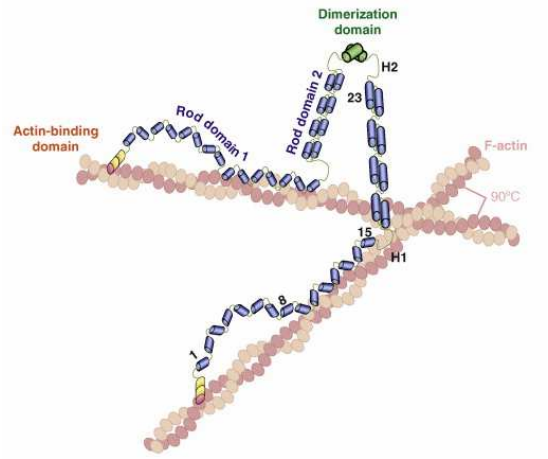

Figure 4: FLN binding to F-actin
The N-terminal ABD and the second ABD within the repeats 9 to 15 interact with filamentous actin. The repeats 1 to 8 allow the proper alignment of the second ABD on the filament, whereas the repeats 16 to 24 are not involved. The dimeric structure enables the orthogonal branching. Picture taken from Zhou et al. (2010).

Besides F-actin binding, FLNs are described to interact with about 90 different proteins including transmembrane receptors, signal molecules and transcription factors. Most of the interactions are mediated by the repeats 16 to 24, the domain of the FLN protein not involved in F-actin binding (Zhou et al., 2010). A few examples for FLN interaction partners and the FLN repeats they bind to are assembled in table 2.

Table 2: FLN interaction partners

Binding partner	Binding site on FLN	Reference
Transmembrane proteins		
CaR extracellular Ca^{2+} receptor	Repeats 14–16	Awata et al. (2001)
Dopamine D2 receptor	Repeats 16–19	Li et al. (2000)
FcγRI	Not known	Ohta et al. (1991)
ICAM-1	Repeats 19–24	Kanters et al. (2008)
β1A, β1D, β2, β3, β7 integrins	Repeat 21	Kiema et al. (2006), Calderwood et al. (2000)
Signaling proteins		
FilGAP	Repeat 23	Ohta et al. (2006)
Protein kinase Cα	Repeats 1–4, hinge2 to repeat 24	Tigges et al. (2003)
SEK1 (MEKK, JNKK)	Repeats 22–23	Marti et al. (1997)
RalA, RhoA, Rac1, Cdc42	Repeat 23–24	Ohta et al. (1999)
ROCK	Repeat 24	Ueda et al. (2003)
Trio	Repeat 23	Bellanger et al. (2000)
Vav	Not known	Del Valle-Perez et al. (2010)
Cytoskeletal and cytoskeleton-associated proteins		
Migfilin	Repeat 21	Ithychanda et al. (2009)
Myotilin	Repeats 19–21	van der Ven et al. (2000)
Supervillin	Repeats 8–10, 20–22	Smith et al. (2010)
Vimentin	Repeats 1–8	Kim et al. (2010)
Transcription factors and nuclear proteins		
BRCA-2	Repeats 21–24	Yuan and Shen (2001)
PEBP2β/CBFβ	Hinge 2 and repeat 24	Yoshida et al. (2005)
SMAD2, SMAD5	Not known	Sasaki et al. (2001)

One of the best studied interactions is the binding of FLN to the cytoplasmic tail of the integrin β chain. FLN repeat 21 was identified to be responsible for this interaction. The FLN interaction site at the cytoplasmic tail of the integrin β chain overlaps with the binding site of another integrin regulating actin-binding protein, talin. FLN and talin compete with each other for integrin binding. While talin acts as activator and facilitates integrin-ICAM-1 binding, FLN inhibits integrin functions. It was shown that an increased binding of FLN to integrin results in a diminished cell migration (Calderwood et al., 2001; Kiema et al., 2006). However, the FLN mediated inhibition of integrins depends on a complex network of different regulation modes. Application of mechanical force and/or phosphorylation of the FLN protein on Ser2152 results in unfolding of FLN repeats and subsequent exposure of the integrin-binding site (Chen et al., 2009). In contrast, phosphorylation of the integrin β_2 cytoplasmic tail on Thr758 prevents FLN binding (Takala et al., 2008). Furthermore, migfilin, another cytoplasmic protein, binds FLN at the same site as the cytoplasmic β integrin tail, dissociates FLN from the integrin and acts thereby as integrin activator (Das et al., 2011; Ithychanda et al., 2009; Lad et al., 2008).

As a consequence of this large number of different interactions, FLNs act as scaffold for a number of signaling pathways and are involved in a variety of cellular processes, including cell differentiation, morphogenesis, transcription regulation, cell adhesion and motility (Razinia et al., 2012; Zhou et al., 2010). Null or specific missense mutations in the different FLN isoforms cause a wide range of human disorders, thereby reflecting the versatile functions of these proteins. For example, loss-of-function mutations in FLNa are associated with periventricular nodular heterotopia (PVHD), a brain malformation characterized by disrupted neuronal migration. In contrast, a second set of human disorders, mediated by FLNa mutations, the otopalatodigital (OPD) spectrum disorders are caused by clustered missense mutations that seem to mediate a change in FLNa functions. OPD disorders are characterized by congenital malformations including skeletal dysplasia, central nervous defects and anomalies regarding the craniofacial, cardiac, genitourinary and intestinal system (Robertson, 2005). In general, mutations in FLNb are responsible for disruptions in bone morphogenesis. However, as in the case of FLNa, different FLNb mutations result in diverse phenotypes and a variety of different disorders including spondylocarpotarsal syndrome (SCT), Larsen syndrome (LS) or atelosteogenesis I and III (AOI and AOIII) (Feng and Walsh, 2004).

1.4.2.2 Filamins in cell motility

Previous studies describe an important role for FLNs in adhesion, spreading and cell migration. However, their exact functions in these processes remain unclear and seem to be highly cell-type dependent. Fittingly, FLNs were shown to co-localize with F-actin networks at the plasma membrane and were found at the leading edge of migrating cells (Stossel et al., 2001). FLNa was recruited to cell extensions during early spreading and application of mechanical force led to accumulation of FLNa at adhesion sites in human gingival fibroblasts (Glogauer et al., 1998; Kim et al., 2008). A first indication of a role for FLNa in migration arose from the analysis of the FLNa deficient human melanoma cell line M2, revealing a markedly impaired locomotion and reduced stiffness and contractility of the cells that resulted in extensive membrane blebbing (Cunningham et al., 1992; Kasza et al., 2009). Loss of FLNa function in human brain resulted in diminished long-range directed neuronal migration within the cerebral cortex associated with PVHD (Fox et al., 1998). Additionally, depletion of FLN expression also led to an impaired spreading and initiation of migration in human fibrosarcoma cells (Baldassarre et al., 2009). Lack of FLNb in endothelial cells resulted in a decreased cell migration capacity (Del Valle-Perez et al., 2010). FLNa and FLNb deficiencies in mouse embryonic fibroblasts as well as FLNa knockdown in human kidney cells caused disrupted cell spreading (Kim et al., 2008; Lynch et al., 2011). While FLN deficiencies clearly interfere with motility in different cell types, also excess of FLN protein can affect motility. For example overexpression of FLNa in mouse cortical neurons led to a diminished migration (Sarkisian et al., 2006). Moreover, increased binding of FLNa to the cytoplasmic chains of β integrins in Chinese hamster ovary and Jurkat cells was associated with a migration defect due to its above-mentioned inhibitory function in integrin regulation (Calderwood et al., 2001).

Despite these findings, not much is known about the role of FLN proteins during neutrophil migration. One previous study with primary neutrophils of transgenic conditional FLNa knock-out mice indicated a role of FLNa in RhoA dependent regulation of myosin II activation. FLNa deficient neutrophils exhibited lower levels of activated myosin II that was associated with a tail retraction effect. Consequently, these cells were characterized by a decrease in speed in 2D migration and an increase in adhesion (Sun et al., 2013).

1.5 Goals of this project

D. discoideum and neutrophils are both highly motile cell types that share a number of similarities with regard to signaling mechanisms during cell motility. However, the role of FLN proteins in *D. discoideum* migration and in neutrophil motility, in particular in the human system remains rather unclear. The main goal of this thesis was to gain insight into the role of FLN proteins in *D. discoideum* and neutrophils.

Analysis of the function of ddFLN was hindered by the fact that the ddFLN null mutant displayed a very subtle phenotype. It was hypothesized that this was not due to a lack of ddFLN functions, but due to the presence of a network of actin-binding proteins that execute redundant functions and can compensate for each other. To overcome this problem, a ddFLN overexpressing strain and a strain expressing a truncated ddFLN protein should be examined in addition to the ddFLN null mutant. Additionally, in previous studies migration was often studied in simple, rather artificial assays where the cells crawl on a flat surface in buffer. Therefore, the different *D. discoideum* strains should be analyzed using varying migration assays. In order to be able to study ddFLN functions also in 3D migration, the aim was to establish a new 3D migration assay for *D. discoideum.*

The second and main project revolved about the role of FLNs in human neutrophils. Hence, the human promyelocytic leukemia cell line HL60 that can be induced into a neutrophil-like state was employed. The first goal was to characterize the expression and localization of the different human FLN isoforms including putative binding partners in these cells. The second aim was to assess the role of human FLNa in the neutrophil-like HL60 cells in detail with the help of a shRNA mediated knockdown. Therefore, the FLNa deficient cells should be analyzed using various migration, adhesion, spreading and phagocytosis assays.

2 Materials and Methods

2.1 Materials

2.1.1 Instruments

AEKTA purifier 100	Amershan Biosciences
Balances	Sartorius
BioDocAnalyzes	Biometra
Certomat BS-T shaker	Satorius
CO_2 Incubator BBD 6220	Heraeus
Fluorescence Spectrometer LS55	Perkin Elmer
Gene pulse electroporator Xcell	BioRad
Gelsystem MiniPROTEAN	BioRad
HeraCell Incubator	Thermo Scientific
NEPA21 electroporator	Nepa Gene
PCR-Thermocycler Tpersonal	Biometra
PCR UNO Thermocycler	Biometra
pH-meter pH720	Inolab WTW series
Power supplies	BioRad, Biometra, Consort
Protein Transfer TF 77XP	Serva
Shaker Orbital Incubator SI500	Stuart
Shaking incubator with temperature control	Memmert
Shakers for *Dictyostelium* cultures	Kühner
Sonificator Sonifier250	Banson
Thermomixer	Eppendorf
Tabletop Film Processor Curix 60	Agfa
Vortex Genie 2	Bender & Hobein

Microscopes

Axiovert 25	Carl Zeiss
Axiovert 200M	Carl Zeiss
LSM 510 Meta confocal microscope	Carl Zeiss

Objectives

5x A-plan 0.12 Ph1	Carl Zeiss
10x A-plan 0.25 Ph1	Carl Zeiss
40x Neofluar 0.75 Ph2	Carl Zeiss
100x Neofluar 1.3 oil immersion Ph3	Carl Zeiss
63x Neofluar 1.4 oil immersion objective	Carl Zeiss
100x Neofluar 1.3 oil immersion objective	Carl Zeiss

Centrifuges

J6-HC	Beckman
Microcentrifuge 5415 D, 5417 R	Eppendorf
Microcentrifuge Mikro 200	Hettich
Optima TL ultracentrifuge	Beckman
Optima MAX-XP ultracentrifuge	Beckman

Rotors

JA-10	Beckman
TLA 100.3	Beckman

2.1.2 Computer programs

Adobe Acrobat Pro Extended	Adobe Systems
Adobe Illustrator CS2	Adobe Systems
ApE plasmid editor v1.10.4	M. Wayne Davis
AxioVision	Carl Zeiss
BioDoc Analyze	Biometra
ClustalX2	Des Higgins
CorelDraw 12	Corel Corporation
EndNote X7	Thomas Reuter
ImageJ 1.44p	Wayne Rasband
Imaris 7.6.5.	Bitplane
Microsoft Office	Microsoft Corporation
SigmaBlot 2000	SPSS Inc.
Zen	Carl Zeiss

2.1.3 Laboratory consumables

1.5 ml centrifuge tubes	Sarstedt
Amershan Hyperfilm ECL	GE Healthcare
Cell culture flasks with filter cap	Nunc
Cell culture plates, 24 wells	Starlab Int.
Cell culture plates, 96 wells	Nunc
Cell culture dishes, Ø 100 mm x 20 mm	Greiner bio-one
Dialysis tubings Type 8	Biomol
DNA Isolation Kit for Tissue and Cells	Roche
Gel-blotting paper 3MM Chr	Whatman
GFP-Nano-Trap	Chromotek
High Pure Plasmid Isolation Kit	Roche
High Pure PCR Product Purification Kit	Roche
High precision cuvettes 10 mm	Helma
Electroporation cuvette 2 mm, 4 mm	Eurogentec
µ-Slide Chemotaxis^{3D}	IBIDI
Nitrocellulose transfer membrane Protran	Whatman
NucleoSpin Gel and PCR Clean-up Kit	Macherey Nagel
PCR tubes Thermo Tube 0.2 ml	Peqlab
Phusion High-Fidelity DNA Polymerase	New England Biolabs
Petri dishes Ø 92 mm x 16 mm	Sarstedt
Pipettes 10 ml, 20 ml	Sartstedt
Pipet tips	Biozym, Gilson, Starlab
Plasmid DNA Purification Maxi Kit	Macherey Nagel
PureLink RNA Mini Kit	Life Technologies
Restriction Enzymes	New England Biolabs
Sterile filter, Filtropur S 0.2, S 0.45	Sartstedt
T4 DNA Ligation Kit	New England Biolabs
Transcriptor High Fidelity cDNA Synthesis Kit	Roche
Tubes 15 ml, 20 ml	Sarstedt
Ultracentrifuge tubes 1.5 ml	Beckman
YG-latex beads Ø 1 µm, 4.5 µm	Polysciences

2.1.4 Reagents

Standard laboratory chemicals were mainly purchased from Biomol, Biorad, Fluka, Invitrogen, Merck, Peqlab, Roche, Roth, Serva or Sigma-Aldrich and had the degree of purity 'p.a.' unless otherwise mentioned. Media and buffers used in this study were prepared with de-ionized water (Millipore), sterilized either by autoclaving or passing through a micro-filter (pore size 0.2 µm).

2.1.5 Antibodies

Primary antibodies

Actin, human	Polyclonal	Santa Cruz Biotechnologies
Calreticulin, *D. discoideum* (252-234-2)	Monoclonal	Müller-Taubenberger et al. (2001)
Coronin 1A, human	Monoclonal	Santa Cruz Biotechnologies
Filamin A, human (9-42)	Polyclonal	Present study
Filamin B, human (18-2)	Polyclonal	Present study
Filamin rod domain, *D. discoideum* (82-471-14)	Monoclonal	Brink et al. (1990)
Filamin ABD, *D. discoideum* (82-421-5)	Monoclonal	Brink et al. (1990)
GFP (K3-184-2)	Monoclonal	Noegel et al. (2004)
GST (268-44-6)	Monoclonal	Faix et al. (1998)
Phospho-myosin light chain (Ser19)	Polyclonal	Cell Signaling
Tubulin (YL ½)	Monoclonal	Wehland and Willingham (1983)

Secondary antibodies

Goat-anti-rabbit IgG Alexa488-, Cy3-, Alexa633-conjugated	Invitrogen
Goat-anti-mouse IgG Cy3-conjugated	Invitrogen
Anti-mouse, -rabbit, -rat IgG horseradish peroxidase-linked (ECL)	GE Healthcare

2.1.6 Vectors

Constructs used in this study

p1ABsr8 ddFLN-GFP	Khaire et al. (2007)
pDEX-GFP-ddFLN(rod1-6)	Khaire et al. (2007)
pREP4-FLNa	Fumihiko Nakamura
pBluescript-FLNb	Fumihiko Nakamura

pFastBac1	Invitrogen
pEGFP-C1	Clontech
pGEX-6P-1	GE Healthcare
pKLO.1 FLNa shRNA (number 28, 29, 30, 31, 32)	Sigma

Constructs generated in this study

pFastBac1 FLAG-FLNa full length	NotI/XbaI
pFastBac1 FLAG-FLNa(ABD-8)	EcoRI/KpnI
pFastBac1 FLAG-FLNa(9-18)	EcoRI/SalI
pFastBac1 FLAG-FLNa(19-24)	BamHI/HindIII
pEGFP-C1 FLNa (aa 21 to 2160)	SalI/SacII
pGEX-6P-1 FLNa(H2+24)	BamHI
pGEX-6P-1 FLNb(H2+24)	BamHI/SalI
pGEX-6P-1 FLNb(H1)	BamHI/SalI
pGEX-6P-1 FLNb(H1+)	BamHI/SalI
pGEX-6P-1 FLNa(H1+)	BamHI/SalI
pGEX-6P-1 coronin 1A full length	BamHI/SalI

2.1.7 Bacterial strains

E. coli DH5α	Invitrogen
E. coli DH10Bac	Invitrogen
E. coli BL21 RIL	Stratagene
E. coli ArcticExpress RIL	Stratagene
E. coli B/r GFP	Günther Gerisch
E. coli DH10Bac FLAG-FLNa full-length	Present study
E. coli DH10Bac FLAG-FLNa(ABD-8)	Present study
E. coli DH10Bac FLAG-FLNa(9-18)	Present study
E. coli DH10Bac FLAG-FLNa(19-24)	Present study
Klebsiella aerogenes	

2.1.8 *D. discoideum* strains

Strain	Resistance	Source
AX2 (laboratory wild-type)	-	
AX2 ddFLN null mutant (HG1264)	-	Brink et al. (1990)
AX2 ddFLN-GFP	B 10	Present study
AX2 GFP-ddFLN(rod1-6)	G 10	Present study

2.1.9 HL60 strains

Strain	Resistance	Source
HL60 wild-type	-	ATCC
HL60 FLNa shRNA 28 – 32	puromycin (1µg/ml)	Present study
HL60 FLNa KD shRNA 28 subclone C4	puromycin (1µg/ml)	Present study
HL60 FLNa KD shRNA 28 subclone G4	puromycin (1µg/ml)	Present study

2.2 Methods

2.2.1 Molecular methods

Standard molecular biology protocols were performed to generate various GFP-, GST- and FLAG-tagged protein constructs. Total RNA of undifferentiated and differentiated HL60 cells was isolated with the help of PureLink RNA Mini Kit (Life Technologies) and subsequently converted to cDNA using Transcriptor High-Fidelity cDNA Synthesis Kit (Roche). Phusion High-Fidelity DNA Polymerase (New England Biolabs) was used for polymerase chain reactions (PCRs) according to manufacturer's instructions. PCR products were purified with NucleoSpin Gel and PCR Clean-up Kit (Macherey Nagel), and were cloned into expression vectors using standard restriction enzyme mediated cloning. Plasmid DNA was obtained from *E. coli* shaking cultures using either standard alkaline lysis miniprep or silica-based mini- and maxiprep kits (Roche, Macherey Nagel). Chemically competent *E. coli* cells were prepared according to the $CaCl_2$ method (Dagert and Ehrlich, 1979). The accuracy of the DNA sequences inserted in the respective expression vectors was verified by sequencing using specific primers (Eurofins MWG Operon, Ebersberg).

2.2.2 Biochemical methods

2.2.2.1 Generation of cell lysates

Due to the high susceptibility of ddFLN to partial degradation, *D. discoideum* cells were directly lysed in a urea sample buffer (10% SDS, 9 M urea, 5% 2-mercaptoethanol) (20 µl per 1 x 10^6 cells) and heated at 70°C for 2 minutes.

HL60 cells were lysed in 3x SDS sample buffer (20 µl per 1 x 10^6 cells) and heated at 95°C for 5 minutes. For analysis of levels of phospho-myosin light chain (pMLC), differentiated HL60 cells were first suspended in adhesion buffer (20 mM HEPES, pH 7.4, 150 mM NaCl, 5.5 mM glucose, 1.2 mM $CaCl_2$, 1 mM $MgCl_2$, 0.25% BSA) (Hepper et al., 2012) and then stimulated with 100 nM fMLP for 10 minutes at 37°C. Immediately before and after stimulation with fMLP, cells were lysed in 3x SDS sample buffer (50 µl per 4 x 10^6 cells) and heated at 95°C for 5 minutes.

2.2.2.2 SDS polyacrylamide gel electrophoresis, protein staining and Western blotting

Protein mixtures were separated by standard discontinuous SDS-PAGE (Laemmli, 1970). Proteins were either stained directly in the gel using Coomassie Brilliant Blue R 250 or, for mass spectrometry analysis, with Roti®-Blue quick staining solution. For the detection of proteins in the low nanogram range, high sensitive silver staining was performed. Therefore, the gels were first incubated in fixing solution (40% ethanol, 10% acetate) for a minimum of 30 minutes and subsequently transferred to sensitizing solution (30% ethanol, 0.2% $Na_2S_2O_3$, 0.83 M $C_2H_3NaO_2$, 0.125% freshly added glutaraldehyde) for 30 minutes. Gels were washed three times in ddH_2O (5 minutes each) and stained in silver solution (0.25% $AgNO_3$, 0.015% freshly added formaldehyde) for another 30 minutes. After three additional washing steps in ddH_2O (1 minute each) the gels were exposed to developing solution (23.5 mM Na_2CO_3, 0.015% freshly added formaldehyde) until the desired grade of staining intensity was reached. The reaction was stopped by addition of aqueous EDTA solution.

Alternatively, proteins were transferred onto a nitrocellulose membrane using semi-dry Western blotting in a transfer buffer (25 mM Tris, pH 8.5, 190 mM glycine, 20% methanol, 0.02% SDS). Membranes were blocked in nonfat milk powder in NCP buffer (10 mM Tris, pH 7.3, 150 mM NaCl, 0.05% Tween20) followed by incubation with the appropriate primary and secondary antibodies and subsequent development using Enhanced Chemiluminescence System (ECL). Bands were quantified with the help of ImageJ software (U.S. National Institutes of Health).

2.2.2.3 GST-tagged protein expression in bacteria and purification

For the expression of proteins with an N-terminal GST-tag, respective DNA sequences were cloned into pGEX vector and transformed in BL21 RIL or ArcticExpress RIL *E. coli* strains. Bacteria were grown as shaking cultures in LB medium containing the particular antibiotics overnight at 37°C. Cultures were then diluted 1:20 and grown at 37°C to an OD_{600} of 0.4–0.8. Protein expression was induced by addition of 1 mM IPTG and cells were grown at 37°C for 3 hours or at 16°C overnight. The bacteria were pelleted and resuspended in PBS (137 mM NaCl, 2.7 mM KCl, 8.1 mM Na_2HPO_4, 1.5 mM KH_2PO_4, pH 7.4) containing 1 mM DTT and Complete Protease Inhibitor cocktail (Roche). The cells were opened using sonification and the lysates were centrifuged at 50,000 g for 10 minutes at 6°C. The supernatant was then incubated with Glutathione Sepharose resin B4 (Sigma-Aldrich) for 2–3 hours at 4°C by gentle head over head rotation. The matrix was washed with 10–20 column volumes of PBS containing protease inhibitor and either kept on ice for subsequent protein interaction pull-down experiments or eluted in PBS containing 1 mM DTT and 25 mM reduced glutathione. The purity and functionality of the proteins were analyzed by SDS-PAGE and Coomassie Blue staining.

2.2.2.4 FLAG-tagged protein expression using the baculovirus system

As human FLN protein exhibits a relative high molecular weight (280 kDa), expression of this protein would be difficult in prokaryotic systems. Therefore, full-length FLNa and truncated FLNa proteins were expressed using the eukaryotic Bac-To-Bac baculovirus expression system. Initially, the sequence of interest was cloned with an N-terminal FLAG-tag in the pFastBac1 vector and then transformed in DH10Bac cells. The DH10Bac cells contain a virus shuttle vector (bacimd) and a helper plasmid encoding certain transposition proteins that support the transfer of the sequence of interest into the bacmid via site specific transposition. Successful recombination was verified via blue/white screening. Bacmid DNA was isolated using standard miniprep and was transfected in immortalized insect Sf9 cells. For the transfection, 30–50 µg bacmid DNA was mixed with 200 µl Sf-900 II SFM medium (Invitrogen) and 10 µl Cellfectin (Invitrogen). After incubation for 30 minutes at room temperature, the mix was added to 2 ml cells that were plated at a density of 0.5 x 10^6 cells/ml in a 6-well plate. The transfection mix was removed after an incubation of 5 hours at 28°C and the cells were subsequent cultured in Sf-900 II SFM medium supplemented with 5% fetal bovine serum and gentamycin (0.1 mg/ml) at 28°C for 72 hours. The P_0 virus-containing supernatant was then harvested, sterile-filtered and either stored at 4°C or used for amplification by generating P_1 and P_2 generations. For

protein expression, > 97% viable Sf9 cells were infected at a density of 2 x 10^6 cells/ml with the respective P_2 virus at a ratio of about 1/25 (2 ml P_2 virus and 48 ml cells). Cells were incubated as a shaking culture at 100 rpm and 28°C for 48 hours and harvested by centrifugation (2,000 g, 15 minutes, 4°C). After lysis of the cells in lysis buffer (150 mM NaCl, 50 mM Tris-HCl, pH 7.4, 1 mM EDTA, 1% Triton-X-100 and one Complete Protease Inhibitor cocktail tablet (Roche) per 50 ml buffer), lysates were centrifuged at 30,000 g at 4°C for 10 min. Supernatants were then incubated with anti-FLAG M2 affinity gel (Sigma-Aldrich) (100 µl resin for lysates of a 50 ml culture) for 90 min by gentle head over head rotation at 4°C. The matrix was washed three times in washing buffer (150 mM NaCl, 50 mM Tris-HCl, pH 7.4 and one Complete Protease Inhibitor cocktail tablet (Roche) per 50 ml buffer) and either stored at 4°C for subsequent protein interaction pull-down experiments or eluted by incubation of the matrix with elution buffer (0.5 mg/ml FLAG peptides in washing buffer) for 1 hour at 4°C under slight agitation. The eluate was collected by centrifugation and the concentration of the protein was determined with the help of SDS-PAGE. The protein was then either used in subsequent experiments or frozen in liquid nitrogen and stored at –80°C.

2.2.2.5 Pull-down assays and immunoprecipitation

For the identification of interaction partners in HL60 cells, GST-coronin 1A, FLAG-tagged full-length FLNa protein or truncated FLAG-tagged FLNa proteins bound to the respective matrix was employed. 3 x 10^8 differentiated HL60 cells were allowed to adhere on fibrinogen (100 µg/ml) coated Petri dishes in adhesion buffer (1 x 10^7 cells per one dish) and were stimulated with 100 nM fMLP and 1 mM $MnCl_2$ for 10 minutes at 37°C. Adherent cells were directly lysed by addition of 300 µl lysis buffer (150 mM NaCl, 50 mM Tric-HCl, pH 7.4, 1 mM EDTA, 1% Triton-X-100 and one Complete Protease Inhibitor cocktail tablet (Roche) per 50 ml buffer) to each Petri dish and centrifuged at 16,000 g for 20 minutes at 4°C in a benchtop centrifuge. The supernatant was used for incubation with the various recombinant proteins bound to the respective matrix for 3 hours at 4°C by gentle head over head rotation. The matrix was washed four times with washing buffer (150 mM NaCl, 50 mM Tris-HCl, pH 7.4 and one Complete Protease Inhibitor cocktail tablet (Roche) per 50 ml buffer) in order to reduce unspecific protein binding. By incubation of the matrix for 1 hour at 4°C in the respective elution buffer recombinant proteins and potential bound interaction partners were gently eluted from the matrix. The eluate was precipitated using 50% ice cold trichloroacetic acid for 30 minutes on ice, separated by SDS-PAGE and stained with either Roti®-Blue quick staining solution (Roth), Coomassie Blue or was

analyzed by Western blotting. Bands of interest were cut out from the gel and analyzed by MALDI-TOF mass spectrometry (ZfP, LMU Munich).

Alternatively, co-immunoprecipitations were performed with anti-FLNa antibodies. Therefore, lysates of differentiated adherent HL60 cells were generated as described above using following lysis buffer: 25 mM Tris-HCl, pH 7.5, 150 mM NaCl, 0.5 mM EDTA, 1 mM DTT, 1% Triton-X-100, 1% Na-deoxycholate, 10 mM NaF, 250 µM Na-orthovanadate and one Complete Protease Inhibitor cocktail tablet (Roche) per 50 ml buffer. Supernatant was then incubated with 60 µl anti-FLNa antibody or 10 µg of a random antibody (e.g. anti-EB1 antibody) as a control for 1 hour at 4°C by gentle head over head rotation. Afterwards, 100 µl of protein A Sepharose CL-4B (GE Healthcare), which had been previously blocked in 0.1% BSA for 2 hours, were added to the solution and the suspension was rotated for another hour at 4°C. The matrix was washed four times in lysis buffer before the proteins were eluted with the help of a pH shift using 1 M Glycin, pH 2.7. A solution of 1 M Tris-HCl pH 8.0 was used for neutralization. The eluates were collected; precipitated using 50% ice cold trichloroacetic acid for 30 minutes on ice and subsequently analyzed as described above.

For the identification of proteins interacting with ddFLN in *D. discoideum* cells, GFP-Nano-Trap technique (Chromotek) was used. 5 x 10^7 – 1 x 10^8 cells expressing a recombinant GFP-tagged ddFLN protein were harvested and suspended in homogenization buffer (30 mM Tris-HCl, pH 7.4, 2 mM DTT, 2 mM EDTA, 4 mM EGTA, 5 mM benzamidin, 0.5 mM PMSF, 30% sucrose and one Complete Protease Inhibitor cocktail tablet (Roche) per 10 ml buffer). The cells were pushed through a 0.8 µm nucleopore filter (Whatman) and were centrifuged for 20 minutes at 10,000 g at 4°C. 20 µl GFP-Trap agarose beads were equilibrated in homogenization buffer and incubated with the supernatant for one hour at 4°C by rotation. The beads were subsequently washed according to the manufacturer's instructions and the recombinant GFP-tagged proteins with potential bound interaction partners were eluted by boiling in 3x SDS sample buffer. Proteins were separated by SDS-PAGE and analyzed by Western blotting.

2.2.2.6 Gel filtration using the AEKTA 100 system

For protein size analysis and interaction studies, the gel filtration column superose 6 10/300 GL (GE Healthcare) was used. The column was equilibrated with IEDANBP buffer (10 mM imidazole, 1 mM EGTA, 1 mM DTT, 0.02% NaN_3, 50 mM NaCl, 1 mM benzamidine, 1 mM PMSF; pH 7.3) and the flow rate was set between 0.1–0.5 ml/min. The column was calibrated with the help of protein molecular weight standards range 12.4–450 kDa (Serva). Usually 200 µg purified protein

was injected, 0.5 ml-fractions were collected and analyzed using SDS-PAGE followed by silver staining or Western blotting.

2.2.2.7 Generation of FLNa and FLNb specific antibodies

For antibody generation, suitable domains of FLNa (hinge 2 domain and repeat 24, amino acids 2517 to 2648) and of FLNb (hinge 1 domain and adjacent regions, amino acids 1691 to 1749) were expressed and purified as GST-tagged proteins in bacteria (GST-FLNa(H2+24) and GST-FLNb(H1)). 200 µg of purified GST-tagged protein was mixed with Freud´s adjuvant 100 (Gerbu Biotechnik) and injected subcutaneously in New Zealand white rabbits. Four immunizations were performed at an interval of four weeks. Blood samples were received ten days after the immunization, respectively. Sera were generated by centrifugation of the blood (4,200 g, 10 minutes) and were subsequently tested in Western blot analysis.

The specificity of the antibodies was examined using the respective regions of FLNa and FLNb that were expressed as GST-tagged proteins. The antibodies were originally raised against GST-tagged proteins implying that also antibodies recognizing GST were present in the sera. Therefore, GST-tags were cut off by digestion of the proteins with PreScission Protease (PSP) for 6 hours at 4°C. Resulting fragments were subsequently analyzed by SDS-PAGE, Coomassie Blue staining and Western blotting.

2.2.2.8 Confocal microscopy

Confocal microscopy data were acquired on an inverted Axiovert LSM 510 Meta confocal microscope (Zeiss) with 63x or 100x oil immersion objectives with a numerical aperture of 1.4 and 1.3, respectively. Excitation of fluorophores was achieved with the 488 nm argon ion laser line, the 543 nm and 633 nm helium neon laser lines, and emission was collected using 505 – 530 nm band-pass, 475 nm long-pass, 585 – 615 nm band-pass or 650 nm long-pass filters.

2.2.3 Cell biological methods

2.2.3.1 *D. discoideum*

2.2.3.1.1 Cell culture and transformations

D. discoideum AX2 (laboratory wild-type strain) and mutant strains derived from AX2 were cultured axenically in HL5 medium (Formedium) either in cell culture dishes, in shaking cultures at 150 rpm or on lawns of *K. aerogenes*. For long-term storage, spores were obtained from phosphate agar plates, frozen in Soerensen buffer pH 6.0 (14.6 mM KH_2PO4, 2 mM Na_2HPO_4)

and stored at –80°C. In order to induce starvation, cells were washed trice in Soerensen buffer and were incubated in Soerensen buffer on Petri dishes for 6 hours, until they exhibited the typical elongated cell form ('t6 cells').

To generate overexpression mutants, GFP-tagged FLN constructs were transformed into AX2 cells using electroporation and were expressed under the control of actin-15 promotor. For the transformation, 3 – 5 x 10^7 cells were washed twice in ice cold Soerensen buffer. After an additional washing step in ice cold electroporation buffer (50 mM sucrose, 10 mM KH_2PO_4, pH 6.1), the cells were resuspended in 800 µl ice cold electroporation buffer. The suspension was transferred in a 4 mm electroporation cuvette, mixed with 25 µg DNA and electroporated using a Gene Pulser XCell (Biorad) and the standard settings (square wave, V = 1.0 kV, 1 ms pulse length, two pulses, 5 seconds pulse interval). After incubation for 10 minutes at room temperature, 2 µM $CaCl_2$ and 2 µM $MgCl_2$ were added and the suspension was incubated for another 15 minutes in a culture dish under gentle shaking (50 rpm). Subsequently, HL5 medium was added and the cells were allowed to recover for about 24 hours before the respective antibiotic (either 10 µg/ml blasticidin or G418) was added to select the transformants. Single clones were obtained by spreader dilution on lawns of non-pathogenic *K. aerogenes* and were screened via live-cell microscopy for the presence of the overexpressed GFP-tagged proteins.

2.2.3.1.2 Migration assays in 2D and 3D

Micropipette assay

Approximately 1 x 10^6 t6 cells in one ml Soerensen buffer were plated in low 35 mm standard-bottom µ-dishes (IBIDI) and migration toward a micropipette (Eppendorf), filled with 10 µM cAMP, was visualized using a Axiovert 200M microscope with a 40x/0.75 plan objective. Images were taken at an interval of 10 seconds over a period of ~30 minutes at room temperature.

Under-agarose assay

For the analysis of 2D migration of vegetative cells, under-agarose assays were performed in low 35 mm standard-bottom µ-dishes (IBIDI). 0.7% (w/v) Biozym LE agarose in SM-Medium (10 g/l Bacto Peptone, 1 g/l yeast extract, 1.9 g KH_2PO_4, 0.6 g/l K_2HPO_4, 0.43 g $MgSO_4$, 10 g/l glucose, pH 6.5) was melted, and 2.5 ml of the solution were immediately poured into µ-dishes. After hardening of the agarose, three troughs of 10 mm x 2 mm located 5 mm apart from each other were cut in the center of the dish. Cells were harvested, washed with Soerensen buffer once and resuspended in MB medium (14 g/l Bacto Peptone, 7 g/l yeast extract, 4.26 g MES buffer, pH 6.9). 5 x 10^4 cells in equal volumes were loaded into the two outer troughs and 1 mM folic

acid in MB medium was loaded into the central trough. After 3 to 4 hours of incubation at 22°C inside a moist chamber, directed cell migration was imaged using Axiovert 200M microscope with A-Plan 10x/0.25 Ph1 lenses at an interval of 10 seconds for 1 hour and 40 minutes.

3D collagen assay *(D. discoideum)*

Migration in 3D was assessed using a collagen assay that was adapted from 3D experiments for neutrophils. 1 x 10^6 t6 cells were harvested and suspended in 50 µl Soerensen buffer. Subsequently, 12.5 µl cell suspension were mixed with 1.5 mg/ml rat tail collagen type I (IBIDI), 0.2% $NaHCO_3$, 6.7 mM NaOH and 1.2 mM $CaCl_2$ in Sorensen buffer in a final volume of 75 µl. 6 µl of the cell-collagen mix was then filled into a µ-Slide Chemotaxis^{3D} (IBIDI). After polymerization of the collagen for 30 minutes at room temperature, a cAMP gradient was establish across the observation channel by filling one reservoir with 65 µl of a solution of 100 nM cAMP and the opposing reservoir with 65 µl Soerensen buffer. Migration was recorded for 1 hour and 40 minutes at an interval of 20 seconds using an Axiovert 200M microscope with A-Plan 10x/0.25 Ph1 lenses.

Data processing

Evaluation of migration assays was performed with the help of Imaris software. Speed and directionality of migrating cells were analyzed using the automatic ImarisTrack tool followed by manual cell tracking. Directionality was measured as the displacement in direction of the chemoattractant divided by total track length of the cell. Cells were included into statistical analysis if they displayed a maximum displacement from the origin > 20 µm and a maximum track length of > 50 µm. Statistical analysis was performed by use of the Student´s t-test and data shown represent means plus or minus SDs. *P < 0,05; **P < 0,01; ***P < 0,001.

2.2.3.1.3 Immunofluorescence

Subcellular localization of GFP-tagged FLN proteins was analyzed in immunofluorescence studies with the overexpressing mutant strains. 1 x 10^6 t0 or t6 cells were allowed to settle on a coverslip in HL5 medium or Soerensen buffer for 15 minutes at room temperature. The medium or buffer was removed and the cells were fixed in ice cold methanol at –20°C for 2 minutes. After two washing steps in PBS, filamentous actin was stained with TRITC-phalloidin (Invitrogen). The stained samples were quickly rinsed with ddH2O, embedded in gelvatol mounting medium (0.14 M NaCl, 0.01 M KH_2PO_4/Na_2HPO_4, pH 7.2, 5.7 M polyvinyl alcohol, 0.5 mM glycerol, 0.9 mM DABCO) and stored in the dark at 4°C.

Alternatively, ddFLN-GFP expressing cells were directly fixed within a 3D collagen matrix. Therefore, cells were allowed to migrate within the matrix in a gradient of cAMP for approximately 30 minutes using a 3D µ-slide Chemotaxis^{3D} (IBIDI). Afterwards, Soerensen buffer and cAMP solution were carefully removed from the reservoirs, enclosing the observation channel and gently replaced by a 2% glutaraldehyde-solution containing 0.5% Triton-X-100. The fixation solution was allowed to diffuse through the observation channel for 5 minutes and the matrix was subsequently washed with PBS and stained with TRITC-phalloidin using the same technique.

2.2.3.2 HL60 cells

2.2.3.2.1 Cell culture and induction of differentiation

The promyelocytic HL60 cell line was purchased at American Type Culture Collection (CCL-240) and cultured in RPMI-1640 medium (Sigma-Aldrich), supplemented with 10% heat-inactivated FCS (Sigma-Aldrich) and 2 mM L-glutamine (Sigma-Aldrich) in untreated cell culture flasks at 37°C and 5% CO_2. Cells were centrifuged at 200 g for 5 minutes at room temperature unless noted otherwise. Differentiation into the neutrophil-like state was induced by addition of 1.3% DMSO to the culture medium at a concentration of either 0.2 x 10^6 cells/ml or 1 x 10^7 cells/ml for pull-down assays. Cells were used for the execution of the different experiment on day five or six after addition of DMSO (Collins et al., 1978).

2.2.3.2.2 Stable transduction using lentivral system

In order to generate a stable down-regulation of FLNa expression in HL60 cells, RNA interference and lentiviral transduction was employed. Therefore, five different shRNAs specific for FLNa (no. 28, 29, 30, 31, 32), cloned into pKLO.1 vector, were purchased form Sigma-Aldrich. As a control, a pKLO.1 vector containing scrambled, non-targeting shRNA was applied. HEK293T cells (CRL-11268) were used for the generation of virus-containing supernatant. First, 0.5 x 10^6 cells were plated on 6-well tissue culture plates in 2 ml RPMI-1640 complete medium. For transfection mix 1, 250 µl serum-free Opti-MEM medium (Life Technologies) was mixed with 12 µl Lipofectamine 2000 (Invitrogen) and incubated at room temperature for 5 minutes. Additionally, a second transfection mix, comprising 250 µl serum-free Opti-MEM medium, 1 µg shRNA containing pKLO.1 vector, 2 µg of the envelope vector pVSV-G and 3 µg of the packing vector pCMVΔR8.9, was also incubated for 5 minutes at room temperature. Both transfection solutions were mixed and after incubation for 20 minutes, the mix was slowly added

to the HEK293T cells and the cells were cultured at 37°C. After 24 hours the supernatant was removed from the cells, replaced with fresh PRMI-1640 complete medium and the cells were incubated for another 24 hours. The now virus-containing supernatant was harvested, sterile-filtered (filter pore-size 0.45 µm) and new medium was added to the HEK293T cells. Subsequently, HL60 cells were suspended in RPMI-1640 medium supplemented with 50%, 10% or 1% virus-containing supernatant at a density of 0.2 x 10^6 cells/ml and were seeded in a 24-well plate. After 24 hours, the virus-containing supernatant was again harvested form the HEK293T cells and used to infect the same HL60 cells. After one week all wells containing the same virus were pooled and the HL60 cells were selected using 1 µg/ml puromycin (Sigma-Aldrich). The different cell lines were then tested for down-regulation of FLNa by Western blotting and the cell line displaying the most efficient knockdown (KD) (shRNA 28) was subcloned by limited dilution cloning. Different single clone lines were again tested by Western blotting and two different clones were chosen for further analysis.

2.2.3.2.3 Transient transfection and live-cell imaging

For transient transfection of FLNa, FLNa cDNA (comprising amino acid 21 to 2640) was cloned in the pEGFP-C1 vector. 1 x 10^6 differentiated HL60 cells were harvested and washed in serum-free Opti-MEM medium (Life Technologies). The cells were then suspended in 100 µl serum-free Opti-MEM medium, mixed with 10 µg DNA in a 2 mm electroporation cuvette and transfected using the NEPA21 electroporator (Nepa Gene) under following conditions: pulse voltage 150V, pulse length 5 ms, pulse interval 50 ms, pulse number 2. Immediately after the electroporation, the cells were transferred in RPMI-1640 complete medium, cultured 12 hours at 37°C and were then used for live-cell imagining. Therefore, a Zigmond chamber assay (s. 2.2.3.2.6) was performed and transfected cells were imaged during migration in an fMLP gradient at a 5-seconds interval using confocal microscopy.

2.2.3.2.4 Immunofluorescence

Subcellular localization of proteins was studied by immunofluorescence analysis. Therefore, coverslips were coated with fibrinogen (100 µg/ml) for either 2 hours at room temperature or overnight at 4°C and washed subsequently twice with PBS. 1 x 10^6 differentiated HL60 cells in RPMI-1640 complete medium were allowed to adhere onto the coated coverslips for 15 minutes at 37°C and were stimulated with 100 nM fMLP for 10 minutes at 37°C. After removal of the medium, cells were fixed with ice cold methanol at –20°C for 2 minutes. After two washing steps

in PBS, the fixed samples were then stained with the appropriate primary and secondary antibodies for 1 hour, respectively. After rinsing the coverslips quickly in ddH20, they were embedded in gelvatol mounting medium and stored in the dark at 4°C.

2.2.3.2.5 Measurement of cell adhesion and spreading

Cell spreading and adhesion experiments were carried out simultaneously in two different buffer systems: in mHBSS buffer (20 mM HEPES, pH 7.2, 150 mM NaCl, 55 mM glucose, 4 mM KCl, 1.2 mM $MgCl_2$ supplemented with 0.25% BSA) (Servant et al., 1999) and in adhesion buffer (s. 2.2.2.1).

For analysis of cell spreading, differentiated HL60 cells were harvested and resuspended in the respective buffer at a density of 1 x 10^6 cells/ml and one ml of the cell suspension were plated on fibrinogen (100 µg/ml) coated coverslips. Cells were allowed to adhere for 15 minutes at 37°C and were then stimulated with 100 nM fMLP. 2 or accordingly 3 minutes after addition of fMLP, cells were fixed with methanol for 2 minutes at –20°C. For each coverslip, six bright field images at random positions were acquired using an Axiovert 200M microscope (Zeiss) with a 100x/1.4 oil objective. Spreading was analyzed by measurement of the area of the spreaded cells with the help of ImageJ software.

In order to analyze adhesion, 5 x 10^4 differentiated HL60 cells were harvested, resuspended in the respective buffer and were plated on fibrinogen (100 µg/ml) or fibronectin (50 µg/ml) coated wells of 96-well plates. For the generation of standard curves for each cell line, a 100%, 75%, 50% and 25% dilution of the cell suspension was seeded in wells, coated with poly-L-lyisn. After an incubation of 30 minutes at 37°C, the cells were stimulated by addition of 100 nM fMLP for 30 minutes at 37°C. Subsequently, non-attached cells in the fibrinogen and fibronectin coated wells were rinsed away by a gentle wash step in the respective buffer. After fixation with 1% glutaraldehyde for 20 minutes, cells were washed twice in ddH_2O. Subsequently, the wells were allowed to either air dry for approximately 45 minutes or were dried overnight at 4°C. The dried cells were then stained with 0.1% crystal violet (Sigma-Aldrich) and finally lysed with 10% acetic acid for 15 minutes. Extinction of the suspension was measured in triplicates at a wavelength of 590 nm using Ultrospec 2100 Pro spectrophotometer. Values of the poly-L-lysin samples were used for the generation of standard curves for each cell line and adhesion on fibrinogen or fibronectin was then calculated as percentage of cells adherent to poly-L-lysin.

2.2.3.2.6 Migration assays in 2D and 3D

Zigmond chamber assay (2D migration)

Chemotactic migration of HL60 cells in 2D was analyzed in Zigmond chambers as previously described (Zigmond and Hirsch, 1973). Briefly, 3 x 10^4 differentiated HL60 cells were harvested, washed once in mHBSS buffer and were allowed to adhere on a fibrinogen (100 µg/ml) coated streak in the middle of a 33 mm x 24 mm coverslip at 37°C for 20 minutes. The coverslip was then put face down in the chamber so that the adherent cells are positioned directly above the observation bridge in the middle of the two channels. One channel was filled with mHBSS buffer while the other was filled with 10 nM fMLP solution, thereby creating an fMLP gradient across the observation bridge.

Collagen assay (3D Migration)

For analysis of 3D migration, 3 x 10^6 differentiated HL60 cells were harvested, washed once in mHBSS buffer and were resuspended in 90 µl mHBSS. 12.5 µl of the cell suspension were mixed with 1 mg/ml rat tail collagen type I (IBIDI) and 0.2% $NaHCO_3$ in mHBSS buffer in a final volume of 75 µl. 6 µl of the cell-collagen mix was then filled into a µ-Slide Chemotaxis^{3D} (IBIDI) and the mix was allowed to polymerize for 30 minutes at 37°C in a moist chamber. Subsequently, an fMLP gradient was establish across the observation channel by filling one reservoir with 65 µl of a solution of 10 nM fMLP and the opposing reservoir with 65 µl mHBSS buffer.

Data processing

In both cases, images were taken in a heated chamber every 20 seconds using Axiovert 200M microscope (Zeiss) with a 5x/0.12 plan objective over a time period of 3 hours. Speed and directionality of migrating cells were analyzed with the automatic ImarisTrack tool of the Imaris software (Bitplane) followed by manual cell tracking. Directionality was measured as the displacement in direction of fMLP divided by total track length of the cell. Cells were included into statistical analysis if they displayed a maximum displacement from the origin > 20 µm and a maximum track length of > 50 µm.

2.2.3.2.7 Phagocytosis assay

E. coli B/r GFP bacteria were grown in shaking cultures in LB medium containing 100 µg/ml ampicillin at 37°C. The expression of the GFP protein was induced by addition of 1 mM IPTG and the cells were grown overnight at 37°C. The bacteria were harvested and heat-inactivated at 95°C for 20 minutes in a water bath. The OD_{600} was measured and the density of the bacteria

solution was estimated using a standard growth curve. For the analysis of phagocytosis the bacteria were opsonized in human serum for 30 min at 37°C and subsequently washed trice in mHBSS buffer.

Differentiated HL60 cells were resuspended in mHBSS buffer (density 1.5 x 10^6 cells/ml) and were incubated with the serum-opsonized GFP-expressing *E. coli* at a cell-to-bacteria ratio of 1:100 at 37°C. Phagocytosis was stopped after 10 minutes by addition of 4% paraformaldehyde and fixed cells were centrifuged on coverslips (500 g, 5 minutes). Per coverslip, 6 pictures at random positions were captured using an Axiovert 200M microscope with a 40x/0.75 plan objective (Zeiss). Phagocytosis positive cells were counted, a cell containing at least one bacterium was considered positive.

Alternatively, phagocytosis was analyzed using fluorescence spectroscopy. Therefore, green fluorescent YG latex beads (Ø 1 µm) were serum-opsonized as described above for the bacteria. Differentiated HL60 cells were harvested, resuspended in mHBSS buffer and adjusted to a density of 2 x 10^6 cells/ml. After transfer in a 25 ml Erlenmeyer flask, the cell solutions were gently shaken at 75 rpm at 37°C. Serum-opsonized latex beads were added at a cell-to-bead ratio of 1:50. One ml of the cell-bead solution was extracted immediately after addition of the latex beads (‘0 minutes’) and after 5, 10, 20, 30 and 45 minutes, respectively. The non-internalized beads were removed by two gentle centrifugation steps (100 g, 3 min). After resuspension in buffer, the fluorescence of the internalized beads was measured in a fluorimeter using 441 nm light for excitation.

3 Results

3.1 The role of ddFLN in *D. discoideum* migration

For *D. discoideum* it is suggested that different actin-binding proteins, among them ddFLN, execute redundant and overlapping functions and can therefore compensate for each other. This makes the analysis of the function of ddFLN difficult. To circumvent this problem, ddFLN mutant strains expressing GFP-tagged ddFLN proteins were assessed in addition to the ddFLN null mutant, HG1264.

3.1.1 Expression of GFP-tagged ddFLN fusion proteins in AX2 wild-type cells

A ddFLN overexpressing strain was generated by transforming AX2 wild-type cells with a ddFLN-GFP construct. Additionally, a truncated construct, where the ABD was completely replaced by a GFP (GFP-ddFLN(rod1-6)), was also expressed in AX2 wild-type cells (Figure 5A). The transformation efficiency was assessed using fluorescence microscopy. By staining of the cells with phalloidin that was used as a general cell marker, we could establish that in both strains clearly more than 95% of the cells were expressing the GFP-tagged fusion protein (Figure 5B,C).

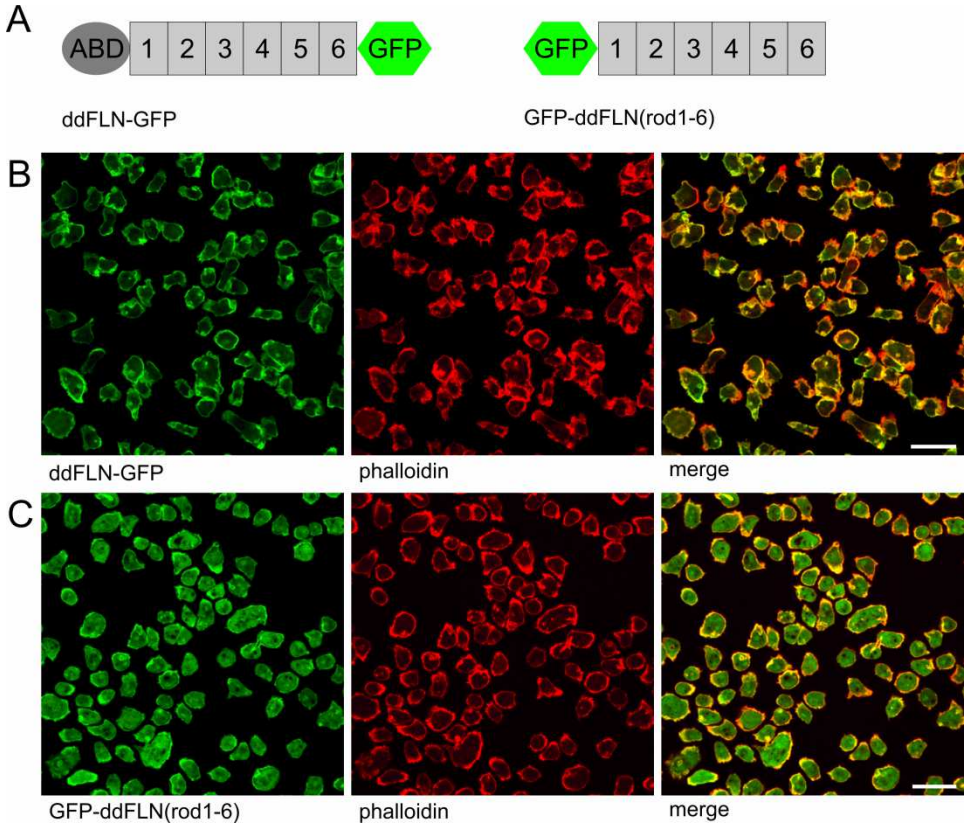

Figure 5: Expression of ddFLN-GFP and ddFLN-GFP(rod1-6) in AX2 wild-type cells
A) Schematic representation of the ddFLN GFP-fusion proteins: ddFLN-GFP and GFP-ddFLN(rod1-6). B,C) The cells were fixed with methanol and stained with phalloidin (red). Comparison of the expression of the GFP-tagged fusion proteins with the phalloidin staining revealed a transformation efficiency of about 95% for both the ddFLN-GFP (B) and the GFP-ddFLN(rod1-6) (C) expressing strain. Scale bars = 20 µm.

The localization of the ddFLN GFP-tagged fusion protein was analyzed in immunofluorescences using the LSM 510 confocal microscope in vegetative (t0) and starved cells (t6). The full-length ddFLN-GFP displayed a strong co-localization with actin at the cortex of t0 cells and at the leading edge in migrating t6 cells (Figure 6).

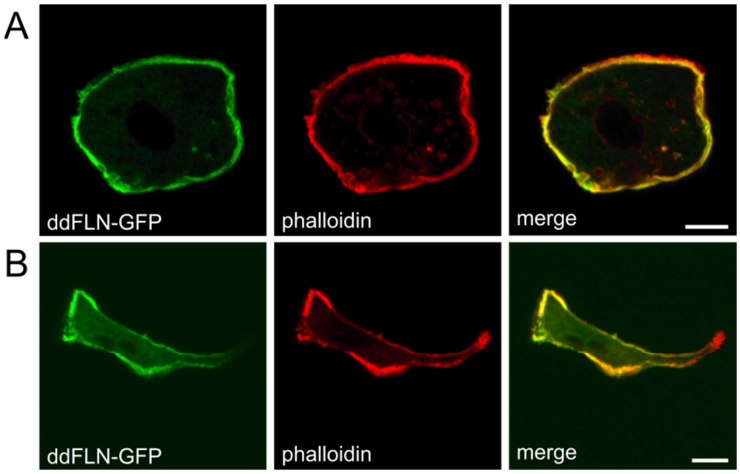

Figure 6: Localization of ddFLN-GFP in AX2 wild-type cells
DdFLN-GFP expressing cells were fixed with methanol and stained with phalloidin (red). A) In t0 cells, ddFLN-GFP co-localize with F-actin at the cortex. B) During migration in t6 cells, ddFLN-GFP is recruited to the leading edge. Scale bars = 2.5 µm.

The C-terminal GFP-tag does not interfere with the ability of the ddFLN-GFP protein to dimerize as it was already shown elsewhere (Khaire et al., 2007).

Despite the absence of the ABD in the GFP-ddFLN(rod1-6) construct, the truncated ddFLN protein also located to the F-actin rich structures in the cell, to the cortex in t0 cells and to the leading edge in t6 cells. Most likely by overexpression the amount of the fusion protein enriched in the cytosol was much higher as for the full-length ddFLN-GFP construct (Figure 7).

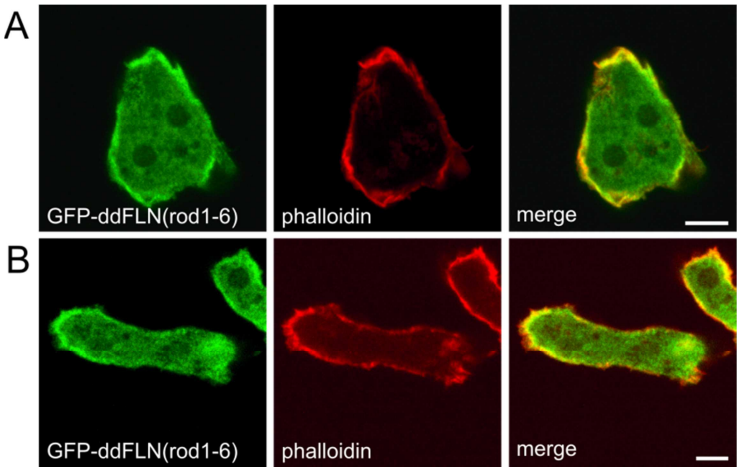

Figure 7: Localization of GFP-ddFLN(rod1-6) in AX2 wild-type cells
GFP-ddFLN(rod1-6) expressing cells were fixed with methanol and stained with phalloidin (red). A) In t0 cells, GFP-ddFLN(rod1-6) co-localizes with F-actin at the cortex. B) In t6 cells, GFP-ddFLN(rod1-6) is recruited to the leading edge. A much higher amount of the GFP fusion protein was found in the cytosol in comparison with the full-length construct. Scale bars = 2.5 µm.

The presence of the GFP-ddFLN(rod1-6) construct at F-actin rich sites was due to the ability of this truncated protein to dimerize with endogenous ddFLN protein, located at the cortex and the leading edge, respectively. The existence of such heterodimers was already verified by co-immunoprecipitation experiments in a previous study (Khaire et al., 2007). However, we confirmed the presence of heterodimers in the GFP-ddFLN(rod1-6) expressing strain generated in this study and additionally tested if the heterodimers were still present after induction of starvation. Therefore, a GFP-trap was performed using t0 and t6 GFP-ddFLN(rod1-6) expressing cells. By using an antibody specific for the ABD of ddFLN (82-421-5), which is only present in the endogenous protein, we verified that the GFP-ddFLN(rod1-6) protein dimerizes with the endogenous ddFLN protein in vegetative (t0) and in starved (t6) cells (Figure 8).

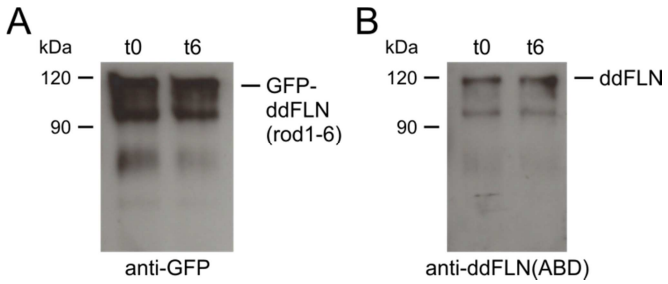

Figure 8: GFP-ddFLN(rod1-6) forms heterodimers with endogenous ddFLN protein.
Lysates of GFP-ddFLN(rod1-6) expressing t0 and t6 cells were incubated with GFP-trap beads and eluates were separated by SDS-PAGE. A) Western blot analysis with an anti-GFP antibody (K3-184-2) displayed the GFP-ddFLN(rod1-6) protein used as bait. B) In Western blot analysis with an antibody specific for the ABD of ddFLN (82-421-5), the endogenous ddFLN protein was identified to interact with the GFP-ddFLN(rod1-6) protein.

We suggest that due to this formation of heterodimers the GFP-ddFLN(rod1-6) fusion protein acts as a kind of competitive inhibitor and might be therefore a helpful tool to study the function of ddFLN.

3.1.2 Different ddFLN mutant strains

In order to analyze the function of ddFLN during locomotion, the ddFLN overexpressing strain (ddFLN-GFP) and the GFP-ddFLN(rod1-6) expressing strain were compared with AX2 wild-type cells as a control and additionally with the primary ddFLN null mutant HG1264 in different migration assays. Therefore, the expression levels of ddFLN and the different fusion proteins were assessed by Western blotting using an anti-ddFLN antibody, specific for the rod domain of the protein (82-471-14) (Figure 9). This antibody reacts both with the endogenous ddFLN protein and with the GFP-tagged fusion proteins.

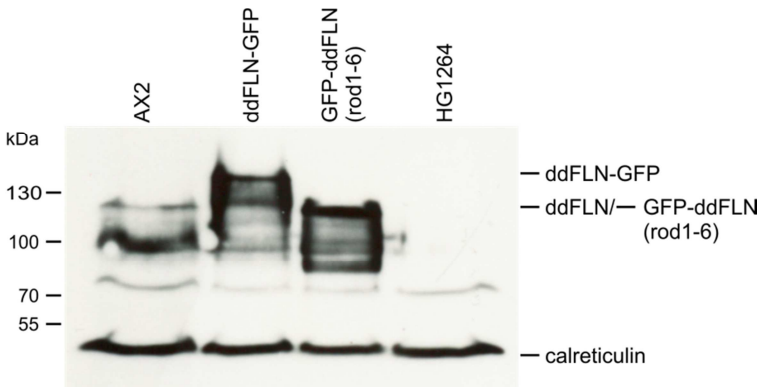

Figure 9: Expression level of ddFLN and ddFLN fusion proteins
Lysates of AX2 wild-type cells, ddFLN-GFP cells, GFP-ddFLN(rod1-6) cells and HG1264 cells were analyzed by SDS-PAGE and Western blotting using an antibody specific for the ddFLN rod domain (82-471-14). Endogenous ddFLN and GFP-ddFLN(rod1-6) exhibit roughly the same size (about 120 kDa). DdFLN-GFP migrates at approximately 140 – 150 kDa. Calreticulin was used as loading control.

DdFLN is highly susceptible to partial fragmentation in lysates. This made it impossible to determine the exact expression levels of endogenous ddFLN in comparison to the ddFLN GFP-tagged fusion proteins. Therefore, the whole amount of ddFLN protein (endogenous protein with the fusion proteins) was determined. We detected that the ddFLN-GFP protein was expressed at levels about 2.5 to 3 times (Figure 9, second lane) and the GFP-ddFLN(rod1-6) protein at levels about 3 to 3.5 times (Figure 9, third lane) of the expression level of the endogenous ddFLN protein (data not shown). In the ddFLN null mutant HG1264, no ddFLN expression was detectable (Figure 9, fourth lane).

3.1.3 Migration toward cAMP in a micropipette assay

First, the role of ddFLN was reviewed in 2D migration under buffer using a micropipette assay. T6 cells were allowed to migrate toward a micropipette filled with cAMP and speed of the migrating cells was analyzed using Imaris software (Figure 10). The ddFLN deficient mutant strain HG1264 exhibited no significant changes in the migration in comparison with AX2 wild-type cells. However, speed of ddFLN-GFP cells was significantly reduced whereas speed in GFP-ddFLN(rod1-6) cells was significantly increased in comparison to AX2 wild-type cells.

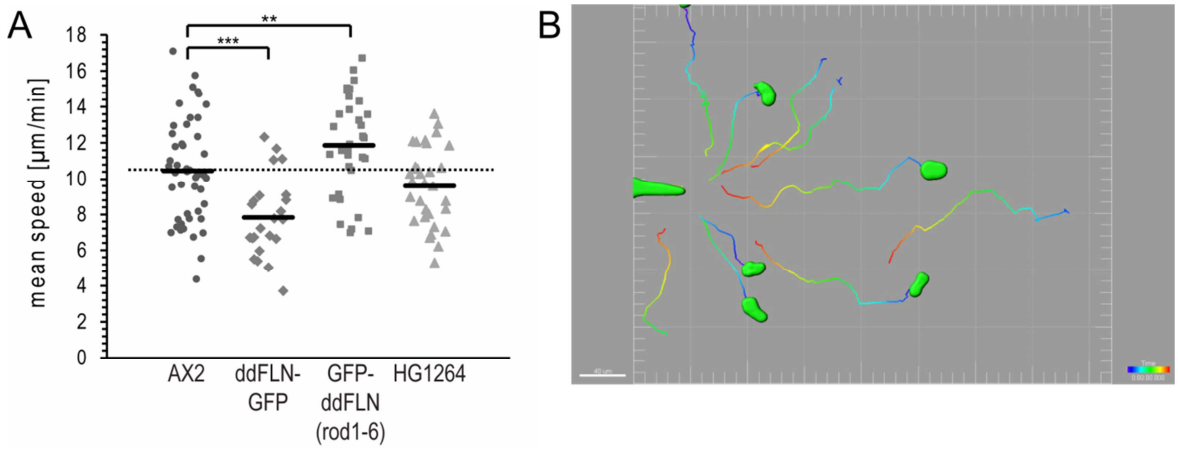

Figure 10: Analysis of ddFLN mutants in a micropipette assay
Migration speed of the different ddFLN mutant strains was compared with AX2 wild-type cells in cAMP-induced chemotaxis using a micropipette assay. A) Dot plots show the overall distribution, dotted line indicates the mean value of AX2 wild-type cells. Data are from four to seven independent experiments, respectively (sample size AX2 = 47, ddFLN-GFP = 23, GFP-ddFLN(rod1-6) = 34, HG1264 = 33). Speed was significantly reduced in the ddFLN-GFP expressing cells and was significantly enhanced in GFP-ddFLN(rod1-6) expressing cells and not changed in HG1264 cells. **P < 0.01; ***P < 0.001. B) Representative example for an evaluated micropipette migration assay with AX2 wild-type cells using Imaris software. The cells (in green) migrate toward the micropipette (left, green). Scale bar = 40 µm.

3.1.4 DdFLN in folic acid-induced chemotaxis in an under-agarose assay

Migration on a flat surface under buffer is rather unphysiological for *D. discoideum* cells. They normally live within and crawl through the soil. An under-agarose assay was used to test the migration of the different ddFLN strains under more restrictive conditions as the cells have here to move under the agarose overlay (Laevsky and Knecht, 2001). Vegetative cells were allowed to migrate toward folic acid for about 100 minutes and were analyzed using Imaris software (Figure 11). DdFLN deficiency had again no effect on migration. However, speed of migration was reduced in the ddFLN-GFP and in the GFP-ddFLN(rod1-6) expressing strain. Directionality was only enhanced in the ddFLN-GFP overexpressing strain.

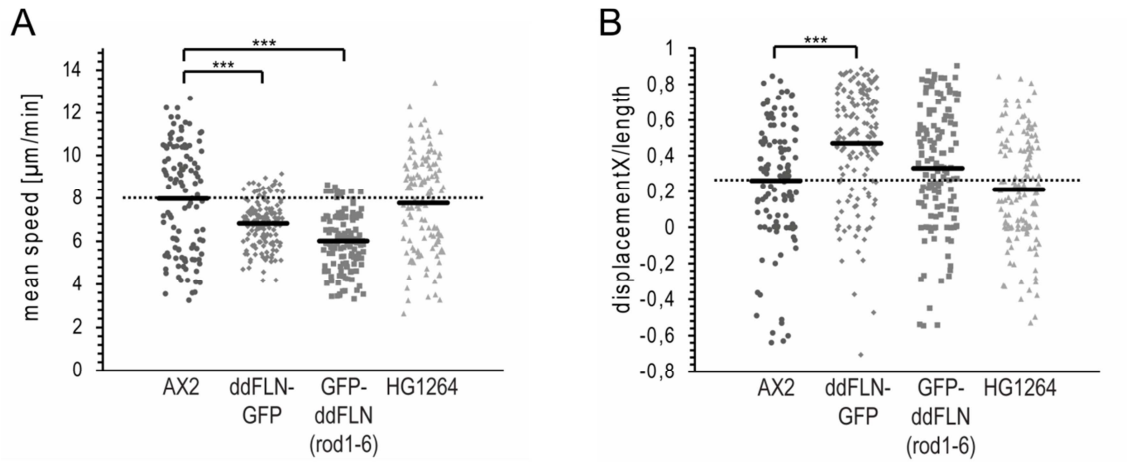

Figure 11: The different ddFLN mutant strains in the under-agarose assay
Under-agarose assays were performed to analyze folic acid-induced chemotaxis under restrictive conditions. Dot plots show the overall distribution, dotted lines indicate the mean values of AX2 wild-type cells. Data are from three independent experiments, respectively (sample size AX2 = 114, ddFLN-GFP = 151, GFP-ddFLN(rod1-6) = 133, HG1264 = 129). A) Speed was significantly reduced in ddFLN-GFP expressing as well as in GFP-ddFLN(rod1-6) expressing cells. B) Directionality was measured as the displacement of the migrating cell in direction of the folic acid ('displacement X') divided by total track length. The ddFLN-GFP expressing cells displayed a significantly increased directionality. ***P < 0.001.

3.1.5 Role of ddFLN in 3D migration

Migration in 3D, where the cell can interact with the substrate on all sides, increasingly become the focal point of migration studies as it is in many cases more suitable to mimic the natural environment of the cells. *D. discoideum* not only has to move through 3D structures within the soil but also migrates as single-cells within the multicellular slug. A number of 3D assays for these cells had been already developed using different substrates including ficoll or agarose (Barry and Bretscher, 2010; Zhao et al., 2013). In this study we tested for the first time if collagen

matrices are a suitable tool to study cAMP-induced migration of starved *D. discoideum* cells in 3D. A collagen 3D migration assay for neutrophils is routinely used in our lab. The assay was adapted to the Soerensen buffer system so that it could be employed for *D. dicsoideum*. It was necessary to increase the collagen concentration of 1 mg/ml (used for neutrophils) to 1.5 mg/ml as the *D. discoideum* cells were less adherent and seemed to 'drop through' the lesser dense matrix. Subsequently, we determined by bright field microscopy that starved *D. discoideum* cells were really arranged in 3D within a matrix of 1.5 mg/ml collagen type I and that they can move through the matrix in response to a cAMP stimulus. Meanwhile, we observed that the cells seemed to move through the matrix using blebs in many cases (Figure 12A).

In order to assess the localization of ddFLN in cells migrating in 3D, ddFLN-GFP cells were fixed within a collagen matrix and stained with phalloidin for F-actin. DdFLN-GFP localized to actin rich protrusion at the leading edge as well as at the rear of the migrating cell (Figure 12B).

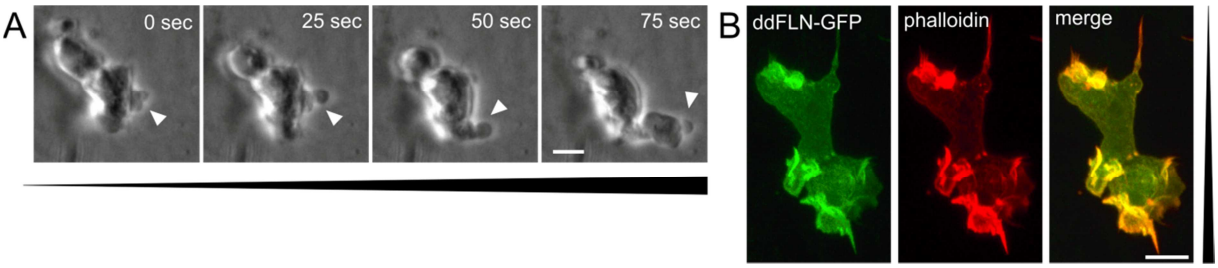

Figure 12: *D. discoideum* cells move through a 3D collagen matrix.
A) Live-cell imaging was performed with AX2 cells migrating within a collagen matrix in a gradient of cAMP. The black line width indicates the concentration gradient of the chemoattractant. Consecutive images at indicated time points were extracted from the original recording that was performed with a frame rate of 5 seconds. White arrow heads indicate bleb formation at the front of the migrating cell. Scale bar = 10 µm. B) DdFLN-GFP expressing cells were allowed to migrate within a 3D collagen matrix, fixed with glutaraldehyde and stained with phalloidin (red). The line at the right indicates the direction of the gradient with the highest concentration at the bottom. Z-stakes were taken using confocal microscopy, the image is a summation projection. DdFLN-GFP localizes to actin rich protrusions at the front and also to the rear of the cell. Scale bar = 5 µm.

Subsequently, migration of t6 cells of the different ddFLN mutant strains was analyzed within a collagen matrix in a gradient of cAMP (Figure 13). All of the ddFLN mutant strains (HG1264, ddFLN-GFP, GFP-ddFLN(rod1-6)) migrated with a significantly lower speed in comparison with AX2 wild-type cells. Whereas the directionality of the ddFLN-GFP and the GFP-ddFLN(rod1-6) cells was significantly decreased, HG1264 cells displayed a significantly enhanced directionality. However, it is noticeable that the observed effects in the HG1264 strain were rather minor in comparison of those in the other ddFLN mutant strains.

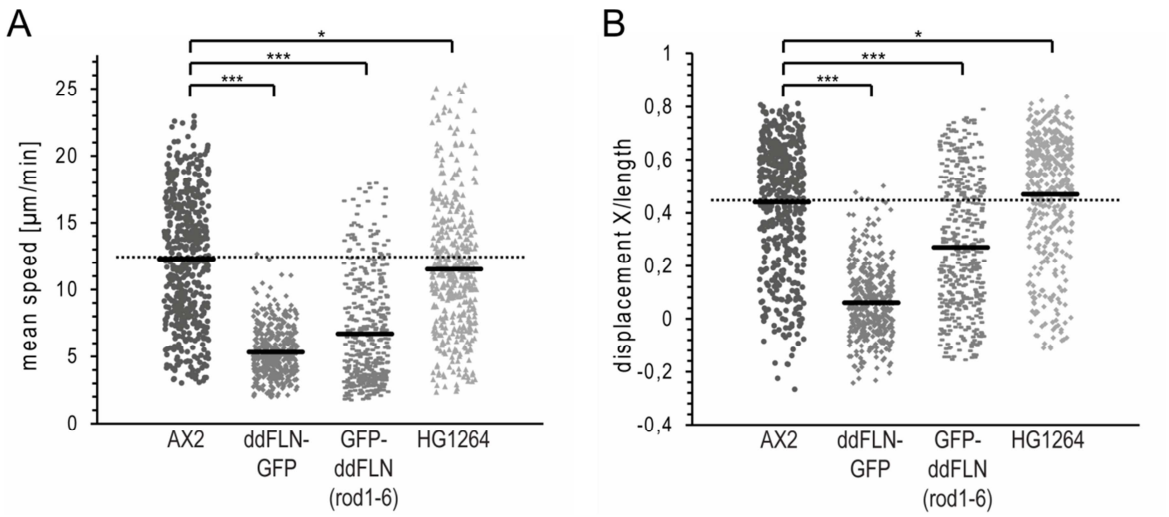

Figure 13: DdFLN mutant strains display a disrupted migration in 3D.
Migration of t6 cells in 3D was analyzed within a collagen matrix in a gradient of cAMP. Dot plots show the overall distribution, dotted lines indicate the mean values of AX2 wild-type cells. Data are from three to four independent experiments, respectively (sample size AX2 = 502, ddFLN-GFP = 398, GFP-ddFLN(rod1-6) = 424, HG1264 = 411). A) Migration speed was reduced in all three ddFLN mutant strains in comparison to AX2 wild-type cells with HG1264 displaying the least affected migration. B) Directionality was slightly enhanced in HG1264 cells, but decreased in ddFLN-GFP and GFP-ddFLN(rod1-6) expressing cells. *P < 0.05; ***P < 0.001.

3.1.6 DdFLN mutant strains in cell migration

DdFLN mutant strains were analyzed in various migration assays. Chemotaxis of starved cells toward cAMP was studied in a micropipette assay and also within a 3D collagen matrix. Additionally, migration of vegetative cells was investigated in under-agarose assays with folic acid as chemoattractant. While overexpression of full-length ddFLN (ddFLN-GFP) and expression of a truncated ddFLN lacking the ABD (GFP-ddFLN(rod1-6)) in AX2 wild-type cells resulted in severe migration defects under all tested conditions, the ddFLN null mutant HG1264 exhibited, in line with previous studies, a very subtle phenotype with only minor effects in the 3D collagen assay. The results of the different ddFLN mutant strains in the three migration assays in comparison to AX2 wild-type cells are summarized in table 3. Arrows display the altered phenotypes found in the ddFLN mutant strains, hyphens indicate no change in comparison to AX2 wild-type cells.

Table 3: Different ddFLN mutant strains in cell migration

	ddFLN-GFP	GFP-ddFLN(rod 1-)	HG1264
Micropipette assay (t6 cells, cAMP)			
Speed	↓	↑	-
Under-agarose assay (t0, folic acid)			
Speed	↓	↓	-
Directionality	↑	-	-
3D collagen assay (t6 cells, cAMP)			
Speed	↓	↓	↓ (minor)
Directionality	↓	↓	↑ (minor)

3.2 Human FLNs in neutrophil-like HL60 cells

3.2.1 FLN isoforms in HL60 cells and generation of FLN isoform specific antibodies

The main part of the thesis focused on the function of human FLNs in neutrophil-like HL60 cells. The first question that arose was which of the three FLN isoforms are expressed in these cells. Therefore, PCRs on cDNA, isolated of undifferentiated and differentiated HL60 cells were performed with three distinct primer pairs, specific for the different isoforms (Table 4).

Table 4: Primer sequences used for analysis of expression of FLN isoforms

	Forward primer (5´–3´)	Reverse primer (5´–3´)
FLNa	Ggcttctccgtctggc	cccacctgtgcccc
FLNb	gagtgacatgaacggcctg	cccatggggaagaactcac
FLNc	Gcagctgaacggtgccc	ctcctcaagccggggct

These PCRs revealed that FLNa and FLNb are expressed in undifferentiated and differentiated HL60 cells. An expression of FLNc could not be detected (Figure 14).

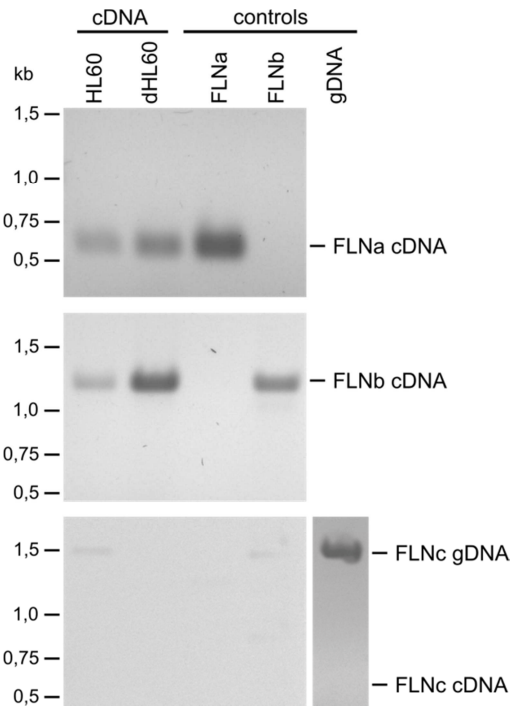

Figure 14: FLNa and FLNb expression is detectable in HL60 cells.
PCRs were performed with cDNA, isolated from undifferentiated (HL60) and differentiated HL60 (dHL60) cells and primer pairs, specific for FLNa (first panel), FLNb (second panel) and FLNc (third panel). As a control, plasmids, containing FLNa and FLNb cDNA and, for the PCR with the FLNc specific primer pairs, genomic DNA were used. FLNa (amplificate of 660 bp) and FLNb (amplificate of 1250 bp) expression could be detected in undifferentiated and differentiated HL60 cells. No indication of a FLNc expression (expected amplificate of 575 bp) was found. Control PCR with genomic DNA and FLNc specific primer pair resulted in an amplificate of the expected size of 1536 bp.

The next step was the examination of the expression of FLNa and FLNb at the protein level. Therefore, specific antibodies against the different FLN isoforms were needed. However, the specificity of available antibodies was questionable due to the high similarity of the isoforms. Accordingly, we raised our own FLNa and FLNb specific antibodies in rabbits. For the generation of the antibodies, both hinge domains seemed suitable as these domains display the greatest divergence along the entire FLN protein. For the creation of the FLNa specific antibodies, the FLNa hinge 2 domain together with the repeat 24 were selected. For the FLNb specific antibodies, the FLNb hinge 1 domain with adjacent regions was employed (Figure 15). Both protein domains were expressed in bacteria as GST-tagged fusion proteins.

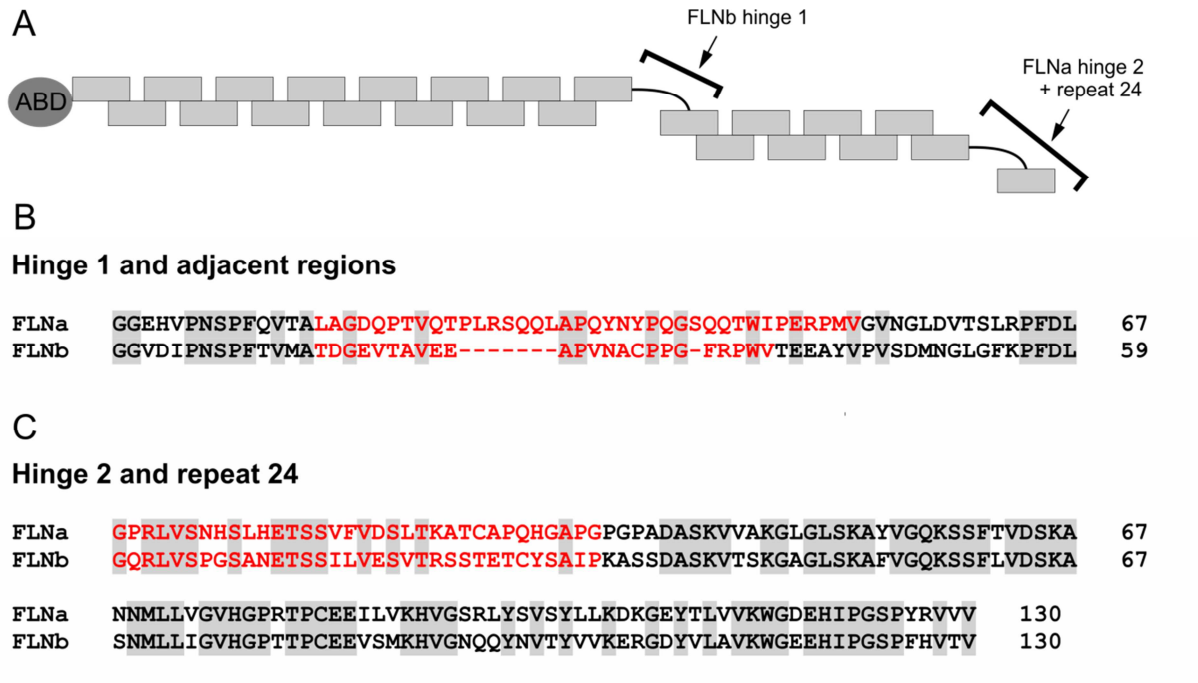

Figure 15: FLNa and FLNb protein domains selected for antibody generation
A) Schematic representation of the FLN proteins. The regions used for antibody production are labeled. B,C) Sequence alignments of the FLN protein domains used for antibody generation. Identical residues are displayed on a grey background. B) Hinge 1 domain is highlighted in red. The adjacent regions (termination of repeat 15 and beginning of repeat 16) are shown in black. FLNa and FLNb display an amino acid sequence identity of 39% in this domain. C) Hinge 2 domain is shown in red and repeat 24 is indicated in black. The amino acid sequences of FLNa and FLNb exhibit an identity of 61% in this region.

In order to test the specificity of the resulting antibodies, the corresponding protein domains of both FLN isoforms were expressed also as GST-tagged proteins (GST-FLNb(H2+24) and GST-FLNa(H1)). However, the antibodies were originally raised against GST-tagged proteins and therefore also antibodies recognizing GST were present in the serum. Consequently, the GST-tag of the FLN proteins had to be removed by digestion with PreScission protease (PSP). The resulting fragments, in particular the cropped FLN domains, were analyzed by Western blotting with both FLN isoform specific antibodies. This analysis demonstrated that both the FLNa and the FLNb antibodies are highly specific for their respective isoform (Figure 16).

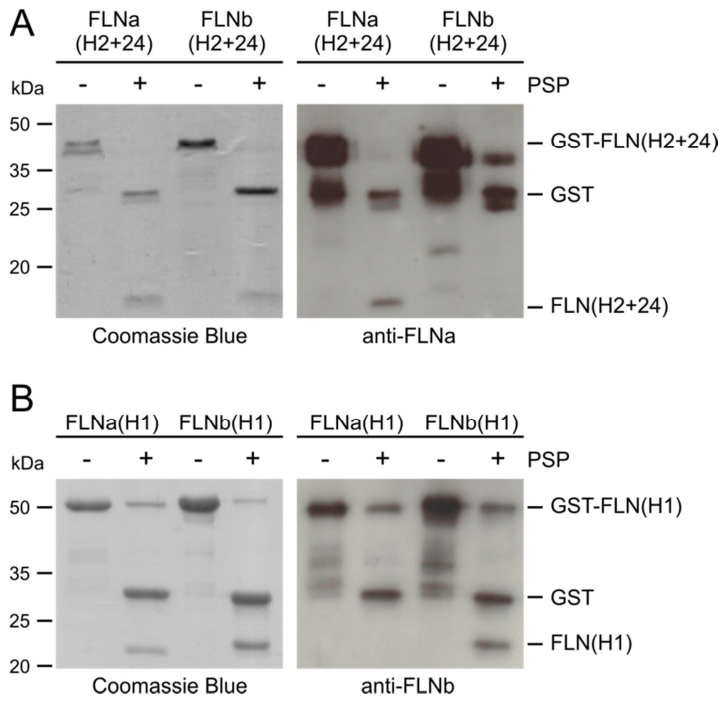

Figure 16: Anti-FLNa and anti-FLNb antibodies are specific for their respective isoform.
GST-tagged FLN hinge 2 domains with repeat 24 (GST-FLNa(H2+24),GST-FLNb(H2+24)) and GST-tagged hinge 1 domains with adjacent region (GST-FLNa(H1), GST-FLNb(H1)) were digested with PreScission protease (PSP). Digestion was verified by SDS-PAGE and Coomassie Blue staining (left panels, respectively). Fragments were tested in Western blot analysis (right panels). A) The cropped FLN(H2+24) fragment migrates at approximately 15–17 kDa. The FLNa specific antibodies recognize only the FLNa(H2+24) domain. B) The FLNb specific antiserum only reacts with the cropped FLNb(H1) protein, not with the FLNa(H1) domain (migrating at approximately 20–22 kDa).

Equipped with FLN isoform specific antibodies, we assessed the protein levels of FLNa and FLNb in neutrophil-like HL60 cells (Figure 17). Analysis of total cell lysates of undifferentiated and differentiated HL60 cells revealed a very low, hardly detectable expression of FLNb. Western blot analysis of lysates of mouse macrophages demonstrated the functionality of FLNb specific antibodies (Figure 17A, right panel). In contrast, a strong FLNa expression was detected in undifferentiated and differentiated HL60 cells (Figure 17A, left panel). Furthermore, the FLNa expression level increased during differentiation by approximately one third of the expression in the undifferentiated cells (Figure 17B), indicating that FLNa is clearly the major isoform in neutrophil-like HL60 cells.

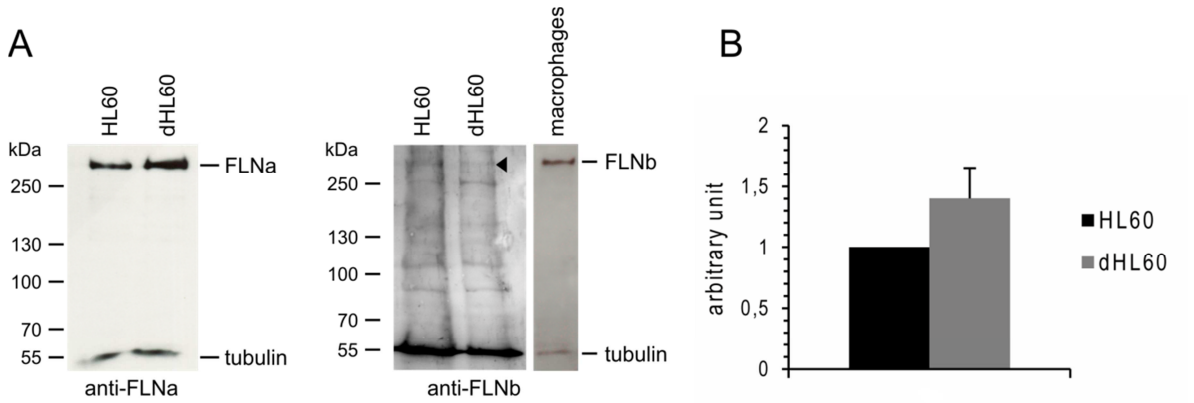

Figure 17: FLNa and FLNb protein expression levels in HL60 cells
A) Representative Western blot analysis with lysates of undifferentiated (HL60) and differentiated HL60 cells (dHL60) and antibodies specific for FLNa and FLNb are shown. Tubulin expression was used as loading control. A prominent FLNa expression was detected and its expression increased during differentiation (left panel). FLNb expression was hardly detectable (indicated by arrow head). Lysate of mouse macrophages was used as a positive control for the FLNb specific antibodies (right panel). B) Results of densitometry analysis of FLNa expression in undifferentiated (HL60) and differentiated HL60 cells (dHL60). Values of undifferentiated HL60 cells were normalized to one. Data are shown as mean of five independent experiments (± SD). Expression of FLNa increases during differentiation by approximately 40%.

3.2.2 Localization of FLNa in neutrophil-like HL60 cells

As FLNa was identified as the major isoform in the HL60 cells, the study focused on this isoform. Localization of FLNa in the differentiated cells was analyzed by immunofluorescence studies using the FLNa specific antibodies. We found that in unpolarized cells that exhibited no clear leading edge FLNa co-localized with F-actin at the cortex. However in polarized cells, FLNa was recruited more to the rear of the cell. Figure 18 displays two representative cells.

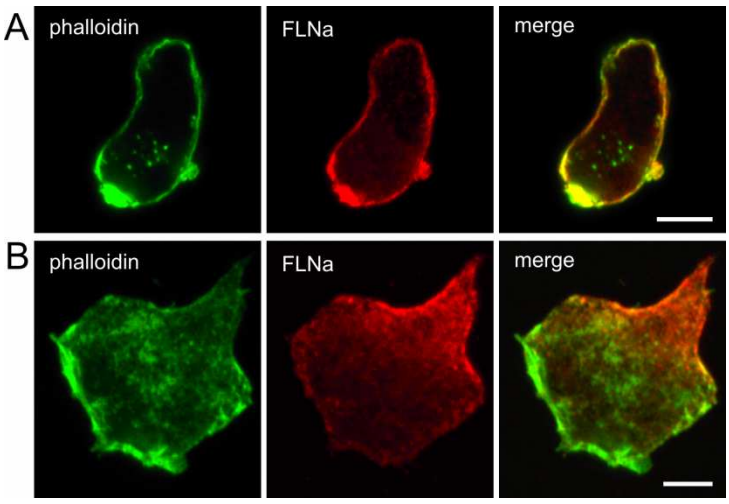

Figure 18: Localization of FLNa in neutrophil-like HL60 cells
Differentiated HL60 cells were allowed to adhere to fibrinogen, stimulated with fMLP and fixed with methanol. The cells were incubated with FLNa specific antibodies (red) and F-actin was stained with phalloidin (green). A) In unpolarized cells, FLNa was located at the cortex. B) In polarized cells with a clear F-actin rich leading edge FLNa was recruited more to the uropod. Scale bars = 5 µm.

This finding was further investigated using live-cell microscopy. Therefore, differentiated HL60 cells were transiently transfected with a FLNa-GFP construct (comprising FLNa amino acids 21 to 2640) by electroporation. Subsequently, the cells were allowed to migrate in a Zigmond chamber within a gradient of fMLP. Cells that displayed a strong FLNa-GFP expression were imaged during migration using a LSM 510 confocal microscope (Figure 19). In line with the results of the immunofluorescence studies, FLNa located more to the rear and sides of the migrating cell.

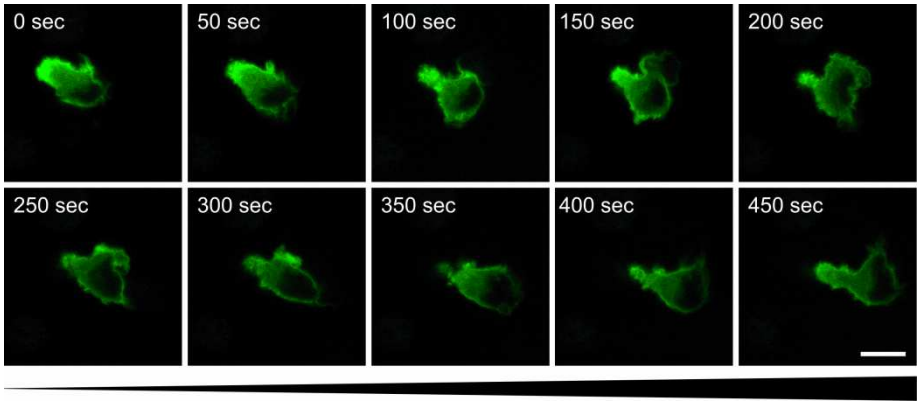

Figure 19: Live-cell microscopy with FLNa-GFP expressing neutrophil-like HL60 cells
Differentiated HL60 cells were transiently transfected with FLNa-GFP and allowed to migrate in an fMLP gradient in a Zigmond chamber. Live-cell microscopy was performed and a representative cell is shown, the highest fMLP concentration is at the right. Consecutive images at indicated time points were extracted from the original recording that was performed with a frame rate of 5 seconds. FLNa is located to the rear of the cell during migration. Scale bar = 10 µm.

3.2.3 Generation and characterization of FLNa knockdown cell lines

In order to investigate the function of FLNa, HL60 cell lines lacking FLNa expression were established (FLNa KD). Five different shRNAs specific for FLNa were used to generate pools of stably transduced cell lines by lentiviral transduction followed by selection with puromycin. The shRNA producing the most efficient knockdown was selected by assessing the FLNa expression levels with Western blotting (data not shown). Subsequently, the cells were subcloned by limited dilution cloning. Cloned knockdown cell lines were again screened for FLNa deficiency. Two independent cell lines (subclone C4 and G4), showing the most distinct decrease in FLNa expression, were chosen for further analysis. Simultaneously, a control cell line was generated by transduction of a scrambled, non-coding shRNA. Western blot analysis with lysates of undifferentiated cells revealed that in both knockdown cell lines the remaining FLNa expression levels amount to less than ~5% in comparison to the control cell line. Similar results were

obtained using lysates of differentiated cells, indicating that the knockdown is stable during differentiation (Figure 20).

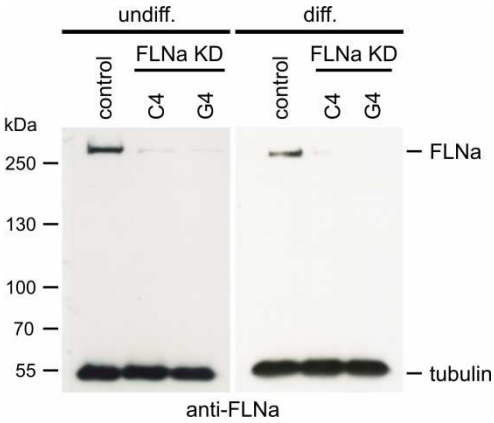

Figure 20: FLNa KD in undifferentiated and differentiated HL60 cells
FLNa expression levels of two different subclones (C4 and G4) in undifferentiated (left panel) and in differentiated (right panel) cells were compared to the levels of control cells by Western blotting with total cell lysates, using anti-FLNa antibodies. Tubulin expression was used as loading control. FLNa expression was reduced below ~5% in both subclones C4 and G4 in comparison to control cells.

3.2.3.1 Influence of FLNa KD on FLNb expression levels and phalloidin staining

Western blot analysis with lysates of differentiated and undifferentiated cells and the FLNb specific antibodies was performed. No influence of the FLNa KD on the FLNb expression level was detectable, either in the undifferentiated or in the differentiated HL60 cells (Figure 21). This finding indicates that FLNb did not simply compensate for the loss of FLNa.

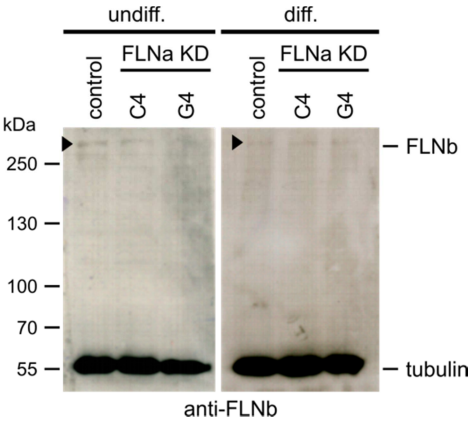

Figure 21: FLNa KD has no influence on the FLNb expression level.
Western blots with total cell lysates of undifferentiated (left panel) and differentiated (right panel) cells were performed with FLNb specific antibodies. Tubulin expression was used as loading control. FLNa KD cells exhibited no different FLNb expression in comparison to control cells. Arrow heads indicate the FLNb protein.

In order to directly compare the FLNa expression levels in knockdown and control cells in the immunofluorescence, FLNa KD cells were stained with the live dye TAMRA (red), mixed with control cells and after fixation stained for FLNa (green). Comparison of the (unlabeled) control cells to the (red) knockdown cells revealed that these two cell lines were clearly distinguishable by the markedly reduced expression level of FLNa (green) (Figure 22A).

FLNa was shown to contribute to the stabilization of the cortical actin filaments (Cunningham et al., 1992; Esue et al., 2009). Therefore, the influence of the FLNa deficiency on the F-actin

network was analyzed. Control cells were mixed with knockdown cells. F-actin was stained with phalloidin (green). Cells were additionally stained for FLNa (red) in order to distinguish between control and knockdown cells. Careful comparison of the phalloidin staining (green) of the FLNa positive control cells (red) with the FLNa deficient cells (unlabeled) revealed no noticeable effect of the knockdown on the F-actin network (Figure 22B).

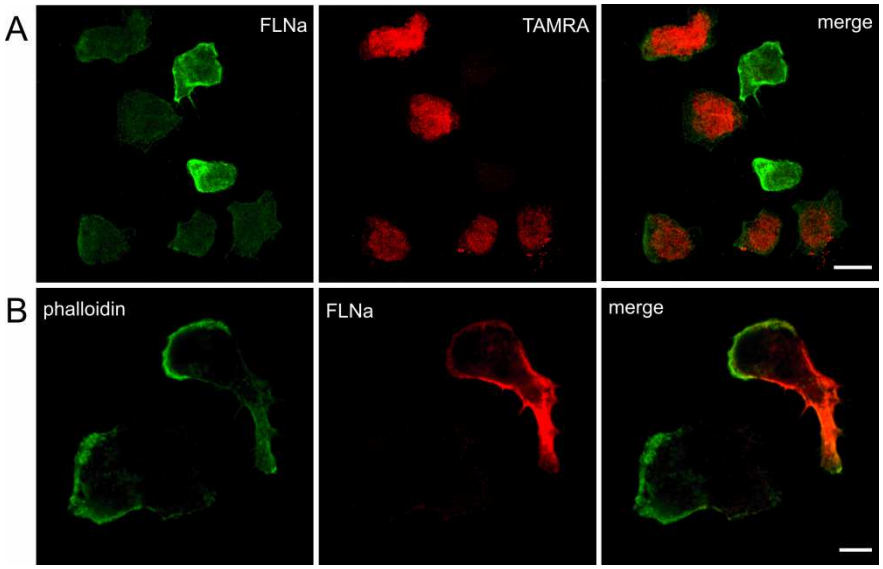

Figure 22: FLNa deficiency does not lead to obvious changes in the F-actin network.
A) FLNa KD cells were stained with the live dye TAMRA (red), mixed with control cells (unstained) and stained for FLNa (green). Comparison of (unlabeled) control cells to (red) FLNa KD cells revealed a strong deficiency in FLNa expression (green) in the knockdown cells. Scale bar = 10 µm. B) FLNa KD cells were mixed with control cells and stained for FLNa (red) and F-actin with phalloidin (green). FLNa staining was used to distinguish between knockdown cells (no FLNa) and control cells (red FLNa staining). Comparison of phalloidin staining revealed no apparent difference in F-actin networks. Scale bar = 5 µm.

3.2.3.2 FLNa modulates myosin II activation during 2D migration.

The role of FLNa in 2D migration was investigated with Zigmond chamber assays. The cells were allowed to migrate within a gradient of fMLP for 3 hours. Speed and directionality were analyzed with the help of Imaris software. Both FLNa KD cell lines displayed a significantly reduced speed of migration compared to control cells. The effect was more prominent in the subclone G4 (Figure 23A). In contrast, the directionality of the migrating cells was not affected in the FLNa deficient cells (Figure 23B).

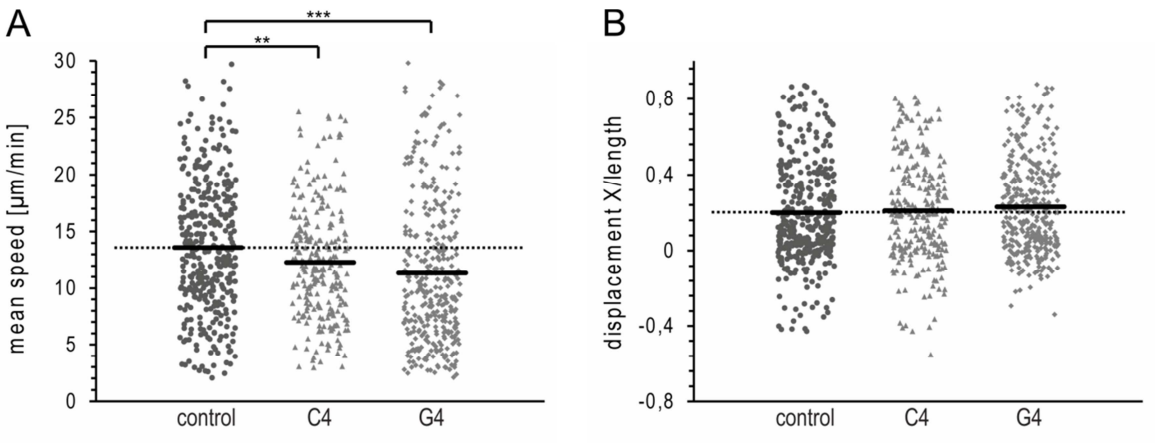

Figure 23: Knockdown of FLNa causes a decrease in speed in 2D migration.
2D migration was assessed using Zigmond chamber assays. Dot plots show the overall distribution, dotted lines indicate the mean values of the control. Data are from three independent experiments for the control cell line and from four independent experiments for FLNa KD subclones C4 and G4, respectively (sample size control = 360, C4 = 243, G4 = 354). A) Comparison of speed revealed a significant decrease in both FLNa KD cell lines (C4 and G4) compared to control cells. **P < 0.01; ***P < 0.001. B) Directionality was measured as the displacement of the migrating cell in direction of fMLP ('displacement X') divided by total track length. Directionality was not affected by knockdown of FLNa expression.

The localization of FLNa at the rear of migrating cells described above, hinted toward an influence of FLNa more at the modulation of the uropod by regulation of myosin II. To test if the decrease in speed in the 2D migration studies was myosin II dependent, levels of activated myosin II were investigated in the FLNa KD and control cell lines. Activation of myosin II is accompanied by the phosphorylation of the myosin light chain at Ser19 (pMLC). Western blot analysis with an antibody specific for pMLC was performed before and after stimulation of the cells with fMLP (Figure 24). In unstimulated cells (0 sec), levels of pMLC were unaffected in FLNa KD cells. However, after stimulation of the cells with fMLP for 10 minutes (600 sec) an increased activation of myosin II, accompanied by an elevation of phosphorylation at myosin light chain Ser19 (pMLC), was detected in the control cells but not in the FLNa deficient cells.

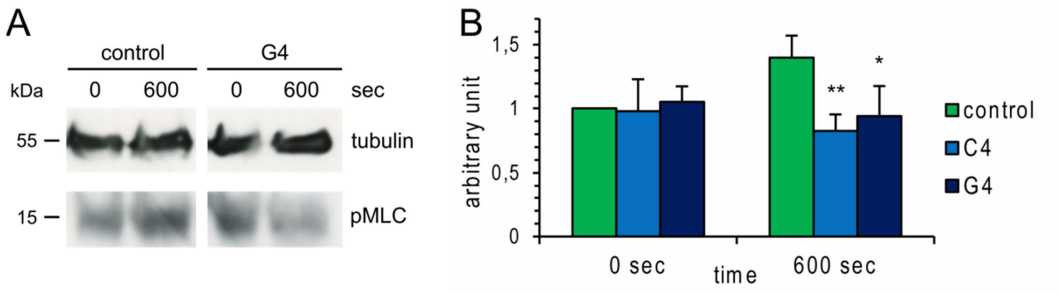

Figure 24: Levels of activated myosin II are reduced in FLNa KD cells.
Levels of myosin light chain 2, phosphorylated at Ser19 (pMLC) in unstimulated cells (0 sec) and 10 minutes (600 sec) after stimulation with fMLP were analyzed by Western blotting in control cells and in both FLNa KD cell lines. A) A representative Western blot with lysates of control and FLNa KD G4 cells is shown. Tubulin expression was used as a loading control. B) Results of densitometry analysis of pMLC expression. Data are from four independent experiments and are shown as means ± SDs, the value of unstimulated control cells (0 sec) was normalized to 1. No significant difference in pMLC levels in unstimulated cells (0 sec) was detected. 10 minutes after addition of fMLP (600 sec), pMLC levels were significantly reduced in both FLNa knockdown cell lines (C4 and G4) in comparison to control cells. *P < 0.05; **P < 0.01.

3.2.3.3 FLNa in 3D migration

In addition to migration in 2D, movement of the cells within a 3D environment was analyzed. Cells were embedded in a collagen matrix and migrated in a gradient of fMLP for 3 hours. Imaris software was used for evaluation. Speed was significantly reduced in both FLNa KD subclones in comparison to control cells (Figure 25A). However, FLNa deficient cells exhibited no differences in directionality (Figure 25B).

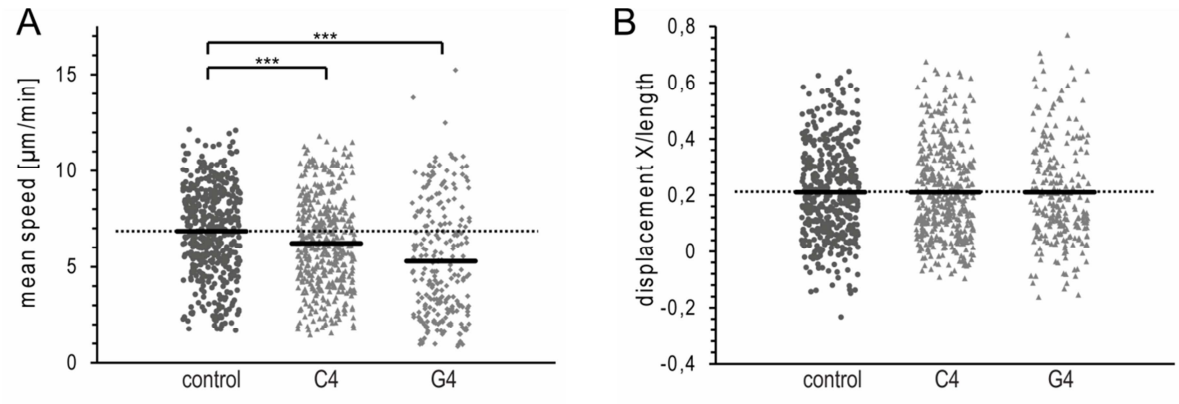

Figure 25: FLNa deficient cells moved significantly slower under 3D conditions.
Migration in 3D of FLNa KD cells in comparison to control cells was analyzed with the help of collagen assays. Dot plots show the overall distribution, dotted lines indicate the mean values of the control cell line. Data are from four independent experiments (sample size control = 457, C4 = 425, G4 = 238). A) Speed of the migrating cells was significantly reduced in FLNa KD cells (subclone C4 and G4). ***P < 0.001. B) No significant difference was detected in the directionality between the control cells and the FLNa KD cell lines.

3.2.3.4 FLNa is dispensable for cell adhesion.

The role of FLNa in cell adhesion on fibrinogen and fibronectin was investigated. The amount of adherent cells on both coatings was determined using Crystal Violet staining followed by measurement of the extinction at 590 nm. Two different buffer systems were described for neutrophils and neutrophil-like cells (mHBSS buffer and adhesion buffer) (Hepper et al., 2012; Servant et al., 1999). The assay was performed simultaneously under both conditions to test if the buffer had any influence on the adhesion properties of the cells. Both FLNa KD cell lines exhibited no significant differences in adhesion on fibrinogen and fibronectin in comparison to the control cell line neither in mHBSS buffer nor in adhesion buffer (Figure 26).

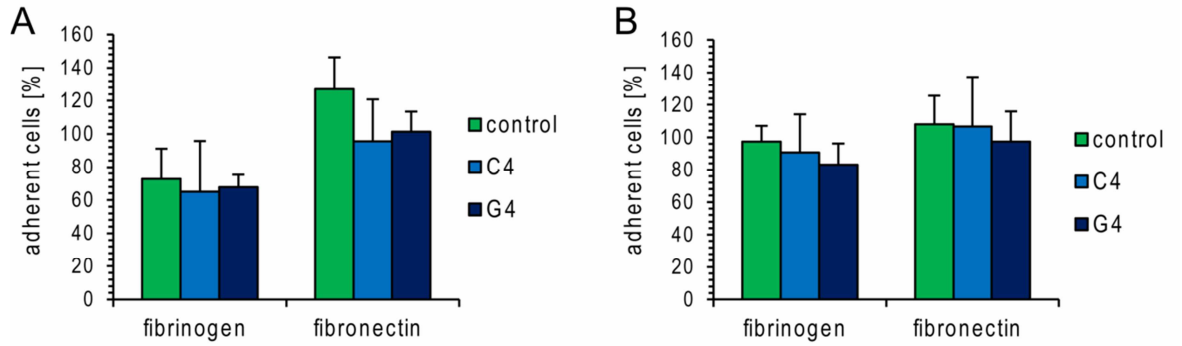

Figure 26: FLNa is dispensable for adhesion.
Adhesion of FLNa KD cells (subclones C4 and G4) were compared to control cells on fibrinogen as well as on fibronectin. Data represent adhesion in percentage of cells adherent to poly-L-lysin. Data are shown as means ± SDs and are from four independent experiments, respectively. Assays were performed in mHBSS buffer (A) and in adhesion buffer (B). No significant difference in adhesion of FLNa KD cells in comparison to control cells was detected.

3.2.3.5 The role of FLNa in cell spreading

Cell spreading was analyzed on fibrinogen. The cells were stimulated with fMLP for 2 or 3 minutes and subsequently the cell area was measured of both FLNa KD cell lines in comparison to the control cells. The assay was again performed simultaneously in mHBBS buffer and in adhesion buffer. In mHBSS buffer, knockdown of FLNa had no influence on the cell area during spreading neither 2 minutes (Figure 27A) nor 3 minutes (data not shown) after stimulation with fMLP. However, experiments performed in adhesion buffer revealed a significant increase of the cell area of both FLNa KD cell lines 2 minutes after stimulation with fMLP (Figure 27B). Notably, this effect vanished already 3 minutes after stimulation with fMLP, as a significant influence of the FLNa KD on the cell area was no longer detectable at this time point (data not shown). This finding is shown in figure 27C with two representative microscope pictures of spreading cells in adhesion buffer at 2 and 3 minutes after addition of fMLP.

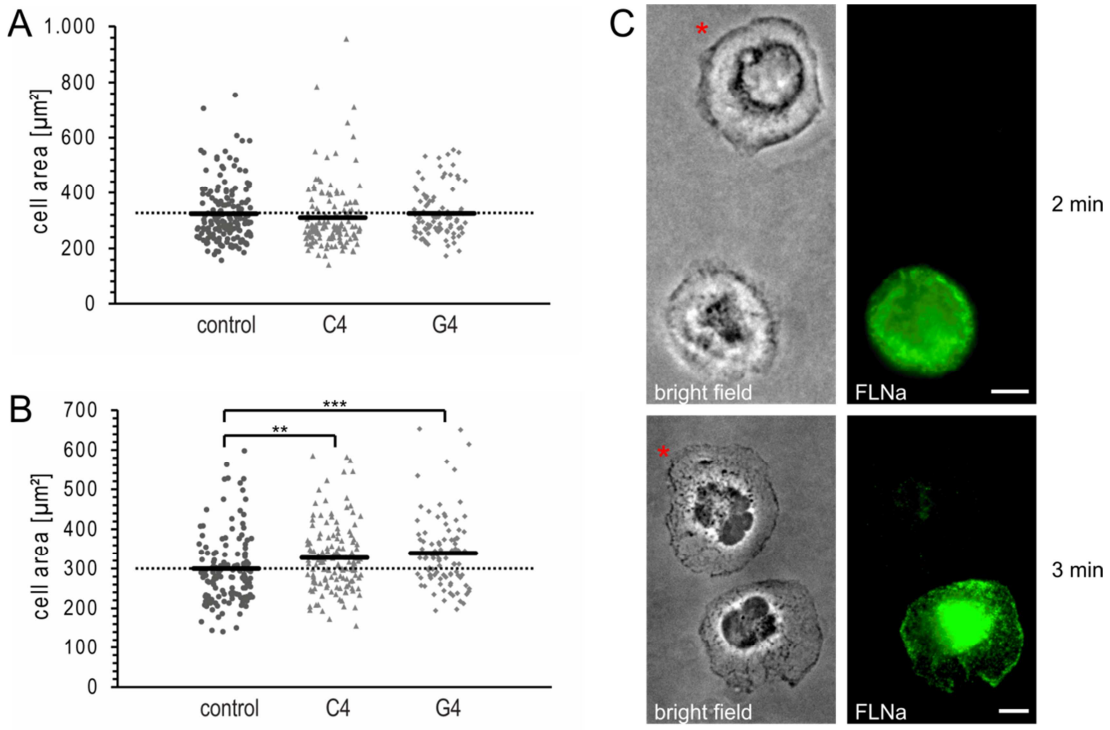

Figure 27: FLNa in cell spreading
A,B) Cell spreading on fibrinogen was analyzed by measurement of cell area 2 minutes after stimulation with fMLP. Dot plots show the overall distribution, dotted lines indicate the mean values of the control cell line. Data are from six independent experiments, respectively. A) Cell spreading experiments in mHBSS buffer revealed no significant difference between knockdown and control cells (sample size control = 166, C4 = 135, G4 = 98). B) In adhesion buffer a significant increase in cell area in both FLNa KD cell lines was detectable (sample size control = 130, C4 = 137, G4 = 96). **P < 0.01; ***P < 0.001. C) Representative microscope images of cell spreading in adhesion buffer are shown. Control cells were mixed with FLNa KD cells, stimulated with fMLP for 2 minutes (upper panel) or 3 minutes (lower panel), fixed with methanol and stained for FLNa (green). FLNa staining was used to distinguish between control cells (unstained, marked with a red star) and FLNa KD cells (green). Scale bar = 5 µm.

3.2.3.6 FLNa is involved in the regulation of phagocytosis.

Phagocytosis is another crucial function of neutrophils. A participation of FLN proteins in this process was not described so far for mammalian phagocytes. In order to test if FLNa is involved in phagocytosis, localization of FLNa during this process was assessed. Immunofluorescences were performed with differentiated HL60 cells, mixed with serum-opsonized green fluorescent YG latex beads (Ø 4.5 µm). Subsequently, cells were incubated with anti-FLNa antibodies. A strong recruitment of FLNa to the phagocytic cup in cells engulfing a latex bead was observed (a representative cell is shown in Figure 28), indicating that FLNa plays indeed a role in phagocytosis.

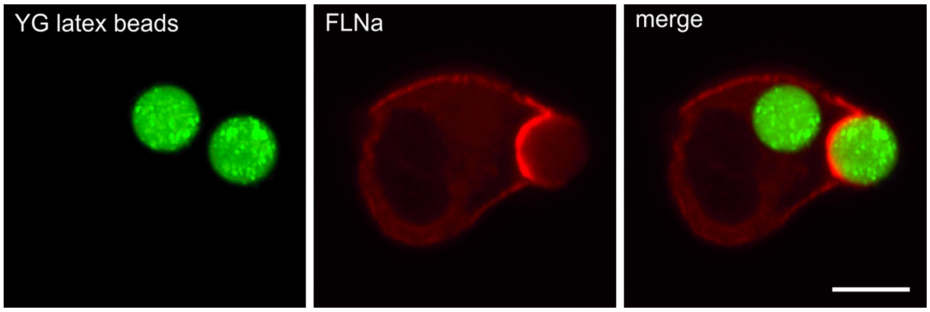

Figure 28: FLNa is recruited to the phagocytic cup.
Confocal microscopy was performed with differentiated HL60 cells phagocytosing serum-opsonized YG-latex beads (Ø 4.5 µm, green). Cells were stained for FLNa (red). FLNa was recruited to the phagocytic cup. Scale bar = 5 µm.

To investigate the function of FLNa during phagocytosis further, FLNa KD cells or control cells were mixed with serum-opsonized GFP-expressing *E. coli* at a bacteria-to-cell ratio of 100:1. Phagocytosis was stopped after 10 minutes and the phagocytosis positive cells (cells that had engulfed at least one bacterium) were counted. Both FLNa KD cell lines revealed a significant decrease in phagocytosis in comparison to control cells (Figure 29).

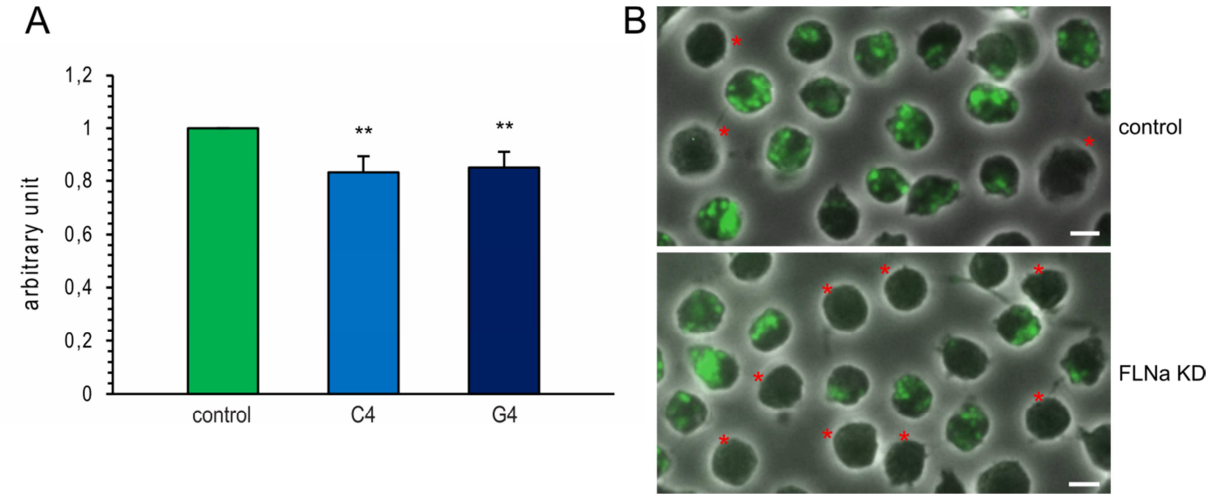

Figure 29: FLNa deficient cells display a reduced phagocytosis of serum-opsonized *E. coli*.
Phagocytosis was analyzed with serum-opsonized GFP-expressing *E.coli*, incubated with differentiated HL60 cells at a bacteria-to-cell ratio of 100:1 for 10 minutes. Phagocytosis was stopped by addition of 4% paraformaldehyde. For quantitative analysis the number of positive cells, containing at least one bacterium, was determined. A) Bar chart represents means ± SDs of four independent experiments, whereas values of control cells were normalized to one (sample size control = 4372, C4 = 4347, G4 = 4469). Phagocytosis was significantly reduced in FLNa KD strains. **P < 0.01. B) Representative results of the phagocytosis assay of control cells (upper panel) in comparison to FLNa KD cells (lower panel) are shown. Phagocytosis negative cells were marked with a red star. Scale bar = 50 µm.

However in this experiment, phagocytosis was measured only at one time point and the precise amount of engulfed bacteria was not taken into consideration. Therefore, a more sophisticated phagocytosis assay was subsequently executed. Differentiated HL60 cells were incubated with serum-opsonized green fluorescent YG latex beads (Ø 1 µm) in shaking culture. At different time points (0, 5, 10, 20, 30 and 45 minutes) samples of the cell-bead suspension were extracted and the free beads were removed by two centrifugation steps. Phagocytosis was measured as the fluorescence of the internalized beads using the fluorescence spectrometer LS55. However, uptake of the serum-opsonized latex beads in was not altered in the FLNa deficient cells in comparison to control cells (data not shown).

3.2.4 FLNa interaction partners in neutrophil-like HL60 cells

To further illuminate the role of FLNa in the neutrophil-like HL60 cells, we set out to identify new FLNa interaction partners in these cells. Therefore, pull-down assays with a recombinant FLAG-FLNa protein, bound to anti-FLAG M2 affinity beads, were performed. Additionally, co-immunoprecipitation assays were executed with FLNa specific antibodies bound to Sepharose A resin. The antibody recognized and bound endogenous FLNa protein. In both cases, the FLNa protein interacted with potential binding partners in lysates of differentiated, adherent HL60 cells. Subsequently, FLNa protein were pulled down together with interaction partners, separated using SDS-PAGE, and proteins were stained with Roti®-Blue quick staining solution. Selected bands of interest were cut out from the gel, analyzed by mass spectrometry and several potential FLNa interaction partners were identified.

3.2.4.1 FLNa interaction with coronin 1A

The actin-binding protein coronin 1A was detected to interact with FLNa in a pull-down with FLAG-FLNa by mass spectrometry. To verify this interaction, the pull-down assay was repeated and coronin 1A was identified as binding partner by Western blot analysis (Figure 30A). Furthermore, a GST-coronin 1A protein was expressed and used as bait in a reversed pull-down assay. FLNa was clearly identified among the proteins precipitated with GST-coronin 1A by Western blotting (Figure 30B).

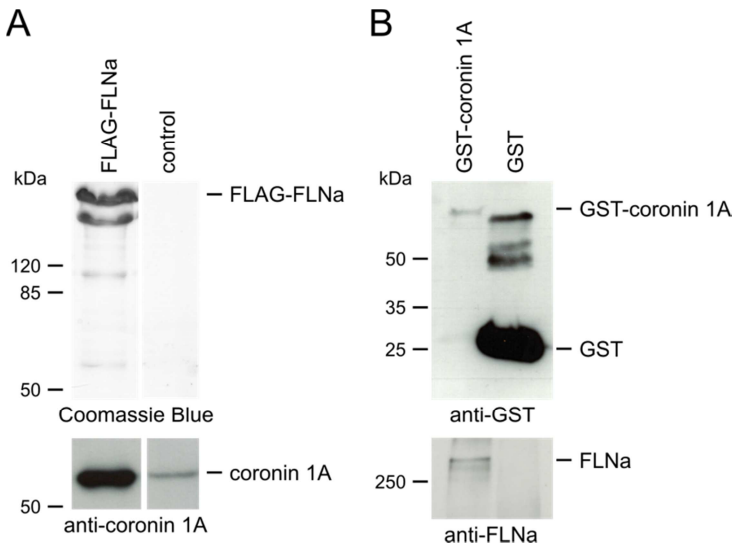

Figure 30: FLNa interacts with coronin 1A.
A) Pull-down experiments were performed with lysates of differentiated adherent HL60 cells and beads, coated with FLAG-FLNa or with empty beads (control). Pull-down was analyzed by SDS-PAGE. Upper panel shows the bait protein FLAG-FLNa in the Coomassie Blue staining. Western blotting with anti-coronin 1A antibody (lower panel) displayed a strong coronin 1A band (migrating at ~55 kDa) in the pull-down with FLAG-FLNa and only a weak signal in the control (empty beads). B) GST-coronin 1A or GST coated beads were used as bait in a pull-down assay with lysates of differentiated adherent HL60 cells. The pellets were analyzed with SDS-PAGE and Western blotting with anti-GST antibody (upper panel): bait proteins (GST-coronin 1A and GST) are shown. Analysis of the pull-down using Western blotting and anti-FLNa antibodies (lower panel) revealed FLNa protein only in the pull-down with GST-coronin 1A.

In a next step the FLNa domain, responsible for the interaction with coronin 1A was determined. Three different sections of the FLNa protein were expressed as FLAG-tagged proteins: FLAG-tagged FLNa actin-binding domain with the repeats 1 to 8 (FLAG-FLNa(ABD-8)), FLAG-tagged FLNa repeats 9 to 18 (FLAG-FLNa(9-18)) and FLAG-tagged FLNa repeats 19 to 24 (FLAG-FLNa(19-24)). In pull-down assays with these three proteins coronin 1A was found to precipitate only with the FLAG-FLNa(9-18) protein (Figure 31). To exclude the possibility that the observed FLNa-coronin 1A interaction occurred only due to the actin-binding properties of both proteins, pull-down assays with the different FLAG-tagged FLNa proteins were screened for actin. By Western blotting, actin was only found in the pull-down with the FLAG-FLNa(ABD-8) protein. No actin was found in the approach with the FLAG-FLNa(9-18) protein indicating that the interaction of FLNa with coronin 1A was not mediated by actin (Figure 31A, undermost panel).

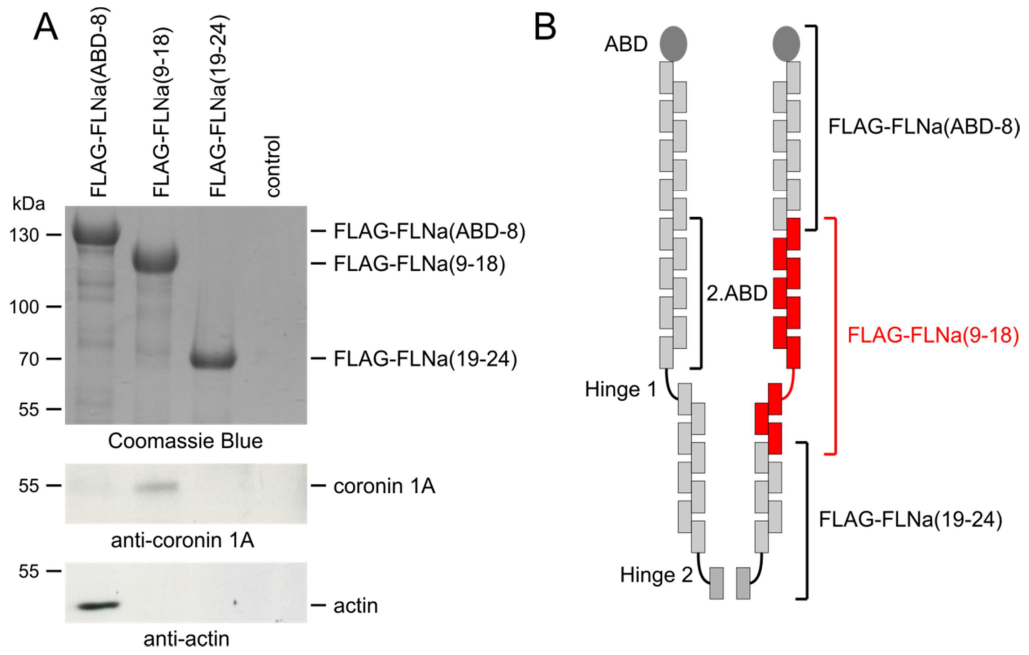

Figure 31: Coronin 1A interacts with the FLNa repeats 9 to 18.
A) To map the FLNa domain responsible for interaction with coronin 1A, pull-down assays with lysates of differentiated adherent HL60 cells and beads coated with FLAG-FLNa(ABD-8), FLAG-FLNa(9-18) or FLAG-FLNa(19-24) were performed and analyzed by SDS-PAGE. First (upper) panel shows the three different FLAG-FLNa bait proteins by Coomassie Blue staining. Western blotting with anti-coronin 1A antibody (second panel) reveals a band for coronin 1A only in the pull-down with FLAG-FLNa(9-18). Western blot analysis with anti-actin antibodies (third panel) indicates that actin only binds to FLAG-FLNa(ABD-8) protein. B) Schematic representation of the FLNa protein. The region responsible for the interaction with coronin 1A (repeats 9 to 18) is highlighted in red.

Although we were able to confirm a FLNa-coronin 1A interaction, it was still questionable if this was a direct protein-protein interaction or if it was mediated by other proteins, probably in the context of a multi-protein complex. Direct protein-protein interaction studies using an AEKTA superose 6 gel filtration column should be performed to answer this question. Therefore, FLAG-FLNa and GST-coronin 1A were purified. In a first step both proteins were applied individually on the gel filtration column. The collected 0.5 ml fractions were analyzed by Western blotting in order to determine their individual elution range. Individual FLAG-FLNa eluted in rather early fractions (8.5 ml to 12 ml) as it was expected due to its high molecular mass and homodimeric structure (Figure 32A). However, the main part of the GST-coronin 1A protein was found to elute at an even higher molecular weight (fractions 7.5 to 8 ml). As recombinant coronin 1A was well known to be highly insoluble, we concluded that the main part of the GST-coronin 1A was denatured (Yan et al., 2007). Only a small amount of GST-coronin 1A protein was detected in the later fractions 11.5 to 12.5 ml. These fractions represent most likely soluble GST-coronin 1A in its trimeric structure (Figure 32B). Unfortunately, the amount of soluble GST-coronin 1A protein was not high enough to perform protein-protein interaction studies in more detail.

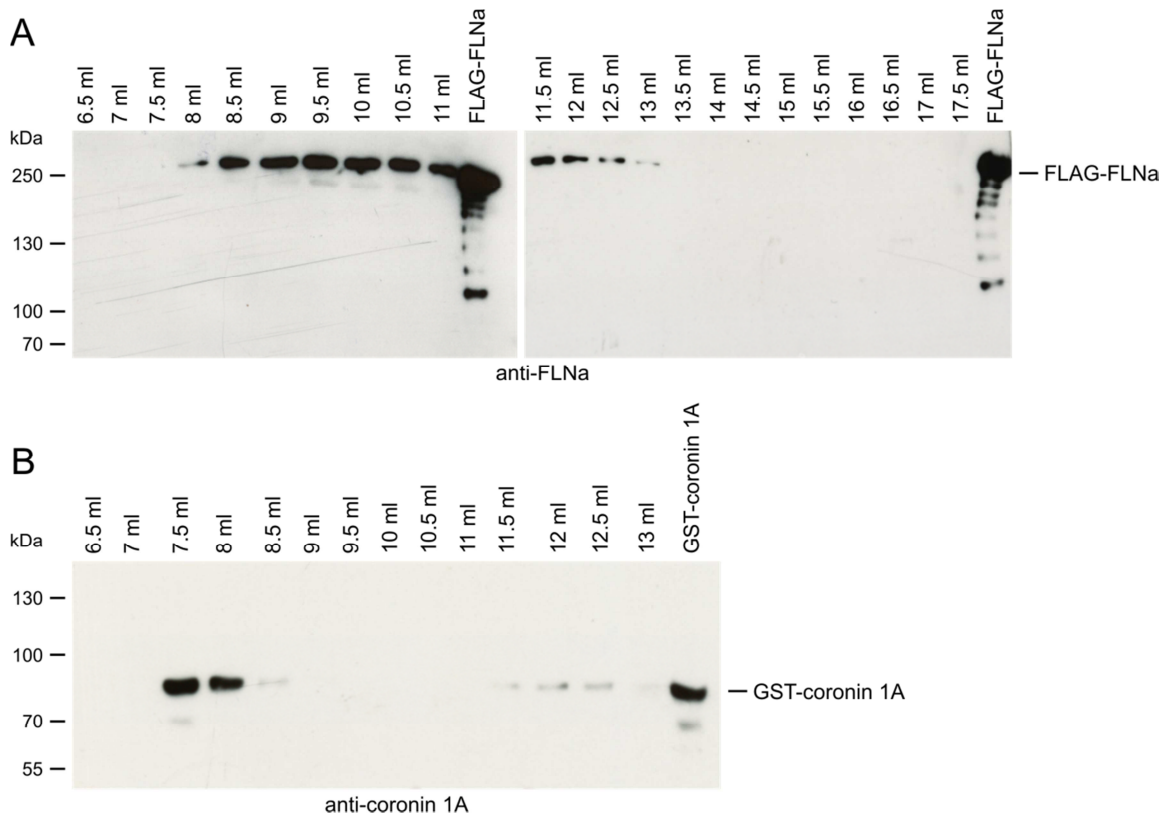

Figure 32: Gel filtration studies with FLAG-FLNa and GST-coronin 1A
200 µg purified FLAG-FLNa and GST-coronin 1A protein were applied onto the AEKTA superose 6 gel filtration column. The collected fractions (0.5 ml) were analyzed by Western blotting with anti-FLNa and anti-coronin 1A specific antibodies, respectively. A) FLAG-FLNa was found in the fractions ~8.5 to 12 ml. B) The main part of the GST-coronin 1A protein eluted in the fractions 7.5 to 8 ml and represent most likely denatured protein aggregates. A weak signal in the fractions 11.5 to 12.5 indicates the presence of a small amount of soluble GST-coronin 1A, probably displaying a trimeric structure.

In order to gain nevertheless some insight into the functional relevance of the FLNa-coronin 1A interaction, the potential occurrence of this interaction during migration, spreading and phagocytosis was investigated. Co-immunofluorescences with differentiated HL60 cells were performed under varying conditions (representative cells are shown in Figure 33). The cells were stained with anti-FLNa and anti-coronin 1A antibodies, respectively. In polarized cells, stimulated with fMLP, coronin 1A was recruited to the leading edge whereas FLNa located, as previously described, more to the rear of the cell (Figure 33A). During cell spreading we found both, FLNa and coronin 1A, enriched at the cortex of the spreading cell (Figure 33B). For the examination of phagocytosis, cells were mixed with serum-opsonized latex beads. Immunofluorescence analysis of these cells revealed that FLNa and coronin 1A co-localized at the phagocytic cup (Figure 33C).

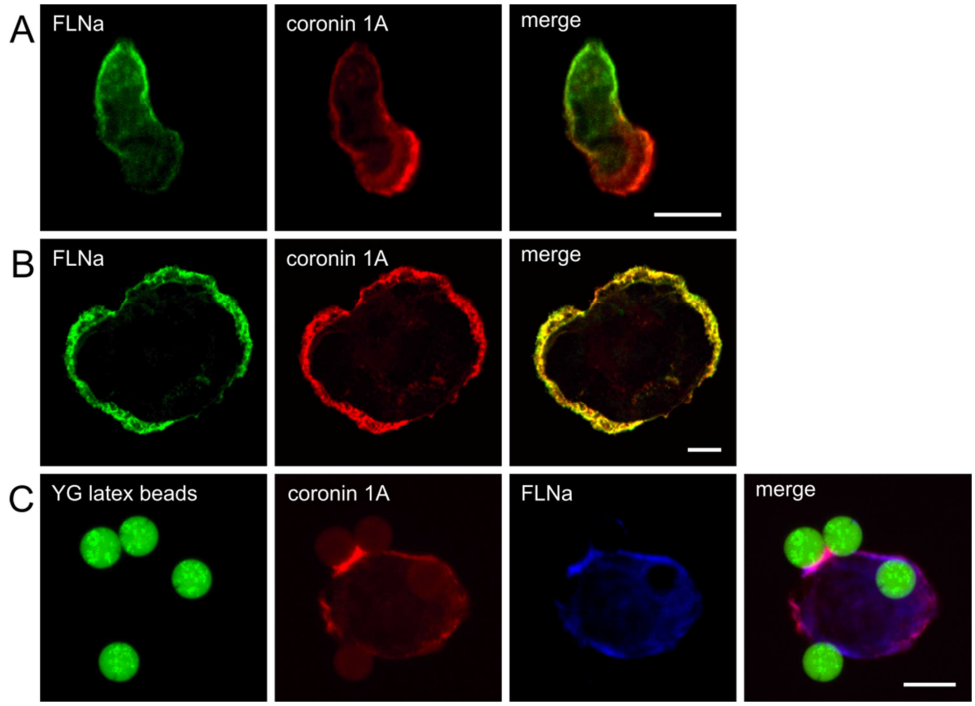

Figure 33: Localization of FLNa and coronin 1A during migration, spreading and phagocytosis
Co-immunofluorescences with differentiated HL60 cells under different conditions were performed. The cells were fixed with methanol and stained for FLNa and coronin 1A, respectively. A) Cells were stimulated with fMLP for 10 minutes. In a polarized cell, FLNa (green) localized at the uropod, whereas coronin 1A (red) was recruited to the leading edge. B) Localization of both proteins was assessed during cell spreading. Cells were fixed 2 minutes after addition of fMLP. A strong co-localization of FLNa (green) and coronin 1A (red) was detected at the cortex. C) Cells were mixed with serum-opsonized green fluorescent YG latex beads (Ø 4.5 µm) and incubated for 10 minutes. Fixed cells were stained for coronin 1A (red) and FLNa (blue). Both proteins were recruited to the phagocytic cup. Scale bars = 5 µm.

3.2.4.2 FLNa binds potentially to DOCK11 and CLIP-170.

Besides coronin 1A, further potential FLNa interaction partners were identified by mass spectrometry (Figure 34). Two of the most interesting are DOCK11, a Cdc42 GEF and the microtubule plus-end binding protein CLIP-170.

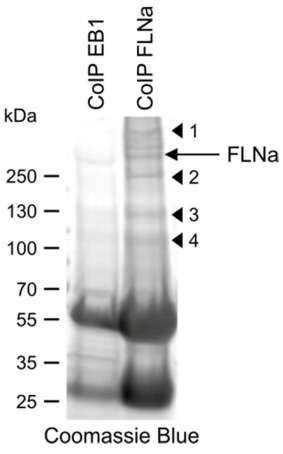

Figure 34: Potential FLNa interaction partner identified by mass spectrometry
Co-immunoprecipitation assay was performed with anti-FLNa antibodies ('CoIP FLNa'). Anti-EB1 antibodies were used as control ('CoIP EB1'). Antibodies were incubated with lysates of differentiated adherent HL60 cells. FLNa together with potential interaction partner was coupled to protein A Sepharose and proteins were eluted from the resin. Proteins were separated by SDS-PAGE, stained with Roti®-Blue quick staining solution and analyzed by mass spectrometry. The identified proteins are indicated with black arrows: 1 = β-spectrin, 2 = DOCK11, 3 = CLIP-170, 4 = formin-like protein 1.

However, FLNa interaction neither with DOCK11 nor with CLIP-170 could be confirmed by pull-down assays and Western blotting. Also subsequent co-localization studies of FLNa and DOCK11 using immunofluorescence approaches were not sufficient to verify the interaction (Figure 35).

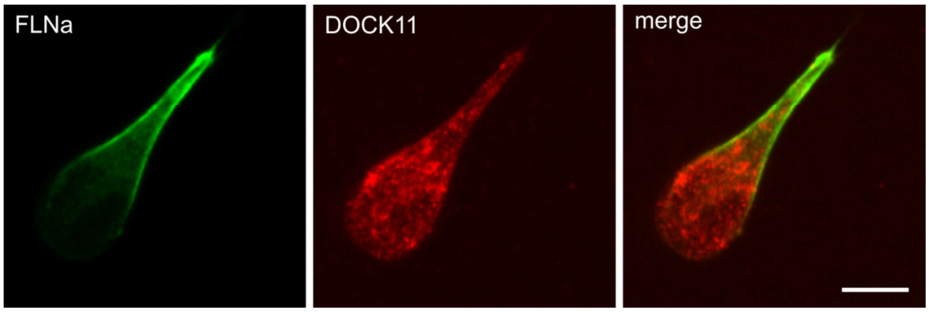

Figure 35: Localization of FLNa and DOCK11 in neutrophil-like HL60 cells
Differentiated HL60 cells were fixed with methanol and stained for FLNa (green) and DOCK11 (red). DOCK11 is distributed in dotted structures throughout the cytoplasm. While a co-localization of DOCK11 with FLNa at the cortex was detectable at some regions, an unequivocal interaction between these both proteins could not be verified. Scale bar = 5 µm.

4 Discussion

The main goal of this study was to characterize the function of FLN proteins in *D. discoideum* and neutrophils. FLNs are highly conserved actin-crosslinking proteins. In a first part of the study different filamin *D. discoideum* (ddFLN) mutant strains were analyzed in varying cell migration assays. Our results revealed that ddFLN plays a role during *D. discoideum* cell migration and is presumably involved in the maintenance of cortical stabilization. The second part addressed the function of human FLNs in neutrophil-like HL60 cells. We identified FLNa as major isoform in the HL60 cells and found a rather unusual localization of FLNa at the rear of migrating neutrophil-like HL60 cells. Furthermore, FLNa deficiency resulted in a surprisingly subtle phenotype. Knockdown of FLNa had no or only minor effects on cell adhesion and spreading. We detected a FLNa dependent defect in myosin II activation that is responsible for decreased migration speed in 2D and presumably also in 3D. Additionally, FLNa was involved in the regulation of phagocytosis of serum-opsonized bacteria, but had no effect on phagocytosis of serum-opsonized latex beads. Furthermore, coronin 1A was identified as a new FLNa interaction partner.

4.1 DdFLN is important for amoeboid migration.

D. discoideum mutant strains, deficient in different actin-binding domains, including ddFLN, displayed surprisingly subtle phenotypes with no or only minor effects on cell migration (Andre et al., 1989; Brink et al., 1990; Schleicher et al., 1988). A model of redundancy was suggested, in which certain cellular processes are multiply guaranteed (Rivero et al., 1999; Rivero et al., 1996b; Witke et al., 1992). This makes it rather difficult to gain some functional insight into the role of ddFLN during cell motility. Therefore, we created a ddFLN overexpressing strain by expressing a ddFLN-GFP construct in AX2 wild-type cells. Additionally, a strain expressing a truncated ddFLN lacking the ABD (GFP-ddFLN(rod1-6)) was generated. By immunofluorescence and Western blot analysis we determined that in both strains the transformation efficiency was about 95% and the GFP-tagged fusion proteins were expressed at levels two or three times of the levels of endogenous ddFLN protein. Full-length ddFLN-GFP localized at the cortex and at the leading edge of migrating cells in line with previous findings (Condeelis et al., 1988; Lemieux et al., 2014). The truncated GFP-ddFLN(rod1-6) protein exhibited a higher amount of protein within the cytoplasm as the full-length construct, but was also recruited to the cortex and leading edge due to the formation of heterodimers with the endogenous ddFLN protein (Khaire et al., 2007). We verified the presence of heterodimers in t0 and t6 cells using a GFP-trap pull-down and suggest

that the GFP-ddFLN(rod1-6) protein might influence the ddFLN function by acting as a competitive inhibitor.

The first ddFLN null mutant HG1264, generated by nitrosoguanidine treatment in 1990, displayed no effects in cell migration. However, migration was tested only for starved cells in the cAMP-induced chemotaxis with cells crawling on a flat surface under buffer. We revised the role of ddFLN in cell migration and assessed additionally its function in the folic acid-induced chemotaxis under restrictive conditions and in 3D migration. Using the modern evaluation software Imaris allowed a more sophisticated in depth analysis of the migrating cells.

When the function of ddFLN during cAMP-induced chemotaxis was revised using a micropipette assay, we found that in the ddFLN deficient mutant HG1264, migration speed was not significantly changed compared to the AX2 wild-type cells. This finding is highly consistent with previous studies using ddFLN null mutants (Brink et al., 1990; Rivero et al., 1999; Rivero et al., 1996b). Contrary, the ddFLN-GFP as well the GFP-ddFLN(rod1-6) expressing strain revealed significant effects on migration speed. These results suggest strongly that ddFLN plays indeed a role in cAMP-induced chemotaxis und support the model of redundancy. It seems feasible that the compensatory functions of other actin-binding proteins are ineffective after overexpression of full-length or truncated ddFLN proteins. Interestingly, overexpression of the full-length ddFLN resulted in a decrease of speed, whereas expression of the truncated GFP-ddFLN(rod1-6) protein led to an enhancement of speed. Based on these results we propose a role of ddFLN in the stabilization of the cortical actin cytoskeleton. This suggests that overexpression of the full-length protein leads to an increased stiffness of the actin cortex. Mobility of the cells would be restricted due to this more rigid cortex. Conversely, the formation of heterodimers in the GFP-ddFLN(rod1-6) expressing cells might lead to an attenuation of the actin cytoskeleton as the presence of ddFLN dimers with only one ABD would clearly interfere with the ddFLN crosslinking ability. A weakened cell cortex might be able to enhance the mobility of the cells.

In the folic acid chemotaxis under agarose, ddFLN deficiency (HG1264) did not have any influence on speed or directionality of the migrating cells. Overexpression of the full-length ddFLN (ddFLN-GFP) caused under these conditions again a decrease in speed and additionally a significant increase in the directionality was observed. These findings are in agreement with the above discussed hypothesis of an enhanced stiffness of the cell cortex due to the overexpressed ddFLN protein: The more rigid cells were handicapped in their movement under the agarose. At the same time, the overexpressed ddFLN-GFP protein could lead to a stabilization of the leading edge and suppression of lateral pseudopods, thereby mediating a better oriented cell migration.

Interestingly, expression of the truncated GFP-ddFLN(rod1-6) protein resulted also in a reduced speed, but did not have any influence on the directionality. These contradictory effects of the GFP-ddFLN(rod1-6) domain on speed in the cAMP- and folic acid-induced chemotaxis might be due to the fact that both migration modes are regulated by different receptors and signaling pathways.

Additionally, previous studies demonstrated that *D. discoideum* cells, migrating under an agarose overlay, switch to another alternative bleb-driven migration mode or sometimes to a mixture of bleb- and pseudopod-driven motility (Tyson et al., 2014; Zatulovskiy et al., 2014). Blebs are typically rounded smooth protrusions of the plasma membrane and provide a pseudopod-independent mechanism with which certain cells, as tumor cells or *D. discoideum* cells, can mediate the extension of the leading edge (Charras and Paluch, 2008). Blebbing was found to be mediated by Rho-ROCK-myosin and Rac GTPases dependent signaling (Fackler and Grosse, 2008). Interestingly, FLNa deficiency in human melanoma cells M2 resulted in extensive membrane blebbing (Cunningham et al., 1992). Our own results together with a previous study already hinted towards a regulatory role of FLNa in RhoA-mediated myosin activation (Sun et al., 2013). However, analysis of ddFLN null mutant cells revealed no abnormal blebbing behavior but it cannot be excluded that here again compensation by other actin-binding proteins might occur (Langridge and Kay, 2006). In the light of these considerations, it is possible that the decrease in stability of the actin cytoskeleton, mediated by the truncated ddFLN fusion protein interfered with the bleb retraction and thereby detained the migrating cells. The defect in migration in the GFP-ddFLN(rod1-6) expressing cells might be also attributed to a failure in signaling pathways, either specific for folic acid-induced chemotaxis and/or specific for the blebbing-mediated migration mode. As the expression of GFP-ddFLN(rod1-6) resulted in the formation of heterodimers with only one ABD, it is likely that the ABD of ddFLN might mediate interactions, involved in signaling processes in the regulation of migration under these conditions. A very interesting candidate, implicated in such signaling processes, would be the IQGAP related protein GAPA that was shown to interact with the ABD of ddFLN. Moreover, ddFLN was described as a scaffold for an interaction with GAPA and Rac1a that is associated with actin remodeling. DdFLN was also shown to bind to RacB, a protein known to be involved in the regulation of blebbing (Lee et al., 2003; Mondal et al., 2010). Further interaction studies regarding a potential ddFLN-RacB-GAPA association and more in detail analyses of the regulation of bleb-driven migration mode are required to really solve the function of ddFLN in this type of migration.

Apart from the analysis of 2D migration, studies of cell migration within in a 3D environment gain more and more importance, as in many cases 3D matrices are more suitable to mimic the *in vivo* situations. In addition, it was already shown for a number of cell types (tumor cells or immune cells) that migration in 2D often strongly differs from that in 3D (Hazgui et al., 2005; Lämmermann et al., 2008). In this study, a 3D migration assays was established for *D. discoideum* where t6 cells are analyzed in their movement through a collagen matrix in a gradient of cAMP. We verified that the cells migrated indeed in 3D within the matrix and we observed a large portion of the cells moving forward by a bleb-driven migration mode. This finding is consistent with the assumption that bleb-driven migration mode is favored in 3D environments (Fackler and Grosse, 2008). In immunofluorescence analysis within the 3D collagen matrix, ddFLN-GFP was detected in actin rich protrusion at the leading edge as well as at the rear of the migrating cell. Based on this finding, we conclude that the *D. discoideum* cells moved through the collagen matrix using blebs that we could detect in the bright field images and actin rich pseudopods, detected in the fluorescent images. This assumption is in line with the finding that formation of blebs and pseudopods might occur simultaneously and can cooperate during cell migration (Tyson et al., 2014).

Interestingly, ddFLN deficiency resulted indeed in a migration defect under these conditions. The HG1264 strain migrated with a lower speed compared to the wild-type cells whereas the directionality was increased. However, it is noticeable that the observed effects in the HG1264 strain were rather minor. It seems that compensation of other actin-binding proteins did occur but was not sufficient to completely rescue cell motility after loss of ddFLN in the 3D collagen environment. Similar to the results of the under-agarose assays, overexpression of ddFLN (ddFLN-GFP) as well as the expression of the truncated GFP-ddFLN(rod1-6) caused a prominent decrease of speed. As both, 3D migration and migration under an agarose overlay are supposed to induce bleb-driven migration, it seems likely that a similar mechanism might be responsible for the reduced migration speed (Fackler and Grosse, 2008; Zatulovskiy et al., 2014). In the case of the GFP-ddFLN(rod1-6) expressing strain this might be either a defect in blebbing and/or in a signaling pathway. We also think it is conceivable that an increased rigidity of the cell cortex, mediated by the overexpressed ddFLN-GFP, would cause, here too, a diminished motility of the cell. However, in contrast to the increase in directionality for the ddFLN overexpressing cells in the under-agarose assay, both ddFLN-GFP and GFP-ddFLN(rod1-6) cells displayed a strongly disoriented migration in the 3D collagen assay. This decrease in directionality might be caused by defects in chemoattractant sensing induced by expression of the GFP-tagged ddFLN fusion

proteins. It is also possible that the effect on the directionality is attributed to purely mechanical issues as it is possible that cells with a more rigid cortex are no longer able to squeeze themselves through the small mesh sized collagen matrix. Consequently, these cells would migrate preferably through larger gaps, losing thereby their oriented forward movement. This hypothesis might also provide an explanation for the slight increase of directionality in the HG1264 strain: ddFLN deficiency might result in an enhanced elasticity of the cell that could probably account for the reduced migration speed. However, at the same time, these more elastic cells might be able to squeeze themselves through more narrow gaps, which would result in straighter, more oriented motility.

In conclusion, we determined with the help of various migration assays and different ddFLN mutant strains that ddFLN plays indeed a role in cell motility, although the ddFLN null strain (HG1264) exhibited no or only minor motility phenotypes. We found a strong indication for a role of ddFLN in maintenance of a stable cell cortex and the leading edge. Additionally, the results suggest that *D. discoideum* cells use under restrictive conditions (under-agarose assay) and in 3D (collagen assay) an alternative mode of migration than during movement on a 2D surface in buffer (micropipette assay). We detected hints pointing towards a ddFLN function in membrane blebbing and/or signaling during this kind of migration.

4.2 The role of human FLNs in neutrophil-like HL60 cells

The role of FLN proteins was studied in neutrophil-like HL60 cells. Neutrophils are highly motile cells that patrol the blood and interstitium and antagonize invading pathogens. To fulfill this function they need to execute fast-paced processes as adhesion, spreading, migration and phagocytosis. Crucial for this essential task is their ability to undergo rapid and expansive changes in morphology and cell shape which requires the dynamic modulation of F-actin networks by various F-actin binding and signaling proteins. Sensible candidates to be involved in the regulation of neutrophil motility are the FLNs, as numerous studies already identified these proteins as important modulators of spreading, adhesion and locomotion in various cell types (Nakamura et al., 2011; Razinia et al., 2012). Furthermore, it was already shown that FLNa is important in uropod retraction via activation of RhoA and myosin II in primary mouse neutrophils (Sun et al., 2013).

4.2.1 FLNa is the major isoform in HL60 cells.

In a first step, the expression of the three different FLN isoforms was assessed in the HL60 cells. On the transcriptional level, there were indications of a FLNa and FLNb expression, but no hints of a FLNc expression. With our own generated highly specific FLNa and FLNb specific antibodies, FLNa was identified as major isoform in the HL60 cells, while FLNb was only weakly expressed. This finding is highly consistent with the results form primary mouse neutrophils and with a study using the myeloblastic PBL985 cell line, a derivate of the HL60 cell line, indicating that FLNa is the main isoform expressed in neutrophils and neutrophil-like cells (Burande et al., 2009; Sun et al., 2013). Furthermore, FLNa expression was strongly up-regulated during DMSO-induced differentiation. This finding seems rather contrary to a previous study indicating that FLN degradation mediated by ASB2 (specificity subunit of an E3 ubiquitin ligase complex) was crucial for myeloid differentiation in the myeloblastic PBL985 cell line and promyelocytic NB4 cell line (Heuzé et al., 2008). However, FLNa protein was clearly expressed in leukocytes (Boxer et al., 1976; Sun et al., 2013). Therefore, it is convincing that FLNa expression must be restored after termination of the differentiation which might explain the high FLNa expression levels in the differentiated HL60 cells in this study. It is also noticeable that in the study with the myeloblastic PBL985 and promyelocytic NB4 cells, retinoic acid was used to induce the differentiation of the cells into the neutrophil-like state. Furthermore, expression of ASB2, the protein responsible for the degradation of FLNa, was specifically induced by retinoic acid (Heuzé et al., 2008; Kohroki et al., 2001). Therefore, one can conclude that by using DMSO, differentiation of the cells into the neutrophil-like state was induced along other, ASB2 and FLN degradation independent pathways.

Consistent with previous reports, FLNa strongly co-localized with F-actin at the cortex (Stossel et al., 2001). Analysis of FLNa localization during migration by immunofluorescence or by live-cell imaging with cells transiently transfected with a FLNa-GFP construct, revealed a markedly enrichment of FLNa at the rear of the migrating cell. In contrast, various studies reported a localization of FLNa at the leading edge in different cell types for example in the human melanoma cell line A7 (Klaile et al., 2005; Stossel et al., 2001). However, the previous analysis of primary mouse neutrophils pointed also towards a primary function of FLNa at the uropod (Sun et al., 2013). This suggests that FLNa had no influence on the formation and regulation of the leading edge of migrating neutrophils but seemed to be rather involved in uropod related functions.

4.2.2 Influence of FLNa deficiency in HL60 cells on neutrophil functions

In order to investigate the role of FLNa more in detail, FLNa deficient cell lines (subclones C4 and G4) with less than ~5% residual FLNa expression levels were created by shRNA mediated knockdowns. Western blot analysis revealed that the knockdown was stable during differentiation of the cells into the neutrophil-like state.

FLNa deficiency did not affect the FLNb expression level. Intriguingly, loss of FLNa in primary mouse neutrophils led to an up-regulation of FLNb expression. But the general FLNb protein amount in the FLNa knockout mouse neutrophils was still very low, equivalent to only 1.5% of the total FLNa protein amount in the wild-type cells. It is questionable if these very low levels of FLNb protein were able to compensate for the loss of FLNa (Sun et al., 2013). Other studies reported compensation after loss of FLNa expression by other FLN isoforms. However, in these cases, expression of the compensating FLN isoform was either rather high in the first place or was markedly up-regulated (Baldassarre et al., 2009; Sheen et al., 2002). As this was not the case in our analysis, it is most likely that FLNb was not able to simply compensate for the lack of FLNa expression.

FLNa immunofluorescence was an efficient tool to distinguish between knockdown and control cells. Careful comparison of phalloidin staining of FLNa positive control cells with the FLNa negative knockdown cells did not reveal any obvious influence of the FLNa deficiency on the overall organization of the filamentous actin. Although, FLN proteins were shown to be potent F-actin crosslinker that are important for the maintenance of the cortical stability for example in human melanoma cells, other studies already described FLN proteins as dispensable for organization of the filamentous actin networks in other cell types (Cunningham et al., 1992; Feng et al., 2006; Flanagan et al., 2001; Nakamura et al., 2007). We conclude that in the neutrophil-like HL60 cells, FLNa was no longer necessary for F-actin crosslinking, but seemed to adopt several new tasks, perhaps in the regulation of signaling pathways.

When analyzing neutrophil migration, it is important to note that neutrophils not only migrate on a surface (2D migration) but that they also crawl through tissue (3D migration). The mode of migration is considerably different in a 2D or 3D context (Lämmermann et al., 2008). FLNa deficient cells, tested in 2D migration (Zigmond chamber assays) and in 3D migration (collagen assays) displayed in both cases similar effects: Directionality was not affected by the knockdown of FLNa suggesting that the cells were still able to sense the gradient and cell polarization was independent of FLNa. However, speed was significantly reduced in 2D and in 3D migration for both FLNa deficient subclones, especially for the subclone G4. This might be due to the fact that

both subclone cell lines contained slightly different levels of residual FLNa expression suggesting that the exact level of FLNa protein is essential for the regulation of migration. Unfortunately, we failed to quantify the exact amount of residual FLNa expression in the knockdown cell lines. The FLNa expression level in the deficient cells was almost below the detection limit and we were not able to obtain trustworthy measurements with our methods.

In a previous study, knockout of FLNa in mouse neutrophils resulted also in a decrease in speed in Zigmond chamber assays. This migration defect was caused by a reduced RhoA mediated activation of myosin II (Sun et al., 2013). As FLNa was mainly concentrated at the uropod in migrating cells, it seemed likely that a similar mechanism accounted for the observed decreased migration in 2D in the neutrophil-like HL60 cells. Levels of activated myosin II in unstimulated cells were not affected. However, the control cells displayed an increase in myosin II activation after stimulation with fMLP that is accompanied by the phosphorylation of myosin II light chain on Ser19. This enhanced myosin II activation was absent in both FLNa KD cell lines. It is possible that this defect in myosin II activation is also responsible for the decrease in speed in the FLNa deficient cells in the 3D migration. A previous study with dendritic cells already indicated that myosin II was also crucial for migration in 3D. Here it was necessary to mediate the contraction of the cell body that is required by the cell to squeeze itself through narrow gaps within the matrix (Lämmermann et al., 2008).

It is important to note that the effects of the FLNa deficiency were surprisingly subtle in both 2D and 3D migration, in particular in contrast with the previous study using FLNa deficient primary mouse neutrophils (Sun et al., 2013). One cannot exclude that this remote phenotype in the neutrophil-like HL60 cells is due to slight differences in the regulation and functions of human and mouse FLNa although they are both highly homologous. However, it is more likely that the residual FLNa levels in our knockdown cells are able to partly rescue the migration defect, indicating that already low levels of FLNa are sufficient to influence neutrophil migration.

Surprisingly, examination of cell adhesion on fibrinogen and on fibronectin did not reveal a significant influence of FLNa. This finding stands in sharp contrast with previous results, describing a significant increase of adhesion after loss of FLNa in mouse neutrophils and in human myeloblastic PBL985 cells (Lamsoul et al., 2011; Sun et al., 2013). The contradictory results with the HL60 cells might be due to the residual FLNa levels in the knockdown cell lines that might be enough to mediate normal adhesion. It was also shown that FLNa plays an inhibitory role in integrin activation (Calderwood et al., 2001). This would also lead to the

assumption that cells deficient in FLNa might show an increased adhesion due to an enhanced activation of integrins. However, the FLNa KD cells showed a slight reduction of adhesion.

In addition, FLNa deficiency did not have any influence on cell spreading on fibrinogen in mHBSS buffer. However, under conditions with elevated levels of extracellular Ca^{2+} (in adhesion buffer), the cell area of spreading cells was significantly increased in both FLNa KD cell lines compared to control cells. Comparison of measurements of cell area of the control cells under conditions without (mHBSS buffer) and with additional extracellular Ca^{2+} (adhesion buffer) revealed no difference. Based on these findings, FLNa seemed not to be required for the process of cell spreading itself but might be more involved in regulation of signaling. Indeed there are already evidences that FLNa plays a role in modulation of the activity of Ca^{2+} sensing and Ca^{2+} permeable receptors. Additionally, it was shown to be required for dampening potentially lethal Ca^{2+} influx through stretch-activated Ca^{2+} permeable channels (Glogauer et al., 1998; Zhang and Breitwieser, 2005). Nevertheless, it is crucial to note that here again the effect of FLNa KD was rather low and turned out to be very short-termed. It is also important to point out that other studies describe a crucial function of FLNa in regulation of cell spreading by a clearly integrin-dependent manner, for example in HEK293 cells (Kim et al., 2008). This study however, failed to identify a comparable function in the neutrophil-like HL60 cells and suggests that FLNa operates in an integrin-independent manner in neutrophil adhesion and spreading.

Another important function of neutrophils is the phagocytosis. A participation of FLN proteins in this process was not described so far for mammalian phagocytes. In immunofluorescence studies of differentiated HL60 cells phagocytosing serum-opsonized latex beads, a strong recruitment of FLNa to the phagocytic cup was detected, indicating that FLNa indeed is associated with the process of phagocytosis. In experiments with serum-opsonized GFP-expressing bacteria, phagocytosis was significantly reduced in both FLNa deficient strains. However, in subsequent experiments with serum-opsonized latex beads, we failed to detect a diminished phagocytosis in the FLNa KD cells. This might hint towards a role of FLNa, not in complement-mediated recognition of pathogens via Fc-receptors and complement receptors but rather in the pattern recognition receptor (PRR) mediated phagocytosis (Thomas and Schroder, 2013; Vidarsson and van de Winkel, 1998). Both the bacteria and the latex beads were serum-opsonized but only in case of the bacteria, where additional invariant structural motifs (pathogen-associated molecular patterns, PAMPs) are available for recognition through phagocytes, phagocytosis was affected by FLNa deficiency. This might also explain the rather subtle effect of the FLNa KD on phagocytosis of serum-opsonized bacteria (decrease was not

above 20%): Although the PRR mediated phagocytosis was disrupted, the complement mediated pathway was still intact.

In conclusion, this study showed, in line with previous findings, a FLNa dependent defect in myosin II activation that is responsible for decreased migration speed in 2D and presumably also in 3D (Sun et al., 2013). FLNa seemed to be rather dispensable for the process of adhesion and cell spreading. However, there were hints pointing towards a role of FLNa in Ca^{2+} signaling during cell spreading. Additionally, we determined a novel role of FLNa in phagocytosis, perhaps in the PRR-mediated recognition of pathogens. Of course, one has to consider the possibility that the residual levels of FLNa expressed in the knockdown cells or even the very remotely expressed FLNb might be able to partly rescue the effects of the FLNa deficiency. One should draw attention to the fact that the inhibitory interaction of FLN with the cytoplasmic tails of various β integrins was already shown to be important for adhesion, spreading and migration processes in diverse cell types (Calderwood et al., 2001; Das et al., 2011; Takala et al., 2008). In contrast, we could not detect any indications of an influence of the FLNa protein on integrin dependent functions in the FLNa deficient neutrophil-like HL60 cells. Interestingly, several studies clearly identified FLNs as mechanoprotective proteins that were recruited to the cytoplasmic tails of β_2 integrins after the application of mechanical force (Chen et al., 2009; D'Addario et al., 2001; Razinia et al., 2012). We therefore want to raise the possibility that FLNa-integrin interaction might be initiated only under shear stress conditions in neutrophil-like HL60 cells, which might explain why FLNa seemed to execute rather minor functions in static environments. Intriguingly, a similar situation was already described for another neutrophil actin-binding protein, the mammalian actin-binding protein 1 (mAbp1) (Hepper et al., 2012).

4.2.3 FLNa interacts with coronin 1A.

The present study clearly argued for a role of FLNa not in F-actin crosslinking, but rather as a signaling and scaffolding protein. Therefore, we set out to identify new FLNa interaction partners in the neutrophil-like HL60 cells. With the help of pull-down assays coronin 1A was identified as FLNa interacting protein by mass spectrometry and Western blotting. Mammalian coronins are another family of highly conserved actin-binding proteins which consists of 7 members. Coronin 1A (also known as coronin 1, p57 or TACO for tryptophan aspartate-containing coat protein) is leukocyte specific and very abundant in neutrophils (Moriceau et al., 2009; Pieters, 2008). Despite this high coronin 1A expression level, the exact role and function of coronins in neutrophils appear rather unclear. Analysis of human neutrophils, transduced with a dominant

negative coronin 1A fragment revealed a role of coronin 1A in chemotaxis, adhesion, spreading and phagocytosis (Yan et al., 2007). However, in a subsequent study using primary neutrophils of coronin $1A^{-/-}$ mice, adhesion, spreading, chemotaxis and phagocytosis was not affected, indicating that coronin 1A was dispensable for F-actin mediated processes in neutrophils (Combaluzier and Pieters, 2009). Additionally, coronin 1A was described to have antiapoptotic activity in neutrophil-like PLB985 cells and was found to associate with NADPH oxidase in primary neutrophils (Grogan et al., 1997; Moriceau et al., 2009).

We were able to determine the repeats 9 to 18 as the FLNa domain responsible for the interaction with coronin 1A. Intriguingly, a second actin-binding domain was identified within this FLNa region (Nakamura et al., 2007). However, we verified that the FLNa-coronin 1A interaction was not mediated by binding of both proteins to F-actin as only the most N-terminal FLNa fragment (FLNa(ABD-8)) was able to precipitate with actin. The fact that only FLNa repeats 9 to 18 are involved in coronin 1A binding was rather surprising, as most of the FLNa interactions described so far, for example with integrins, small GTPases and certain GEFs and GAPs, occur with the more C-terminal part within the repeats 19 to 24, the region not involved in F-actin binding (Zhou et al., 2010). Only a small number of proteins were identified to interact with the FLNa repeats 9 to 18, among them furin, CD28 and the tumor necrosis factor receptor-associated factor ½ (Arron et al., 2002; Liu et al., 1997; Tavano et al., 2006). Another interesting binding partner in this region is the Ca^{2+} sensing receptor (CaR) that interacts with the FLNa repeats 14 to 16 (Awata et al., 2001). We already speculated about a role of FLNa in the regulation of Ca^{2+} signaling in the context of cell spreading. Additionally coronin 1A was also shown to be involved in Ca^{2+} dependent regulation of T cell survival (Mueller et al., 2008). Therefore, it is tempting to propose a joint role of FLNa and coronin 1A in regulating Ca^{2+} signaling pathways in neutrophils, but verifying this hypothesis needs further examination.

Unfortunately, we failed to perform direct protein-protein interaction studies with recombinant FLAG-FLNa and GST-coronin 1A due to the high insolubility of coronin 1A (Yan et al., 2007). Therefore, it is important to note that we were not able to determine if FLNa interacts either directly with coronin 1A or if this interaction is indirect, probably in the context of a multi-protein signaling complex.

Nevertheless we tried to gain first insights into the functional relevance of the FLNa-coronin 1A interaction. Therefore, the localization of both proteins during different cellular processes was analyzed. In migrating cells, stimulated with fMLP, FLNa was recruited more to the uropod, but coronin 1A to the leading edge as previously described (Yan et al., 2007). Hence, it seems

unlikely that a FLNa-coronin 1A interaction is of great significance for this process. In contrast, examination of spreading cells revealed a strong co-localization of FLNa and coronin 1A at the cell cortex. Additionally, we detected a co-localization of FLNa with coronin 1A at the phagocytic cup of a cell engulfing serum-opsonized latex beads. These findings might point towards a collective function of both proteins during cell spreading and phagocytosis.

By mass spectrometry analysis, additional potential FLNa interaction partners were identified in the neutrophil-like HL60 cells, among them CLIP-170 and DOCK11. CLIP-170 (cytoplasmic linker protein of 170 kDa) is a microtubule plus end binding protein that regulates microtubule dynamics, and is involved in the regulation of spreading and phagocytosis in macrophages (Binker et al., 2007; Maekawa and Schiebel, 2004). Furthermore, an interaction of FLNa and CLIP-170 was already described in fibroblasts. Both proteins were recruited to focal adhesion and CLIP-170 was suggested to mediate interaction of the microtubule and actin systems via FLNa after the application of tensile forces (D'Addario et al., 2003). In contrast, not much is known about DOCK11 (dedicator of cytokinesis or zizimin2). DOCK11 is a Cdc42 specific GEF that is expressed in lymphoid organs. In dendritic cells, DOCK11 was shown to be involved in the regulation of filopodia (Lin et al., 2006; Sakabe et al., 2012). Further interaction studies are required to investigate the presence and functional relevance of a FLNa interaction with either DOCK11 or CLIP-170.

References

Akashi, K., D. Traver, T. Miyamoto, and I.L. Weissman. 2000. A clonogenic common myeloid progenitor that gives rise to all myeloid lineages. *Nature*. 404:193-197.

Andre, E., M. Brink, G. Gerisch, G. Isenberg, A. Noegel, M. Schleicher, J.E. Segall, and E. Wallraff. 1989. A Dictyostelium mutant deficient in severin, an F-actin fragmenting protein, shows normal motility and chemotaxis. *J Cell Biol*. 108:985-995.

Annesley, S.J., E. Bandala-Sanchez, A.U. Ahmed, and P.R. Fisher. 2007. Filamin repeat segments required for photosensory signalling in Dictyostelium discoideum. *BMC Cell Biol*. 8:48.

Arron, J.R., Y. Pewzner-Jung, M.C. Walsh, T. Kobayashi, and Y. Choi. 2002. Regulation of the subcellular localization of tumor necrosis factor receptor-associated factor (TRAF)2 by TRAF1 reveals mechanisms of TRAF2 signaling. *J Exp Med*. 196:923-934.

Artemenko, Y., T.J. Lampert, and P.N. Devreotes. 2014. Moving towards a paradigm: common mechanisms of chemotactic signaling in Dictyostelium and mammalian leukocytes. *Cell Mol Life Sci*. 71:3711-3747.

Awata, H., C. Huang, M.E. Handlogten, and R.T. Miller. 2001. Interaction of the calcium-sensing receptor and filamin, a potential scaffolding protein. *J Biol Chem*. 276:34871-34879.

Bagorda, A., V.A. Mihaylov, and C.A. Parent. 2006. Chemotaxis: moving forward and holding on to the past. *Thromb Haemost*. 95:12-21.

Baldassarre, M., Z. Razinia, C.F. Burande, I. Lamsoul, P.G. Lutz, and D.A. Calderwood. 2009. Filamins regulate cell spreading and initiation of cell migration. *PLoS One*. 4:e7830.

Bandala-Sanchez, E., S.J. Annesley, and P.R. Fisher. 2006. A phototaxis signalling complex in Dictyostelium discoideum. *Eur J Cell Biol*. 85:1099-1106.

Barry, N.P., and M.S. Bretscher. 2010. Dictyostelium amoebae and neutrophils can swim. *Proc Natl Acad Sci U S A*. 107:11376-11380.

Bastounis, E., R. Meili, B. Alvarez-Gonzalez, J. Francois, J.C. del Alamo, R.A. Firtel, and J.C. Lasheras. 2014. Both contractile axial and lateral traction force dynamics drive amoeboid cell motility. *J Cell Biol*. 204:1045-1061.

Bechtel, P.J. 1979. Identification of a high molecular weight actin-binding protein in skeletal muscle. *J Biol Chem*. 254:1755-1758.

Bellanger, J.M., C. Astier, C. Sardet, Y. Ohta, T.P. Stossel, and A. Debant. 2000. The Rac1- and RhoG-specific GEF domain of Trio targets filamin to remodel cytoskeletal actin. *Nat Cell Biol*. 2:888-892.

Binker, M.G., D.Y. Zhao, S.J. Pang, and R.E. Harrison. 2007. Cytoplasmic linker protein-170 enhances spreading and phagocytosis in activated macrophages by stabilizing microtubules. *J Immunol*. 179:3780-3791.

Birnie, G.D. 1988. The HL60 cell line: a model system for studying human myeloid cell differentiation. *Br J Cancer Suppl*. 9:41-45.

Borregaard, N., and J.B. Cowland. 1997. Granules of the human neutrophilic polymorphonuclear leukocyte. *Blood*. 89:3503-3521.

Boxer, L.A., S. Richardson, and A. Floyd. 1976. Identification of actin-binding protein in membrane of polymorphonuclear leukocytes. *Nature*. 263:249-251.

Brink, M., G. Gerisch, G. Isenberg, A.A. Noegel, J.E. Segall, E. Wallraff, and M. Schleicher. 1990. A Dictyostelium mutant lacking an F-actin cross-linking protein, the 120-kD gelation factor. *J Cell Biol*. 111:1477-1489.

Brinkmann, V., U. Reichard, C. Goosmann, B. Fauler, Y. Uhlemann, D.S. Weiss, Y. Weinrauch, and A. Zychlinsky. 2004. Neutrophil extracellular traps kill bacteria. *Science*. 303:1532-1535.

Burande, C.F., M.L. Heuze, I. Lamsoul, B. Monsarrat, S. Uttenweiler-Joseph, and P.G. Lutz. 2009. A label-free quantitative proteomics strategy to identify E3 ubiquitin ligase substrates targeted to proteasome degradation. *Mol Cell Proteomics*. 8:1719-1727.

Cai, H., and P.N. Devreotes. 2011. Moving in the right direction: how eukaryotic cells migrate along chemical gradients. *Semin Cell Dev Biol*. 22:834-841.

Calderwood, D.A., A. Huttenlocher, W.B. Kiosses, D.M. Rose, D.G. Woodside, M.A. Schwartz, and M.H. Ginsberg. 2001. Increased filamin binding to beta-integrin cytoplasmic domains inhibits cell migration. *Nat Cell Biol*. 3:1060-1068.

Calderwood, D.A., S.J. Shattil, and M.H. Ginsberg. 2000. Integrins and actin filaments: reciprocal regulation of cell adhesion and signaling. *J Biol Chem*. 275:22607-22610.

Carrigan, S.O., A.L. Weppler, A.C. Issekutz, and A.W. Stadnyk. 2005. Neutrophil differentiated HL-60 cells model Mac-1 (CD11b/CD18)-independent neutrophil transepithelial migration. *Immunology*. 115:108-117.

Charras, G., and E. Paluch. 2008. Blebs lead the way: how to migrate without lamellipodia. *Nat Rev Mol Cell Biol*. 9:730-736.

Chen, H.S., K.S. Kolahi, and M.R. Mofrad. 2009. Phosphorylation facilitates the integrin binding of filamin under force. *Biophys J*. 97:3095-3104.

Chisholm, R.L., and R.A. Firtel. 2004. Insights into morphogenesis from a simple developmental system. *Nat Rev Mol Cell Biol*. 5:531-541.

Chung, C.Y., S. Lee, C. Briscoe, C. Ellsworth, and R.A. Firtel. 2000. Role of Rac in controlling the actin cytoskeleton and chemotaxis in motile cells. *Proc Natl Acad Sci U S A*. 97:5225-5230.

Chung, C.Y., G. Potikyan, and R.A. Firtel. 2001. Control of cell polarity and chemotaxis by Akt/PKB and PI3 kinase through the regulation of PAKa. *Mol Cell*. 7:937-947.

Collins, S.J. 1987. The HL-60 promyelocytic leukemia cell line: proliferation, differentiation, and cellular oncogene expression. *Blood*. 70:1233-1244.

Collins, S.J., R.C. Gallo, and R.E. Gallagher. 1977. Continuous growth and differentiation of human myeloid leukaemic cells in suspension culture. *Nature*. 270:347-349.

Collins, S.J., F.W. Ruscetti, R.E. Gallagher, and R.C. Gallo. 1978. Terminal differentiation of human promyelocytic leukemia cells induced by dimethyl sulfoxide and other polar compounds. *Proc Natl Acad Sci U S A*. 75:2458-2462.

Combaluzier, B., and J. Pieters. 2009. Chemotaxis and phagocytosis in neutrophils is independent of coronin 1. *J Immunol*. 182:2745-2752.

Condeelis, J., A. Hall, A. Bresnick, V. Warren, R. Hock, H. Bennett, and S. Ogihara. 1988. Actin polymerization and pseudopod extension during amoeboid chemotaxis. *Cell Motil Cytoskeleton*. 10:77-90.

Cox, D., J. Condeelis, D. Wessels, D. Soll, H. Kern, and D.A. Knecht. 1992. Targeted disruption of the ABP-120 gene leads to cells with altered motility. *J Cell Biol*. 116:943-955.

Cox, D., D. Wessels, D.R. Soll, J. Hartwig, and J. Condeelis. 1996. Re-expression of ABP-120 rescues cytoskeletal, motility, and phagocytosis defects of ABP-120- Dictyostelium mutants. *Mol Biol Cell*. 7:803-823.

Cunningham, C.C., J.B. Gorlin, D.J. Kwiatkowski, J.H. Hartwig, P.A. Janmey, H.R. Byers, and T.P. Stossel. 1992. Actin-binding protein requirement for cortical stability and efficient locomotion. *Science*. 255:325-327.

D'Addario, M., P.D. Arora, R.P. Ellen, and C.A. McCulloch. 2003. Regulation of tension-induced mechanotranscriptional signals by the microtubule network in fibroblasts. *J Biol Chem*. 278:53090-53097.

D'Addario, M., P.D. Arora, J. Fan, B. Ganss, R.P. Ellen, and C.A. McCulloch. 2001. Cytoprotection against mechanical forces delivered through beta 1 integrins requires induction of filamin A. *J Biol Chem*. 276:31969-31977.

Dagert, M., and S.D. Ehrlich. 1979. Prolonged incubation in calcium chloride improves the competence of Escherichia coli cells. *Gene*. 6:23-28.

Das, M., S.S. Ithychanda, J. Qin, and E.F. Plow. 2011. Migfilin and filamin as regulators of integrin activation in endothelial cells and neutrophils. *PLoS One*. 6:e26355.

Del Valle-Perez, B., V.G. Martinez, C. Lacasa-Salavert, A. Figueras, S.S. Shapiro, T. Takafuta, O. Casanovas, G. Capella, F. Ventura, and F. Vinals. 2010. Filamin B plays a key role in vascular endothelial growth factor-induced endothelial cell motility through its interaction with Rac-1 and Vav-2. *J Biol Chem*. 285:10748-10760.

Devreotes, P.N., and S.H. Zigmond. 1988. Chemotaxis in eukaryotic cells: a focus on leukocytes and Dictyostelium. *Annu Rev Cell Biol*. 4:649-686.

Eichinger, L., B. Köppel, A.A. Noegel, M. Schleicher, M. Schliwa, K. Weijer, W. Witke, and P.A. Janmey. 1996. Mechanical perturbation elicits a phenotypic difference between Dictyostelium wild-type cells and cytoskeletal mutants. *Biophys J*. 70:1054-1060.

Eichinger, L., S.S. Lee, and M. Schleicher. 1999. Dictyostelium as model system for studies of the actin cytoskeleton by molecular genetics. *Microsc Res Tech*. 47:124-134.

Eichinger, L., J.A. Pachebat, G. Glockner, M.A. Rajandream, R. Sucgang, M. Berriman, J. Song, R. Olsen, K. Szafranski, Q. Xu, B. Tunggal, S. Kummerfeld, M. Madera, B.A. Konfortov, F. Rivero, A.T.

Bankier, R. Lehmann, N. Hamlin, R. Davies, P. Gaudet, P. Fey, K. Pilcher, G. Chen, D. Saunders, E. Sodergren, P. Davis, A. Kerhornou, X. Nie, N. Hall, C. Anjard, L. Hemphill, N. Bason, P. Farbrother, B. Desany, E. Just, T. Morio, R. Rost, C. Churcher, J. Cooper, S. Haydock, N. van Driessche, A. Cronin, I. Goodhead, D. Muzny, T. Mourier, A. Pain, M. Lu, D. Harper, R. Lindsay, H. Hauser, K. James, M. Quiles, M. Madan Babu, T. Saito, C. Buchrieser, A. Wardroper, M. Felder, M. Thangavelu, D. Johnson, A. Knights, H. Loulseged, K. Mungall, K. Oliver, C. Price, M.A. Quail, H. Urushihara, J. Hernandez, E. Rabbinowitsch, D. Steffen, M. Sanders, J. Ma, Y. Kohara, S. Sharp, M. Simmonds, S. Spiegler, A. Tivey, S. Sugano, B. White, D. Walker, J. Woodward, T. Winckler, Y. Tanaka, G. Shaulsky, M. Schleicher, G. Weinstock, A. Rosenthal, E.C. Cox, R.L. Chisholm, R. Gibbs, W.F. Loomis, M. Platzer, R.R. Kay, J. Williams, P.H. Dear, A.A. Noegel, B. Barrell, and A. Kuspa. 2005. The genome of the social amoeba Dictyostelium discoideum. *Nature*. 435:43-57.

Esue, O., Y. Tseng, and D. Wirtz. 2009. Alpha-actinin and filamin cooperatively enhance the stiffness of actin filament networks. *PLoS One*. 4:e4411.

Fackler, O.T., and R. Grosse. 2008. Cell motility through plasma membrane blebbing. *J Cell Biol*. 181:879-884.

Faix, J., C. Clougherty, A. Konzok, U. Mintert, J. Murphy, R. Albrecht, B. Muhlbauer, and J. Kuhlmann. 1998. The IQGAP-related protein DGAP1 interacts with Rac and is involved in the modulation of the F-actin cytoskeleton and control of cell motility. *J Cell Sci*. 111 (Pt 20):3059-3071.

Faix, J., L. Kreppel, G. Shaulsky, M. Schleicher, and A.R. Kimmel. 2004. A rapid and efficient method to generate multiple gene disruptions in Dictyostelium discoideum using a single selectable marker and the Cre-loxP system. *Nucleic Acids Res*. 32:e143.

Faix, J., M. Steinmetz, H. Boves, R.A. Kammerer, F. Lottspeich, U. Mintert, J. Murphy, A. Stock, U. Aebi, and G. Gerisch. 1996. Cortexillins, major determinants of cell shape and size, are actin-bundling proteins with a parallel coiled-coil tail. *Cell*. 86:631-642.

Feng, Y., M.H. Chen, I.P. Moskowitz, A.M. Mendonza, L. Vidali, F. Nakamura, D.J. Kwiatkowski, and C.A. Walsh. 2006. Filamin A (FLNA) is required for cell-cell contact in vascular development and cardiac morphogenesis. *Proc Natl Acad Sci U S A*. 103:19836-19841.

Feng, Y., and C.A. Walsh. 2004. The many faces of filamin: a versatile molecular scaffold for cell motility and signalling. *Nat Cell Biol*. 6:1034-1038.

Fisher, P.R., A.A. Noegel, M. Fechheimer, F. Rivero, J. Prassler, and G. Gerisch. 1997. Photosensory and thermosensory responses in Dictyostelium slugs are specifically impaired by absence of the F-actin cross-linking gelation factor (ABP-120). *Curr Biol*. 7:889-892.

Flanagan, L.A., J. Chou, H. Falet, R. Neujahr, J.H. Hartwig, and T.P. Stossel. 2001. Filamin A, the Arp2/3 complex, and the morphology and function of cortical actin filaments in human melanoma cells. *J Cell Biol*. 155:511-517.

Fleck, R.A., S. Romero-Steiner, and M.H. Nahm. 2005. Use of HL-60 cell line to measure opsonic capacity of pneumococcal antibodies. *Clin Diagn Lab Immunol*. 12:19-27.

Fox, J.W., E.D. Lamperti, Y.Z. Eksioglu, S.E. Hong, Y. Feng, D.A. Graham, I.E. Scheffer, W.B. Dobyns, B.A. Hirsch, R.A. Radtke, S.F. Berkovic, P.R. Huttenlocher, and C.A. Walsh. 1998. Mutations in filamin 1 prevent migration of cerebral cortical neurons in human periventricular heterotopia. *Neuron*. 21:1315-1325.

Friedl, P., S. Borgmann, and E.B. Bröcker. 2001. Amoeboid leukocyte crawling through extracellular matrix: lessons from the Dictyostelium paradigm of cell movement. *J Leukoc Biol*. 70:491-509.

Friedl, P., and K. Wolf. 2010. Plasticity of cell migration: a multiscale tuning model. *J Cell Biol*. 188:11-19.

Fucini, P., B. Koppel, M. Schleicher, A. Lustig, T.A. Holak, R. Muller, M. Stewart, and A.A. Noegel. 1999. Molecular architecture of the rod domain of the Dictyostelium gelation factor (ABP120). *J Mol Biol*. 291:1017-1023.

Fucini, P., A.J. McCoy, M. Gomez-Ortiz, M. Schleicher, A.A. Noegel, and M. Stewart. 1997a. Crystallization and preliminary X-Ray diffraction characterization of a dimerizing fragment of the rod domain of the Dictyostelium gelation factor (ABP-120). *J Struct Biol*. 120:192-195.

Fucini, P., C. Renner, C. Herberhold, A.A. Noegel, and T.A. Holak. 1997b. The repeating segments of the F-actin cross-linking gelation factor (ABP-120) have an immunoglobulin-like fold. *Nat Struct Biol*. 4:223-230.

Furuike, S., T. Ito, and M. Yamazaki. 2001. Mechanical unfolding of single filamin A (ABP-280) molecules detected by atomic force microscopy. *FEBS Lett*. 498:72-75.

Glogauer, M., P. Arora, D. Chou, P.A. Janmey, G.P. Downey, and C.A. McCulloch. 1998. The role of actin-binding protein 280 in integrin-dependent mechanoprotection. *J Biol Chem*. 273:1689-1698.

Grogan, A., E. Reeves, N. Keep, F. Wientjes, N.F. Totty, A.L. Burlingame, J.J. Hsuan, and A.W. Segal. 1997. Cytosolic phox proteins interact with and regulate the assembly of coronin in neutrophils. *J Cell Sci*. 110 (Pt 24):3071-3081.

Han, J.W., L. Leeper, F. Rivero, and C.Y. Chung. 2006. Role of RacC for the regulation of WASP and phosphatidylinositol 3-kinase during chemotaxis of Dictyostelium. *J Biol Chem*. 281:35224-35234.

Hartwig, J.H., and T.P. Stossel. 1975. Isolation and properties of actin, myosin, and a new actinbinding protein in rabbit alveolar macrophages. *J Biol Chem*. 250:5696-5705.

Hauert, A.B., S. Martinelli, C. Marone, and V. Niggli. 2002. Differentiated HL-60 cells are a valid model system for the analysis of human neutrophil migration and chemotaxis. *Int J Biochem Cell Biol*. 34:838-854.

Hazgui, S., N. Bonnet, J. Cutrona, B. Nawrocki-Raby, M. Polette, L. Chouchane, P. Birembaut, and J.M. Zahm. 2005. 3D culture model and computer-assisted videomicroscopy to analyze migratory behavior of noninvasive and invasive bronchial epithelial cells. *Am J Physiol Cell Physiol*. 289:C1547-1552.

Hepper, I., J. Schymeinsky, L.T. Weckbach, S.M. Jakob, D. Frommhold, M. Sixt, M. Laschinger, M. Sperandio, and B. Walzog. 2012. The mammalian actin-binding protein 1 is critical for spreading and intraluminal crawling of neutrophils under flow conditions. *J Immunol*. 188:4590-4601.

Heuzé, M.L., I. Lamsoul, M. Baldassarre, Y. Lad, S. Leveque, Z. Razinia, C. Moog-Lutz, D.A. Calderwood, and P.G. Lutz. 2008. ASB2 targets filamins A and B to proteasomal degradation. *Blood*. 112:5130-5140.

Higgs, H.N., and T.D. Pollard. 1999. Regulation of actin polymerization by Arp2/3 complex and WASp/Scar proteins. *J Biol Chem*. 274:32531-32534.

Ithychanda, S.S., M. Das, Y.Q. Ma, K. Ding, X. Wang, S. Gupta, C. Wu, E.F. Plow, and J. Qin. 2009. Migfilin, a molecular switch in regulation of integrin activation. *J Biol Chem*. 284:4713-4722.

Jacob, C., M. Leport, C. Szilagyi, J.M. Allen, C. Bertrand, and V. Lagente. 2002. DMSO-treated HL60 cells: a model of neutrophil-like cells mainly expressing PDE4B subtype. *Int Immunopharmacol*. 2:1647-1656.

Janssen, K.P., L. Eichinger, P.A. Janmey, A.A. Noegel, M. Schliwa, W. Witke, and M. Schleicher. 1996. Viscoelastic properties of F-actin solutions in the presence of normal and mutated actin-binding proteins. *Arch Biochem Biophys*. 325:183-189.

Jin, T., X. Xu, J. Fang, N. Isik, J. Yan, J.A. Brzostowski, and D. Hereld. 2009. How human leukocytes track down and destroy pathogens: lessons learned from the model organism Dictyostelium discoideum. *Immunol Res*. 43:118-127.

John Condeelis, S.G., Maryanne Vahey. 1982. Isolation of a new actin-binding protein from Dictyostelium discoideum. *Cell Motility*. 2:273-285.

Johnston, J.J., P. Rintels, J. Chung, J. Sather, E.J. Benz, Jr., and N. Berliner. 1992. Lactoferrin gene promoter: structural integrity and nonexpression in HL60 cells. *Blood*. 79:2998-3006.

Kanters, E., J. van Rijssel, P.J. Hensbergen, D. Hondius, F.P. Mul, A.M. Deelder, A. Sonnenberg, J.D. van Buul, and P.L. Hordijk. 2008. Filamin B mediates ICAM-1-driven leukocyte transendothelial migration. *J Biol Chem*. 283:31830-31839.

Kasza, K.E., F. Nakamura, S. Hu, P. Kollmannsberger, N. Bonakdar, B. Fabry, T.P. Stossel, N. Wang, and D.A. Weitz. 2009. Filamin A is essential for active cell stiffening but not passive stiffening under external force. *Biophys J*. 96:4326-4335.

Kesner, B.A., S.L. Milgram, B.R. Temple, and N.V. Dokholyan. 2010. Isoform divergence of the filamin family of proteins. *Mol Biol Evol*. 27:283-295.

Kessin, R.H. 2001. Dictyostelium: Evolution, Cell Biology, and the Development of Multicellularity. Cambridge University Press, Cambridge, UK.

Khaire, N., R. Müller, R. Blau-Wasser, L. Eichinger, M. Schleicher, M. Rief, T.A. Holak, and A.A. Noegel. 2007. Filamin-regulated F-actin assembly is essential for morphogenesis and controls phototaxis in Dictyostelium. *J Biol Chem*. 282:1948-1955.

Kiema, T., Y. Lad, P. Jiang, C.L. Oxley, M. Baldassarre, K.L. Wegener, I.D. Campbell, J. Ylänne, and D.A. Calderwood. 2006. The molecular basis of filamin binding to integrins and competition with talin. *Mol Cell*. 21:337-347.

Kim, C., C.C. Marchal, J. Penninger, and M.C. Dinauer. 2003. The hemopoietic Rho/Rac guanine nucleotide exchange factor Vav1 regulates N-formyl-methionyl-leucyl-phenylalanine-activated neutrophil functions. *J Immunol*. 171:4425-4430.

Kim, H., F. Nakamura, W. Lee, C. Hong, D. Perez-Sala, and C.A. McCulloch. 2010. Regulation of cell adhesion to collagen via beta1 integrins is dependent on interactions of filamin A with vimentin and protein kinase C epsilon. *Exp Cell Res*. 316:1829-1844.

Kim, H., A. Sengupta, M. Glogauer, and C.A. McCulloch. 2008. Filamin A regulates cell spreading and survival via beta1 integrins. *Exp Cell Res*. 314:834-846.

Klaile, E., M.M. Müller, C. Kannicht, B.B. Singer, and L. Lucka. 2005. CEACAM1 functionally interacts with filamin A and exerts a dual role in the regulation of cell migration. *J Cell Sci*. 118:5513-5524.

Klinker, J.F., K. Wenzel-Seifert, and R. Seifert. 1996. G-protein-coupled receptors in HL-60 human leukemia cells. *Gen Pharmacol*. 27:33-54.

Kohroki, J., S. Fujita, N. Itoh, Y. Yamada, H. Imai, N. Yumoto, T. Nakanishi, and K. Tanaka. 2001. ATRA-regulated Asb-2 gene induced in differentiation of HL-60 leukemia cells. *FEBS Lett*. 505:223-228.

Kolaczkowska, E., and P. Kubes. 2013. Neutrophil recruitment and function in health and inflammation. *Nat Rev Immunol*. 13:159-175.

Kolahi, K.S., and M.R. Mofrad. 2008. Molecular mechanics of filamin's rod domain. *Biophys J*. 94:1075-1083.

Kovacevic, I., and E.J. Cram. 2010. FLN-1/filamin is required for maintenance of actin and exit of fertilized oocytes from the spermatheca in C. elegans. *Dev Biol*. 347:247-257.

Kruger, P., M. Saffarzadeh, A.N. Weber, N. Rieber, M. Radsak, H. von Bernuth, C. Benarafa, D. Roos, J. Skokowa, and D. Hartl. 2015. Neutrophils: Between Host Defence, Immune Modulation, and Tissue Injury. *PLoS Pathog*. 11:e1004651.

Kuspa, A., T. Dingermann, and W. Nellen. 1995. Analysis of gene function in Dictyostelium. *Experientia*. 51:1116-1123.

Lad, Y., P. Jiang, S. Ruskamo, D.S. Harburger, J. Ylanne, I.D. Campbell, and D.A. Calderwood. 2008. Structural basis of the migfilin-filamin interaction and competition with integrin beta tails. *J Biol Chem*. 283:35154-35163.

Laemmli, U.K. 1970. Cleavage of structural proteins during the assembly of the head of bacteriophage T4. *Nature*. 227:680-685.

Laevsky, G., and D.A. Knecht. 2001. Under-agarose folate chemotaxis of Dictyostelium discoideum amoebae in permissive and mechanically inhibited conditions. *Biotechniques*. 31:1140-1142, 1144, 1146-1149.

Lämmermann, T., B.L. Bader, S.J. Monkley, T. Worbs, R. Wedlich-Soldner, K. Hirsch, M. Keller, R. Forster, D.R. Critchley, R. Fassler, and M. Sixt. 2008. Rapid leukocyte migration by integrin-independent flowing and squeezing. *Nature*. 453:51-55.

Lämmermann, T., and R.N. Germain. 2014. The multiple faces of leukocyte interstitial migration. *Semin Immunopathol*. 36:227-251.

Lamsoul, I., C.F. Burande, Z. Razinia, T.C. Houles, D. Menoret, M. Baldassarre, M. Erard, C. Moog-Lutz, D.A. Calderwood, and P.G. Lutz. 2011. Functional and structural insights into ASB2alpha, a novel regulator of integrin-dependent adhesion of hematopoietic cells. *J Biol Chem*. 286:30571-30581.

Langereis, J.D. 2013. Neutrophil integrin affinity regulation in adhesion, migration, and bacterial clearance. *Cell Adh Migr*. 7:476-481.

Langridge, P.D., and R.R. Kay. 2006. Blebbing of Dictyostelium cells in response to chemoattractant. *Exp Cell Res*. 312:2009-2017.

Larsson, J., and S. Karlsson. 2005. The role of Smad signaling in hematopoiesis. *Oncogene*. 24:5676-5692.

Lee, E., D.J. Seastone, E. Harris, J.A. Cardelli, and D.A. Knecht. 2003. RacB regulates cytoskeletal function in Dictyostelium spp. *Eukaryot Cell*. 2:474-485.

Lemieux, M.G., D. Janzen, R. Hwang, J. Roldan, I. Jarchum, and D.A. Knecht. 2014. Visualization of the actin cytoskeleton: different F-actin-binding probes tell different stories. *Cytoskeleton (Hoboken)*. 71:157-169.

Ley, K., C. Laudanna, M.I. Cybulsky, and S. Nourshargh. 2007. Getting to the site of inflammation: the leukocyte adhesion cascade updated. *Nat Rev Immunol*. 7:678-689.

Li, K.W., S.M. Turner, C.L. Emson, M.K. Hellerstein, and D.C. Dale. 2011. Deuterium and neutrophil kinetics. *Blood*. 117:6052-6053; author reply 6053-6054.

Li, M., J.C. Bermak, Z.W. Wang, and Q.Y. Zhou. 2000. Modulation of dopamine D(2) receptor signaling by actin-binding protein (ABP-280). *Mol Pharmacol*. 57:446-452.

Li, M.G., M. Serr, K. Edwards, S. Ludmann, D. Yamamoto, L.G. Tilney, C.M. Field, and T.S. Hays. 1999. Filamin is required for ring canal assembly and actin organization during Drosophila oogenesis. *J Cell Biol*. 146:1061-1074.

Lin, Q., W. Yang, D. Baird, Q. Feng, and R.A. Cerione. 2006. Identification of a DOCK180-related guanine nucleotide exchange factor that is capable of mediating a positive feedback activation of Cdc42. *J Biol Chem*. 281:35253-35262.

Liu, G., L. Thomas, R.A. Warren, C.A. Enns, C.C. Cunningham, J.H. Hartwig, and G. Thomas. 1997. Cytoskeletal protein ABP-280 directs the intracellular trafficking of furin and modulates proprotein processing in the endocytic pathway. *J Cell Biol*. 139:1719-1733.

Lynch, C.D., N.C. Gauthier, N. Biais, A.M. Lazar, P. Roca-Cusachs, C.H. Yu, and M.P. Sheetz. 2011. Filamin depletion blocks endoplasmic spreading and destabilizes force-bearing adhesions. *Mol Biol Cell*. 22:1263-1273.

Maekawa, H., and E. Schiebel. 2004. CLIP-170 family members: a motor-driven ride to microtubule plus ends. *Dev Cell*. 6:746-748.

Marti, A., Z. Luo, C. Cunningham, Y. Ohta, J. Hartwig, T.P. Stossel, J.M. Kyriakis, and J. Avruch. 1997. Actin-binding protein-280 binds the stress-activated protein kinase (SAPK) activator SEK-1 and is required for tumor necrosis factor-alpha activation of SAPK in melanoma cells. *J Biol Chem*. 272:2620-2628.

Massena, S., G. Christoffersson, E. Hjertström, E. Zcharia, I. Vlodavsky, N. Ausmees, C. Rolny, J.P. Li, and M. Phillipson. 2010. A chemotactic gradient sequestered on endothelial heparan sulfate induces directional intraluminal crawling of neutrophils. *Blood*. 116:1924-1931.

McCachren, S.S., Jr., J. Nichols, R.E. Kaufman, and J.E. Niedel. 1986. Dibutyryl cyclic adenosine monophosphate reduces expression of c-myc during HL-60 differentiation. *Blood*. 68:412-416.

McCoy, A.J., P. Fucini, A.A. Noegel, and M. Stewart. 1999. Structural basis for dimerization of the Dictyostelium gelation factor (ABP120) rod. *Nat Struct Biol*. 6:836-841.

Mestas, J., and C.C. Hughes. 2004. Of mice and not men: differences between mouse and human immunology. *J Immunol*. 172:2731-2738.

Millius, A., and O.D. Weiner. 2010. Manipulation of neutrophil-like HL-60 cells for the study of directed cell migration. *Methods Mol Biol*. 591:147-158.

Mondal, S., B. Burgute, D. Rieger, R. Muller, F. Rivero, J. Faix, M. Schleicher, and A.A. Noegel. 2010. Regulation of the actin cytoskeleton by an interaction of IQGAP related protein GAPA with filamin and cortexillin I. *PLoS One*. 5:e15440.

Moriceau, S., C. Kantari, J. Mocek, N. Davezac, J. Gabillet, I.C. Guerrera, F. Brouillard, D. Tondelier, I. Sermet-Gaudelus, C. Danel, G. Lenoir, S. Daniel, A. Edelman, and V. Witko-Sarsat. 2009. Coronin-1 is associated with neutrophil survival and is cleaved during apoptosis: potential implication in neutrophils from cystic fibrosis patients. *J Immunol*. 182:7254-7263.

Mueller, P., J. Massner, R. Jayachandran, B. Combaluzier, I. Albrecht, J. Gatfield, C. Blum, R. Ceredig, H.R. Rodewald, A.G. Rolink, and J. Pieters. 2008. Regulation of T cell survival through coronin-1-mediated generation of inositol-1,4,5-trisphosphate and calcium mobilization after T cell receptor triggering. *Nat Immunol*. 9:424-431.

Müller-Taubenberger, A., A.N. Lupas, H. Li, M. Ecke, E. Simmeth, and G. Gerisch. 2001. Calreticulin and calnexin in the endoplasmic reticulum are important for phagocytosis. *EMBO J*. 20:6772-6782.

Muller, W.A. 2011. Mechanisms of leukocyte transendothelial migration. *Annu Rev Pathol*. 6:323-344.

Nakamura, F., J.H. Hartwig, T.P. Stossel, and P.T. Szymanski. 2005. Ca2+ and calmodulin regulate the binding of filamin A to actin filaments. *J Biol Chem*. 280:32426-32433.

Nakamura, F., T.M. Osborn, C.A. Hartemink, J.H. Hartwig, and T.P. Stossel. 2007. Structural basis of filamin A functions. *J Cell Biol*. 179:1011-1025.

Nakamura, F., T.P. Stossel, and J.H. Hartwig. 2011. The filamins: organizers of cell structure and function. *Cell Adh Migr*. 5:160-169.

Nauseef, W.M., and N. Borregaard. 2014. Neutrophils at work. *Nat Immunol*. 15:602-611.

Niederman, R., P.C. Amrein, and J. Hartwig. 1983. Three-dimensional structure of actin filaments and of an actin gel made with actin-binding protein. *J Cell Biol*. 96:1400-1413.

Niggli, V. 1999. Rho-kinase in human neutrophils: a role in signalling for myosin light chain phosphorylation and cell migration. *FEBS Lett*. 445:69-72.

Noegel, A.A., R. Blau-Wasser, H. Sultana, R. Muller, L. Israel, M. Schleicher, H. Patel, and C.J. Weijer. 2004. The cyclase-associated protein CAP as regulator of cell polarity and cAMP signaling in Dictyostelium. *Mol Biol Cell*. 15:934-945.

Noegel, A.A., and J.E. Luna. 1995. The Dictyostelium cytoskeleton. *Experientia*. 51:1135-1143.

Noegel, A.A., S. Rapp, F. Lottspeich, M. Schleicher, and M. Stewart. 1989. The Dictyostelium gelation factor shares a putative actin binding site with alpha-actinins and dystrophin and also has a rod domain containing six 100-residue motifs that appear to have a cross-beta conformation. *J Cell Biol*. 109:607-618.

Nordenfelt, P., S. Bauer, P. Lonnbro, and H. Tapper. 2009. Phagocytosis of Streptococcus pyogenes by all-trans retinoic acid-differentiated HL-60 cells: roles of azurophilic granules and NADPH oxidase. *PLoS One*. 4:e7363.

Ohta, Y., J.H. Hartwig, and T.P. Stossel. 2006. FilGAP, a Rho- and ROCK-regulated GAP for Rac binds filamin A to control actin remodelling. *Nat Cell Biol*. 8:803-814.

Ohta, Y., T.P. Stossel, and J.H. Hartwig. 1991. Ligand-sensitive binding of actin-binding protein to immunoglobulin G Fc receptor I (Fc gamma RI). *Cell*. 67:275-282.

Ohta, Y., N. Suzuki, S. Nakamura, J.H. Hartwig, and T.P. Stossel. 1999. The small GTPase RalA targets filamin to induce filopodia. *Proc Natl Acad Sci U S A*. 96:2122-2128.

Parent, C.A. 2001. Dictyostelium cell dynamics. *Curr Protoc Cell Biol*. Chapter 12:Unit 12 15.

Parent, C.A. 2004. Making all the right moves: chemotaxis in neutrophils and Dictyostelium. *Curr Opin Cell Biol*. 16:4-13.

Park, K.C., F. Rivero, R. Meili, S. Lee, F. Apone, and R.A. Firtel. 2004. Rac regulation of chemotaxis and morphogenesis in Dictyostelium. *EMBO J*. 23:4177-4189.

Phillipson, M., B. Heit, P. Colarusso, L. Liu, C.M. Ballantyne, and P. Kubes. 2006. Intraluminal crawling of neutrophils to emigration sites: a molecularly distinct process from adhesion in the recruitment cascade. *J Exp Med*. 203:2569-2575.

Pieters, J. 2008. Coronin 1 in innate immunity. *Subcell Biochem*. 48:116-123.

Pillay, J., I. den Braber, N. Vrisekoop, L.M. Kwast, R.J. de Boer, J.A. Borghans, K. Tesselaar, and L. Koenderman. 2010. In vivo labeling with 2H2O reveals a human neutrophil lifespan of 5.4 days. *Blood*. 116:625-627.

Popowicz, G.M., M. Schleicher, A.A. Noegel, and T.A. Holak. 2006. Filamins: promiscuous organizers of the cytoskeleton. *Trends Biochem Sci*. 31:411-419.

Pudas, R., T.R. Kiema, P.J. Butler, M. Stewart, and J. Ylänne. 2005. Structural basis for vertebrate filamin dimerization. *Structure*. 13:111-119.

Raper, K.B. 1935. *Dictyostelium discoideum*, a new species of slime mold from decaying forest leaves. *Journal of Agricultural Research* 50:135-147.

Razinia, Z., T. Mäkelä, J. Ylänne, and D.A. Calderwood. 2012. Filamins in mechanosensing and signaling. *Annu Rev Biophys*. 41:227-246.

Rivero, F., R. Furukawa, M. Fechheimer, and A.A. Noegel. 1999. Three actin cross-linking proteins, the 34 kDa actin-bundling protein, alpha-actinin and gelation factor (ABP-120), have both unique and redundant roles in the growth and development of Dictyostelium. *J Cell Sci*. 112 (Pt 16):2737-2751.

Rivero, F., R. Furukawa, A.A. Noegel, and M. Fechheimer. 1996a. Dictyostelium discoideum cells lacking the 34,000-dalton actin-binding protein can grow, locomote, and develop, but exhibit defects in regulation of cell structure and movement: a case of partial redundancy. *J Cell Biol*. 135:965-980.

Rivero, F., B. Köppel, B. Peracino, S. Bozzaro, F. Siegert, C.J. Weijer, M. Schleicher, R. Albrecht, and A.A. Noegel. 1996b. The role of the cortical cytoskeleton: F-actin crosslinking proteins protect against

osmotic stress, ensure cell size, cell shape and motility, and contribute to phagocytosis and development. *J Cell Sci*. 109 (Pt 11):2679-2691.

Robertson, S.P. 2005. Filamin A: phenotypic diversity. *Curr Opin Genet Dev*. 15:301-307.

Rohatgi, R., L. Ma, H. Miki, M. Lopez, T. Kirchhausen, T. Takenawa, and M.W. Kirschner. 1999. The interaction between N-WASP and the Arp2/3 complex links Cdc42-dependent signals to actin assembly. *Cell*. 97:221-231.

Rozenberg, G. 1996. Microscopic Haematology: A practical guide for the laboratory. Harwood Academic Publishers, United Kingdom.

Sahai, E., and C.J. Marshall. 2003. Differing modes of tumour cell invasion have distinct requirements for Rho/ROCK signalling and extracellular proteolysis. *Nat Cell Biol*. 5:711-719.

Sakabe, I., A. Asai, J. Iijima, and M. Maruyama. 2012. Age-related guanine nucleotide exchange factor, mouse Zizimin2, induces filopodia in bone marrow-derived dendritic cells. *Immun Ageing*. 9:2.

Sarkisian, M.R., C.M. Bartley, H. Chi, F. Nakamura, K. Hashimoto-Torii, M. Torii, R.A. Flavell, and P. Rakic. 2006. MEKK4 signaling regulates filamin expression and neuronal migration. *Neuron*. 52:789-801.

Sasaki, A., Y. Masuda, Y. Ohta, K. Ikeda, and K. Watanabe. 2001. Filamin associates with Smads and regulates transforming growth factor-beta signaling. *J Biol Chem*. 276:17871-17877.

Schindl, M., E. Wallraff, B. Deubzer, W. Witke, G. Gerisch, and E. Sackmann. 1995. Cell-substrate interactions and locomotion of Dictyostelium wild-type and mutants defective in three cytoskeletal proteins: a study using quantitative reflection interference contrast microscopy. *Biophys J*. 68:1177-1190.

Schleicher, M., A. Noegel, T. Schwarz, E. Wallraff, M. Brink, J. Faix, G. Gerisch, and G. Isenberg. 1988. A Dictyostelium mutant with severe defects in alpha-actinin: its characterization using cDNA probes and monoclonal antibodies. *J Cell Sci*. 90 (Pt 1):59-71.

Schwaiger, I., A. Kardinal, M. Schleicher, A.A. Noegel, and M. Rief. 2004. A mechanical unfolding intermediate in an actin-crosslinking protein. *Nat Struct Mol Biol*. 11:81-85.

Schwaiger, I., M. Schleicher, A.A. Noegel, and M. Rief. 2005. The folding pathway of a fast-folding immunoglobulin domain revealed by single-molecule mechanical experiments. *EMBO Rep*. 6:46-51.

Servant, G., O.D. Weiner, P. Herzmark, T. Balla, J.W. Sedat, and H.R. Bourne. 2000. Polarization of chemoattractant receptor signaling during neutrophil chemotaxis. *Science*. 287:1037-1040.

Servant, G., O.D. Weiner, E.R. Neptune, J.W. Sedat, and H.R. Bourne. 1999. Dynamics of a chemoattractant receptor in living neutrophils during chemotaxis. *Mol Biol Cell*. 10:1163-1178.

Sheen, V.L., Y. Feng, D. Graham, T. Takafuta, S.S. Shapiro, and C.A. Walsh. 2002. Filamin A and Filamin B are co-expressed within neurons during periods of neuronal migration and can physically interact. *Hum Mol Genet*. 11:2845-2854.

Shizuta, Y., H. Shizuta, M. Gallo, P. Davies, and I. Pastan. 1976. Purification and properties of filamin, and actin binding protein from chicken gizzard. *J Biol Chem*. 251:6562-6567.

Sjögren, F., O. Stendahl, and O. Ljunghusen. 2000. The influence of retinoic acid and retinoic acid derivatives on beta2 integrins and L-selectin expression in HL-60 cells in vitro. *Inflammation*. 24:21-32.

Smith, T.C., Z. Fang, and E.J. Luna. 2010. Novel interactors and a role for supervillin in early cytokinesis. *Cytoskeleton (Hoboken)*. 67:346-364.

Sokol, N.S., and L. Cooley. 1999. Drosophila filamin encoded by the cheerio locus is a component of ovarian ring canals. *Curr Biol*. 9:1221-1230.

Srinivasan, S., F. Wang, S. Glavas, A. Ott, F. Hofmann, K. Aktories, D. Kalman, and H.R. Bourne. 2003. Rac and Cdc42 play distinct roles in regulating PI(3,4,5)P3 and polarity during neutrophil chemotaxis. *J Cell Biol*. 160:375-385.

Stossel, T.P., J. Condeelis, L. Cooley, J.H. Hartwig, A. Noegel, M. Schleicher, and S.S. Shapiro. 2001. Filamins as integrators of cell mechanics and signalling. *Nat Rev Mol Cell Biol*. 2:138-145.

Sun, C., C. Forster, F. Nakamura, and M. Glogauer. 2013. Filamin-A regulates neutrophil uropod retraction through RhoA during chemotaxis. *PLoS One*. 8:e79009.

Takala, H., E. Nurminen, S.M. Nurmi, M. Aatonen, T. Strandin, M. Takatalo, T. Kiema, C.G. Gahmberg, J. Ylänne, and S.C. Fagerholm. 2008. Beta2 integrin phosphorylation on Thr758 acts as a molecular switch to regulate 14-3-3 and filamin binding. *Blood*. 112:1853-1862.

Tavano, R., R.L. Contento, S.J. Baranda, M. Soligo, L. Tuosto, S. Manes, and A. Viola. 2006. CD28 interaction with filamin-A controls lipid raft accumulation at the T-cell immunological synapse. *Nat Cell Biol*. 8:1270-1276.

Thomas, C.J., and K. Schroder. 2013. Pattern recognition receptor function in neutrophils. *Trends Immunol*. 34:317-328.

Tigges, U., B. Koch, J. Wissing, B.M. Jockusch, and W.H. Ziegler. 2003. The F-actin cross-linking and focal adhesion protein filamin A is a ligand and in vivo substrate for protein kinase C alpha. *J Biol Chem*. 278:23561-23569.

Tofts, P.S., T. Chevassut, M. Cutajar, N.G. Dowell, and A.M. Peters. 2011. Doubts concerning the recently reported human neutrophil lifespan of 5.4 days. *Blood*. 117:6050-6052; author reply 6053-6054.

Tseng, Y., K.M. An, O. Esue, and D. Wirtz. 2004. The bimodal role of filamin in controlling the architecture and mechanics of F-actin networks. *J Biol Chem*. 279:1819-1826.

Tsiftsoglou, A.S., I.S. Pappas, and I.S. Vizirianakis. 2003. Mechanisms involved in the induced differentiation of leukemia cells. *Pharmacol Ther*. 100:257-290.

Tyson, R.A., E. Zatulovskiy, R.R. Kay, and T. Bretschneider. 2014. How blebs and pseudopods cooperate during chemotaxis. *Proc Natl Acad Sci U S A*. 111:11703-11708.

Ueda, K., Y. Ohta, and H. Hosoya. 2003. The carboxy-terminal pleckstrin homology domain of ROCK interacts with filamin-A. *Biochem Biophys Res Commun*. 301:886-890.

Ura, S., A.Y. Pollitt, D.M. Veltman, N.A. Morrice, L.M. Machesky, and R.H. Insall. 2012. Pseudopod growth and evolution during cell movement is controlled through SCAR/WAVE dephosphorylation. *Curr Biol*. 22:553-561.

van der Flier, A., and A. Sonnenberg. 2001. Structural and functional aspects of filamins. *Biochim Biophys Acta*. 1538:99-117.

van der Ven, P.F., S. Wiesner, P. Salmikangas, D. Auerbach, M. Himmel, S. Kempa, K. Hayess, D. Pacholsky, A. Taivainen, R. Schroder, O. Carpen, and D.O. Fürst. 2000. Indications for a novel muscular dystrophy pathway. gamma-filamin, the muscle-specific filamin isoform, interacts with myotilin. *J Cell Biol*. 151:235-248.

Vargas, M., P. Sansonetti, and N. Guillen. 1996. Identification and cellular localization of the actin-binding protein ABP-120 from Entamoeba histolytica. *Mol Microbiol*. 22:849-857.

Veltman, D.M., J. Roelofs, R. Engel, A.J. Visser, and P.J. Van Haastert. 2005. Activation of soluble guanylyl cyclase at the leading edge during Dictyostelium chemotaxis. *Mol Biol Cell*. 16:976-983.

Vidarsson, G., and J.G. van de Winkel. 1998. Fc receptor and complement receptor-mediated phagocytosis in host defence. *Curr Opin Infect Dis*. 11:271-278.

Wallach, D., P.J. Davies, and I. Pastan. 1978. Purification of mammalian filamin. Similarity to high molecular weight actin-binding protein in macrophages, platelets, fibroblasts, and other tissues. *J Biol Chem*. 253:3228-3235.

Wallraff, E., M. Schleicher, M. Modersitzki, D. Rieger, G. Isenberg, and G. Gerisch. 1986. Selection of Dictyostelium mutants defective in cytoskeletal proteins: use of an antibody that binds to the ends of alpha-actinin rods. *EMBO J*. 5:61-67.

Wang, K., J.F. Ash, and S.J. Singer. 1975. Filamin, a new high-molecular-weight protein found in smooth muscle and non-muscle cells. *Proc Natl Acad Sci U S A*. 72:4483-4486.

Wehland, J., and M.C. Willingham. 1983. A rat monoclonal antibody reacting specifically with the tyrosylated form of alpha-tubulin. II. Effects on cell movement, organization of microtubules, and intermediate filaments, and arrangement of Golgi elements. *J Cell Biol*. 97:1476-1490.

Welch, H.C., W.J. Coadwell, C.D. Ellson, G.J. Ferguson, S.R. Andrews, H. Erdjument-Bromage, P. Tempst, P.T. Hawkins, and L.R. Stephens. 2002. P-Rex1, a PtdIns(3,4,5)P3- and Gbetagamma-regulated guanine-nucleotide exchange factor for Rac. *Cell*. 108:809-821.

Wilson, K., A. Lewalle, M. Fritzsche, R. Thorogate, T. Duke, and G. Charras. 2013. Mechanisms of leading edge protrusion in interstitial migration. *Nat Commun*. 4:2896.

Witke, W., M. Schleicher, and A.A. Noegel. 1992. Redundancy in the microfilament system: abnormal development of Dictyostelium cells lacking two F-actin cross-linking proteins. *Cell*. 68:53-62.

Wolosewick, J.J., and J. Condeelis. 1986. Fine structure of gels prepared from an actin-binding protein and actin: comparison to cytoplasmic extracts and cortical cytoplasm in amoeboid cells of cortical cytoplasm in amoeboid cells of Dictyostelium discoideum. *J Cell Biochem*. 30:227-243.

Woolf, E., I. Grigorova, A. Sagiv, V. Grabovsky, S.W. Feigelson, Z. Shulman, T. Hartmann, M. Sixt, J.G. Cyster, and R. Alon. 2007. Lymph node chemokines promote sustained T lymphocyte motility without triggering stable integrin adhesiveness in the absence of shear forces. *Nat Immunol*. 8:1076-1085.

Wyckoff, J.B., S.E. Pinner, S. Gschmeissner, J.S. Condeelis, and E. Sahai. 2006. ROCK- and myosin-dependent matrix deformation enables protease-independent tumor-cell invasion in vivo. *Curr Biol*. 16:1515-1523.

Xiao, Z., N. Zhang, D.B. Murphy, and P.N. Devreotes. 1997. Dynamic distribution of chemoattractant receptors in living cells during chemotaxis and persistent stimulation. *J Cell Biol*. 139:365-374.

Xu, J., F. Wang, A. Van Keymeulen, P. Herzmark, A. Straight, K. Kelly, Y. Takuwa, N. Sugimoto, T. Mitchison, and H.R. Bourne. 2003. Divergent signals and cytoskeletal assemblies regulate self-organizing polarity in neutrophils. *Cell*. 114:201-214.

Yamazaki, M., S. Furuike, and T. Ito. 2002. Mechanical response of single filamin A (ABP-280) molecules and its role in the actin cytoskeleton. *J Muscle Res Cell Motil*. 23:525-534.

Yan, M., C. Di Ciano-Oliveira, S. Grinstein, and W.S. Trimble. 2007. Coronin function is required for chemotaxis and phagocytosis in human neutrophils. *J Immunol*. 178:5769-5778.

Yoshida, K., and T. Soldati. 2006. Dissection of amoeboid movement into two mechanically distinct modes. *J Cell Sci*. 119:3833-3844.

Yoshida, N., T. Ogata, K. Tanabe, S. Li, M. Nakazato, K. Kohu, T. Takafuta, S. Shapiro, Y. Ohta, M. Satake, and T. Watanabe. 2005. Filamin A-bound PEBP2beta/CBFbeta is retained in the cytoplasm and prevented from functioning as a partner of the Runx1 transcription factor. *Mol Cell Biol*. 25:1003-1012.

Yuan, Y., and Z. Shen. 2001. Interaction with BRCA2 suggests a role for filamin-1 (hsFLNa) in DNA damage response. *J Biol Chem*. 276:48318-48324.

Zarbock, A., and K. Ley. 2009. Neutrophil adhesion and activation under flow. *Microcirculation*. 16:31-42.

Zatulovskiy, E., R. Tyson, T. Bretschneider, and R.R. Kay. 2014. Bleb-driven chemotaxis of Dictyostelium cells. *J Cell Biol*. 204:1027-1044.

Zhang, K., and J. Chen. 2012. The regulation of integrin function by divalent cations. *Cell Adh Migr*. 6:20-29.

Zhang, M., and G.E. Breitwieser. 2005. High affinity interaction with filamin A protects against calcium-sensing receptor degradation. *J Biol Chem*. 280:11140-11146.

Zhao, S., R. Gao, P.N. Devreotes, A. Mogilner, and M. Zhao. 2013. 3D arrays for high throughput assay of cell migration and electrotaxis. *Cell Biol Int*. 37:995-1002.

Zhou, A.X., J.H. Hartwig, and L.M. Akyürek. 2010. Filamins in cell signaling, transcription and organ development. *Trends Cell Biol*. 20:113-123.

Zigmond, S.H., and J.G. Hirsch. 1973. Leukocyte locomotion and chemotaxis. New methods for evaluation, and demonstration of a cell-derived chemotactic factor. *J Exp Med*. 137:387-410.

Zigmond, S.H., M. Joyce, J. Borleis, G.M. Bokoch, and P.N. Devreotes. 1997. Regulation of actin polymerization in cell-free systems by GTPgammaS and Cdc42. *J Cell Biol*. 138:363-374.

List of figures

List of tables

Acknowledgements

First of all, I want to thank PD Dr. Annette Müller-Taubenberger and Prof. Dr. Michael Schleicher for giving me the opportunity to work on these very interesting topics. Thank you very much for your caring support and mentoring, great scientific input and your willingness to always discuss and answer my questions.

I want to thank all my lab members for their helpfulness, colleagueship, for creating such a great working atmosphere and for having so much fun! Many thanks go to Dr. Matthias Samereier for sharing advice and fruitful discussions. I sincerely thank Dr. Hellen Ishikawa-Ankerhold, Dr. Linda Sanftenberg, Dr. Christoph Gallinger, Dr. Julia Gallinger, Gudrun Trommler, Stephanie Lindholz, Thi-Hieu Ho and Daniela Rieger for their scientific and moral support.

I thank Dr. Fumihiko Nakamura and Prof. Dr. Angelika Noegel for generously providing different DNA constructs. Many thanks also go to Prof. Dr. Barbara Walzog and all members of her research group, especially Doris Brechtefeld, Tanja Vlaovic, Melanie Salvermoser and Michael Winkelmann for sharing precious reagents, lab equipment, scientific knowledge and especially for the opportunity to generate the FLNa knockdown cell lines in their lab.

I express my gratitude to the CRC 914 for financial support during this thesis. I also want to thank the ‘Integrated Research Training Group of the CRC 914 (IRTG 914)’ for generous support and especially or the opportunity to participate at many stimulating scientific activities.

Finally, my very special thanks go to my family and friends for all your support, trust, love and patience in the last few years.